Recent advances and prospective in ruthenium-based materials for electrochemical water splitting

Jie Yu,[†] Qijiao He,[†] Guangming Yang,[‡] Wei Zhou,[‡] Zongping Shao,[, ‡, §] and Meng Ni [*, †, //]*

[†]Department of Building and Real Estate, The Hong Kong Polytechnic University, Hung Hom, Kowloon, Hong Kong 999077, China

[‡]State Key Laboratory of Materials-Oriented Chemical Engineering, College of Chemical Engineering, Nanjing Tech University, No. 5, Xin Mofan Road, Nanjing 210009, PR China

[§]Department of Chemical Engineering, Curtin University, Perth, Western Australia 6845, Australia

[//]Environmental Energy Research Group, Research Institute for Sustainable Urban Development (RISUD), The Hong Kong Polytechnic University, Hung Hom, Kowloon, Hong Kong 999077, China

ABSTRACT: As a highly appealing technology for hydrogen generation, water electrolysis including oxygen evolution reaction (OER) at the anode and hydrogen evolution reaction (HER) at the cathode largely depends on the availability of efficient electrocatalysts. Accordingly, over the past years, much effort has been made to develop various electrocatalysts with super performance and reduced cost. Among them, Ruthenium (Ru)-based materials for OER and HER are very promising due to their prominent catalytic activity, pH-universal application, and the cheapest price among the precious metal family, etc. Herein, recent advances in this hot research field are comprehensively reviewed. A general description about water splitting is presented to understand the reaction mechanism and proposed scaling relations toward activities and key stability issues for Ru-based materials are further given. Followed on, various Ru-involving electrocatalysts are introduced and classified into different groups for improving or optimizing electrocatalytic properties, with a special focus on several significant bifunctional electrocatalysts along with a simulated water electrolyzer. Finally, a perspective on the existing challenges and future progress of Ru-based catalysts toward OER and HER is provided. The main aim here is to shed some light on the design and construction of emerging catalysts for energy storage and conversion technologies.

KEYWORDS: ruthenium-based materials, electrocatalysts, oxygen evolution reaction, hydrogen evolution reaction, water splitting

1. INTRODUCTION

Energy saving and environmental protection are the two most urgent challenges on the way to sustainable development in the 21st century.[1-4] With fastly expanding energy demand, worsening environmental pollution, and increasing concentration of CO_2 in the atmosphere due to the immoderate utilization of fossil fuels, intensive research activities are ongoing to better utilize available clean and renewable energy sources/technologies with less environmental impact.[5, 6] Hydrogen (H_2), as an energy carrier with zero-carbon content and the highest gravimetric energy density among the available fuels, has been regard as the most promising alternative to fossil fuels.[6, 7] However, at present, the industrial hydrogen production is still largely dependent on the catalytic reforming route that converts water and natural gas into H_2 and carbon dioxide, which not only promotes the fossil fuel consumption and CO_2 emissions but also results in low purity of the obtained hydrogen products from the unstable conversion efficiency.[8, 9] Electrochemical water splitting driven by renewable energy sources is a highly appealing technology for pure hydrogen production in a more efficient and sustainable manner.

Hydrogen and oxygen evolution reactions (HER and OER), respectively occurred on the cathode and anode of a water electrolyzer, are two key half reactions in water electrolysis, and the theoretically thermodynamic potential of 1.23 V is required for water splitting.[9, 10] However, the sluggish kinetics and thus the large overpotential towards both OER and HER electrodes become main obstacles for the large-scale implementation of water electrolysis for hydrogen production.[10] Accordingly, efficient

electrocatalysts are required to minimize the overpotentials and enhance water-splitting efficiency. Nowadays, a variety of electrocatalysts were exploited and evaluated for HER and OER, including noble-metal based materials, earth-abundant transition metals oxide (hydroxides), chalcogenides, phosphides, nitrides and carbides, functional metal-free carbon and various composites.[7, 11-13] Extensive efforts have been made to develop low-cost noble metal-free catalyst. These affordable OER and HER alternative electrocatalysts demonstrate superior OER catalytic behavior in alkaline electrolyte, whereas their good HER performance is usually obtained in acidic solution.[14-16] The different pH requirements of these catalysts limit their practical applications. For comparison, noble metal catalysts are still the most active catalysts for both HER and OER in a wide range of pH. For example, Pt/C is widely used as the HER benchmark and IrO_2/RuO_2 is used as the OER benchmark.[14, 15] Thus, noble-metal based electrocatalysts are still the most promising family for both OER and HER.

Ruthenium (Ru) belongs to the Pt-related noble metal family, yet its cost is only 4% of that for Pt.[17] Simultaneously, Ru has the robust anti-corrosion ability, allowing for use in electrolytes with a wide range of pH values.[18] From the mid-nineteenth century when Ru was first reported to present, Ru-based materials have emerged as the appealing and famous catalysts for their efficient catalytic ability for various classical reactions, such as OER, HER, oxygen reduction reaction (ORR), CO oxidation reaction, and methane oxidation reaction, etc.[19, 20] As OER electrocatalysts, extensive research articles on Ru-related materials have been reported continuously in the past several decades, especially for RuO_2.[21-24] When referring to HER, Ru-based electrocatalysts

have been discovered as early as the 1970s.[25] However, until recently, they gained renewed attention owing to their Pt-like hydrogen bond strength (~ 65 kcal mol^{-1}).[26-30] Therefore, considerable research efforts have been made to design the Ru-based catalysts for HER or for overall water splitting with great success. As shown in **Figure 1**a, the number of publications increased significantly in the past 5 years. As a booming field in the energy sector, lots of outstanding reviews about OER or HER have been published, with a focus on non-noble metal catalysts such as nickel-, cobalt-, manganese-, iron- and molybdenum-related materials[31-34] Nonetheless, the current literature is lacking a comprehensive and systematical review on the Ru-based materials as OER/HER electrocatalysts.

In this review, we focus on the recent progress about Ru-involving electrocatalysts towards water splitting. First of all, the history of water splitting, the OER/HER reaction mechanisms, the proposed scaling relations toward activities, and the key stability issues for Ru-based materials are briefly introduced. Then, based on the recent advances in this field, all Ru-based catalysts are classified into several categories in detail: Ru metal, Ru oxides, Ru phosphides, sulfides, or selenides, and other Ru-related compounds. Each large category is also divided into several sub-categories, which is described in **Figure 1**b. For each part, we pay more attention to the emphatical discussion on catalyst synthesis and design, working electrolytes, catalytic performance, and activity/stability-enhancing strategies via representing typical examples. The insight into the origin of super performance can provide guidance for the design of high-performance electrocatalysts for water splitting. In addition, some improvised water

electrolyzers with Ru-based electrocatalysts simultaneously for OER and HER are also highlighted in this review. Lastly, the current scientific challenges and future directions in such a rapidly flourishing field are briefly discussed. Such timely and comprehensive review will attract more interests from specialists worldwide and present a fresh impetus for subsequently more high-level studies.

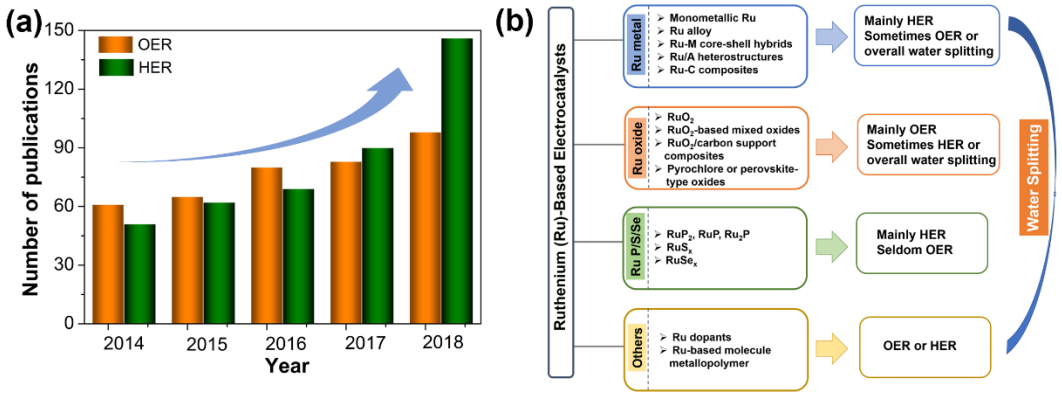

Figure 1. a) Roughly estimated numbers of publications during 2014-2018 from Web of Science, which were obtained by searching the keywords of "ruthenium" and "oxygen evolution" (orange columns), or "ruthenium" and "hydrogen evolution" (green columns). **b)** Diagrammatic illustration for development of Ru-based electrocatalysts toward water splitting.

2. CHARACTERISTICS OF RU-INVOLVING CATALYSTS IN WATER ELECTROLYSIS

2.1. Fundamentals of electrochemical of water splitting. The first research on water electrolysis to generate hydrogen dated back to the early 1800s, yet the crude techniques restricted its generalized use.[35] Nowadays, with the quickly expanded utilization of solar energy, wind energy, and other renewable sources, the electrochemical water splitting technology has been vigorously promoted and contributed to 4% of hydrogen production worldwide.[36] The percentage of hydrogen production from water electrolysis is expected to grow significantly in the coming decades. This is due to the facts that water electrolysis can perform well in a wide range

of pH values with a rather simple overall reaction: $H_2O \rightarrow H_2$ (cathode) + 1/2 O_2 (anode) and the rich renewable energy resources and abundant water reservoir, which theoretically needs a minimum energy input of $\Delta G = 237.1$ kJ mol^{-1} at a thermodynamic potential of 1.23 V.[10] However, to compete with the state-of-the-art hydrogen production technology, such as steam reforming of coal and natural gas, the product cost based on water electrolysis should be greatly reduced, which is highly dependent on the electrode reactions (OER and HER). Significantly, the activity of the two separate half reactions of OER and HER have a large dependence on the pH value of media. To improve the reaction kinetics, the reaction mechanisms for OER and HER in different solutions should be first understood, and extensive research activities have been conducted to understand the reactions over both electrodes of water electrolyzer and the proposed mechanisms are given as follows.

2.1.1. OER mechanism. To realize OER over the electrode, four electrons need to be transferred for per oxygen molecule generation. The electron transfer may be performed in multiple steps. Thus, the OER process is generally believed a complicated multi-step four-electron oxidation process. The theoretical thermodynamic voltage for OER is 1.23 V.[37, 38] Owing to the difficulty in detecting intermediates, multifarious OER mechanisms have been proposed. Here, we pick up the most classical and widely accepted one as an example, which was divided into four steps, as shown below.[37, 39, 40]

In acidic media:

Step 1: $* + H_2O \rightarrow {}^*OH + H^+ + e^-$

Step 2: ${}^*OH \rightarrow {}^*O + H^+ + e^-$

Step 3: $^{*}O + H_2O \rightarrow {}^{*}OOH + H^+ + e^-$

Step 4: $^{*}OOH \rightarrow O_2 + H^+ + e^-$

In alkaline or neutral media:

Step 1: $OH^- \rightarrow {}^{*}OH + e^-$

Step 2: $^{*}OH + OH^- \rightarrow {}^{*}O + H_2O + e^-$

Step 3: $^{*}O + OH^- \rightarrow {}^{*}OOH + e^-$

Step 4: $^{*}OOH + OH^- \rightarrow O_2 + H_2O + e^-$

In which * suggests the active sites of the electrocatalyst. For the four-step process, there are three reaction intermediates ($^{*}OH$, $^{*}O$, $^{*}OOH$), representing the adsorbed oxygen-related species on the surface of catalysts. Typically, under electrochemical oxidation condition, the oxidation of water/hydroxyl ions was initiated to form $^{*}OH$, followed by deprotonation and further oxidation to generate these intermediates of $^{*}O$ and $^{*}OOH$, and ultimately O_2 products. In acidic electrolytes, water molecules serve as the oxygen source, while in neutral or alkaline solutions, oxygen is from hydroxyl ions.

2.1.2. HER mechanism. In the HER process, when releasing one H_2 molecule, only two electrons are transferred. An ideal catalyst requires a theoretical thermodynamic voltage of 0 V to drive HER.[42] Therefore, compared with OER, HER is relatively easy to occur and is a two-step two-electron process, as expressed in the following equations.[42, 43]

Step 1: $H^+ + e^- \rightarrow H_{ads}$ (under acidic condition) / $H_2O + e^- \rightarrow H_{ads} + OH^-$ (under alkaline condition) (Volmer, ~120 mV dec^{-1})

Step 2: $H_2O + H_{ads} + e^- \rightarrow H_2 + OH^-$ (under acidic condition) / $H^+ + H_{ads} + e^- \rightarrow H_2$

(under alkaline condition) (Heyrovsky, ~40 mV dec^{-1})

OR $H_{ads} + H_{ads} \rightarrow H_2$ (Tafel, ~30 mV dec^{-1})

According to the above-mentioned steps, the adsorbed hydrogen intermediate, H_{ads}, is first produced, denoted as Volmer step. Under the acidic condition, hydrogen ions (protons) directly combine with an electron and then are chemically adsorbed on the surface of the electrocatalysts, forming H_{ads}, whereas in alkaline solutions, the hydrogen ions are from the cleaved water molecules. Thus, in general, HER is easier to perform in acidic solutions than in alkaline solutions. The second step is the production of hydrogen molecules, which involves two different routes. One is that one proton can combine with a H_{ads} species formed through the first step to give an H_2 molecule, which is called as Heyrovsky step. The other is that two as-formed neighboring H_{ads} species are directly combined, named as Tafel step. Numerous previous works have revealed that the Tafel slopes can determine HER reaction mechanism, mainly including Volmer-Heyrovsky or Volmer-Tafel mechanism.[27-29, 41]

Figure 2 describes the representative polarization curves of OER (right) /HER (left) for an individual electrocatalyst based on a standard three-electrode system. Albeit the two reactions are contrary (one is regarded as water oxidation, OER; the other is considered as water reduction, HER.), their polarization curves show very similar shape corresponding to several analogous essential evaluation parameters to unravel catalytic behavior. Onset potential (E_{onset}), a potential value obtained at 10 μA cm^{-2}, indicates the occurrence of OER/HER. The extra potential value above the equilibrium potential (1.23 V for OER and 0 V for HER), named as overpotential, η, is generally applied to

account for the potential loss in the OER/HER process.[40] Considering a relevance to solar-to-fuels conversion, the overpotential needed to reach a current density of 10 mA cm^{-2} is more usually used.[10] Smaller absolute values of E_{onset} and η represent better electrocatalytic activity. As can be seen in the insert of **Figure 2**, the replotted curve as overpotential (η) versus the logarithm of the current density (log |j|) is derived from OER/HER polarization curves, and the slope value of linear portions is the Tafel value (a). Besides, the attained current density at the η = 0 revealed intrinsic activity, which is called as exchange current density (j_0). Except for several above parameters, Turnover frequency (TOF), quantifying the specific activity at a catalytic active site, and Faradaic efficiency (FE), reflecting the efficiency of electron transfer, are also used to assess the catalytic properties. However, TOF is strongly associated with the catalyst structure that is difficult to obtain. Thus, TOF is not too often used currently. For the measurement of FE during the OER or HER process, both experimentally quantified gas amount (n_e) and theoretically calculated gas amounts (n_t) are needed, and the ratio of them is the FE value ($FE = n_e/n_t$). The actual gas amount can be detected by the gas chromatography in gastight electrochemical cells. Meanwhile, the theoretical gas production can be calculated by integrating the galvanostatic or potentiostatic electrolysis plot. Additionally, electrochemical impedance spectrum (EIS) analysis is also carried out to probe the interface charge-transfer process of the electrode (charge transfer resistance, R_{ct}) and reveal the electrochemical active surface area through the capacitance (ECSA). An ideal OER/HER catalyst should deliver the small a, R_{ct}, high j_0, ECSA, TOF, and FE. Last but not least, stability has served as a vitally important

criterion to evaluate the practicability. Two conventional testing methods were commonly used: one is the accelerated measurement based on cyclic voltammetry and the other is the chronoamperometry or chronopotentiometry route. Besides them, there are some new methods, such as a flow cell (FC) directly linked to an inductively coupled plasma mass spectrometer (ICP-MS), named as FC-ICP-MS, and differential electrochemical mass spectrometry (DEMS).[44-46] By using FC-ICP-MS, the metal dissolution amounts can be real-timely recorded in parallel to the electrochemical measurement.[44] DEMS could be employed to identify and quantify the products or intermediates during the reaction process. Because the electrochemical currents can be simultaneously observed with the mass spectrometer ion currents, the prominent features in an electrochemical measurement can be revealed by the product analysis.[45, 46] By measuring EIS before and after the electrochemical reaction, the change of active electrode area can be analyzed through capacitance changes, so as to reveal the stability. It is more expected for a good catalyst to perform for a long time.

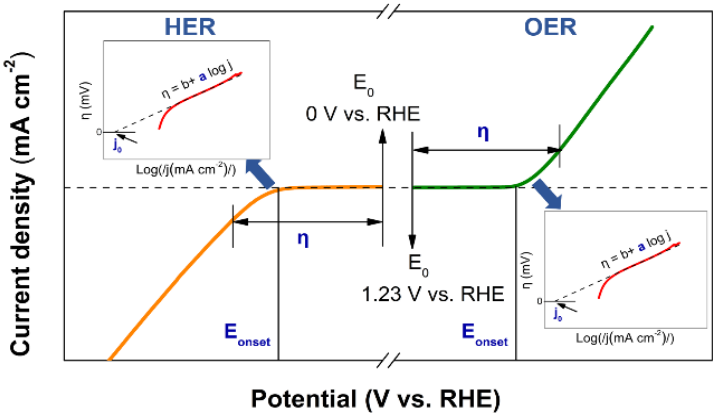

Figure 2. Representative polarization curves of OER (**right**) /HER (**left**). Insert is the Tafel plot obtained from the corresponding polarization curve.

2.2. Classical "Volcano"-shaped curves for revealing OER and HER activity.

Several pioneering works developed some scaling relations to reveal OER or HER

activities, in which “Volcano”-shaped plots offer a straightforward method to compare and visualize the electrocatalytic behavior of various materials, so as to guide the fabrication and design of catalysts.[40, 42, 43, 47, 48] Various catalytic systems depends on different parts of these OER or HER volcanos.

In the OER process, all mechanism steps are thermodynamically uphill. Thus, the potential-determining step should be one with the highest energy barrier.[42] According to many reports on numerous metal oxides, the difference of binding free energy between *OH and *OOH (ΔG_{*O}-ΔG_{*OH}) is large, 3.2 ± 0.2 eV.[42] Accordingly, it is strongly associated with the oxygen-evolving kinetics of an electrocatalyst. Superior OER catalysts should possess a moderate bonding to the O-related reaction intermediates, suggesting that too strong or too weak binding energy is not good for OER. Using the negative theoretical overpotential of numerous metal oxides against the binding free energy of ΔG_{*O}-ΔG_{*OH} obtained from first-principle calculation, Rossmeisl and his co-worker found a scaling relation with the “volcano” model that could disclose the OER activities of various metal oxides, as captured in **Figure 3**a.[43] Among them, RuO_2 theoretically turn out to be the most active toward OER, owing to the closest to optimal bonding force to oxygen species. However, it was difficult to quantitatively compare the theoretical data with different experimental values, as the potential was affected by many factors, such as pH, crystallinity, morphology, particle size, etc.[43] For example, a slight discrepancy could be observed in the case of Co_3O_4. Density functional theory (DFT) results displayed that the OER activities of RuO_2 and Co_3O_4 were very close, while many experimental studies showed Co_3O_4 had a higher

overpotential than RuO_2 by above 0.2 V.[49, 50] Of course, a low OER overpotential for Co_3O_4 with a controlled microstructure can also be found in many previous reports.[50, 51] Therefore, the theoretical values may be of big significance to reveal the optimal activity of an oxide electrocatalyst.

As well acknowledged, the electronic structures of catalysts have a great influence on HER catalytic activity. In 1972, Trasatti et al first captured the experimental data and proposed a theoretical volcano curve by plotting the HER exchange current densities of different metals versus the metal-hydrogen (M-H) bond energy.[47, 48, 52] According to **Figure 3**b, it was found that Pt, Rh, and Ir most near the peak of the volcano with a M–H bond strength of about 65 kcal mol^{-1} ranked in the best HER electrocatalysts corroborated by experiments.[27] Though Ru was absent in this volcano diagram, with a similar bond strength to the most active HER catalysts (~ 65 kcal mol^{-1}), it was highly expected to deliver excellent HER activities. More significantly, in recent years, the outstanding HER performance for Ru also have been uncovered by plentiful reports.[26-29] In this volcano curve, the ascending branch is quite convincing, while the descending branch is questionable due to the oxide-covered metals that were not known at that time. Actually, the appearance of an oxide film would make the reaction rate sluggish by several orders of magnitude.[52] Later, Nørskov's group first used adsorption free energies by DFT to construct a modern volcano plot and thus provided a more reliable and larger set of energies.[53] Yet, it still includes these oxide-covered metals. Based on this work, Schmickler's group further studied the modern volcano plot by adding a few sp metals and discarding these metals covered by oxide

film, as shown in **Figure 3**c and d.[52] When comparing it to the Trasatti's volcano curve, not only an overall similarity was observed for them, once the oxide-covered metals were deleted from the latter, but also a few significant deviations were found due to new experimental values and difference between hydride formation energies and hydrogen adsorption energies. In all these plots, noble metals like Pt, Ir, Pd, etc. always located the top site, suggesting the optimal activity.

2.3. Key issues of Ru-based materials on stability. Regardless of high activity, Ru-based materials suffered from a severe stability issue, particularly in the OER electrocatalytic process. As a benchmark for oxygen-evolution reaction, RuO_2 is extremely unstable due to dissolution from the excessive oxidation at a high overpotential of above 1.4 V during the OER process.[54] The specific reaction can be observed as follow: $RuO_2 + 2H_2O \rightarrow RuO_4\ (aq) + 4H^+ + 4e^-$ (U^0=1.39 V vs RHE).[55] As for metallic Ru, it is somewhat better than RuO_2 in OER activity, but considering the important cathodic corrosion, it suffered from several orders of magnitude higher dissolution rate than the respective oxides.[56, 57] Paoli et al., by employing SEM images, ICP analysis, and electrochemical detection of RuO_4, demonstrated that 90% of metallic Ru was corroded from catalysts electrode through 15 min of continuous electrolysis at 1.5 V vs RHE while for the corresponding oxide this dissolved amount was 30% in a 15-h measurement.[54] Frydendal et al. revealed the dissolution rate of RuO_2 seems to be relatively constant based on an electrochemical quartz crystal microbalance (EQCM).[58] An analogous result in an Au electrode was also subsequently attained[59] and thus these are possibly associated with the known parallelism between OER and dissolution[60].

Besides, a detailed comparative study on the activity and stability of Ru, RuO_2, Ir, and IrO_2 in both acidic and alkaline media was carried out by Mayrhofer's group.[57] The OER activities follow the trends of $IrO_2 < RuO_2 \approx Ir < Ru$, whereas dissolution decreases as $Ru >> Ir > RuO_2 >> IrO_2$ (**Figure 3**e and f) in both electrolytes. It is noteworthy that the dissolution rate of these pure metals is nearly 2-3 orders of magnitude larger over their corresponding oxides, and the corrosion in the base is more intense than in acid. Apart from OER catalytic behavior, their respective HER performance was also detected, with a metallic electrode having more excellent activity. For durability, the dissolution of RuO_2 and IrO_2 is negligible. For the corresponding metallic counterpart, the dissolution is significantly obvious owing to the reduction of native oxides (**Figure 3**g and h), yet which is still greatly lower than that in the OER process. Therefore, metal Ru is both active and relatively stable for HER rather than OER. To strengthen the OER stability of RuO_2 and Ru, a wide range of approaches were applied, resulting in novel Ru-based materials, as described below.

2.4. Mechanism studies based on single crystals or thin films model electrodes.

The reaction mechanisms and active sites in catalyzing oxidation or reduction of small molecules could be well investigated with the utilization of model electrodes. Notably, to eliminate other distractions, most of the previously mentioned models were established based on single crystals or thin films.[22, 61-63] Density functional theory (DFT)-based atomistic modeling is one of the most studied models, which can depict various chemical reactions in detail by their elementary reaction steps.[64]

The deep insights in the surface atomic-scale structures and catalytic reactivity of rutile RuO_2 mainly come from the DFT study. A single-crystalline RuO_2 (110) electrode has been widely reported as an appropriate model system for studying the catalytic processes, due to the thermodynamically most stable property.[65] It exposes two different Ru sites, as depicted in **Figure 3**i: One is a coordinatively unsaturated site uncapped by oxygen, which is bound to five O atoms, named as Ru_{CUS}, and the other is a bridge site, which is coordinated to six O atoms, denoted as Ru_{BRI}.[22, 62, 66-69] According to DFT study, Ertl and his coworkers confirmed that the Ru_{CUS} site shows a type of dangling bond on the model surface,[62] which helps to bind to O-related species (**Figure 3**j),[63, 66] thus explaining Ru_{CUS} site as the active site to catalyze oxidation/reduction of small molecules.[22, 67] Sun et al. theoretically studied the interactions between water and single-crystalline RuO_2 (110) surfaces. They found one hydroxyl group per unit cell was formed on either the bridge (OH_{BRI}/O_{CUS}) or coordinatively unsaturated (O_{BRI}/OH_{CUS}) Ru site under water vapor-poor conditions, while towards higher pressures of water vapor, either a waterlike species was chemisorbed on coordinatively unsaturated Ru (O_{BRI}/H_2O_{CUS}) or two hydroxyl groups were generated at both R_{CUS} and Ru_{BRI} sites (OH_{BRI}/OH_{CUS}).[68]

Although such information didn't directly refer to the OER process, they provided effective guidance to disclose the configuration of the active sites and the OER mechanism. In the conventional OER mechanism for RuO_2 (110), it involves four steps, concertedly transferring four protons and electrons on the Ru_{CUS} site, along with the generation of $^*OH$, $^*O$, and $^*OOH$ intermediates.[22, 43] The formation of -OOH from -O

is regarded as the rate-limiting step.[22, 43] Later, Rao and co-workers combined DFT calculations and surface X-ray scattering measurements. They further identified the surface structure change on RuO_2(110) as a function of potential via using single crystals, so as to propose a new pathway, where the deprotonation of the *OH group on the Ru_{CUS} or Ru_{BRI} used to stabilize *OO on the Ru_{CUS} sites was found to be rate-limiting.[22] Stephens's group systematically explored OER reaction chemistry at RuO_2 thin film electrodes with three different orientations of (111), (101), and (001), and a single-crystal RuO_2 (110) electrode by using DFT studies and experimental routes.[61] The Ru_{CUS} at the (110) and (101) surface can form five Ru-O bonds to the rest of the structure, generating one surface active site toward OER, while the Ru_{CUS} atom at the (001) and (111) facet is only linked by four Ru-O bonds, offering two empty sites. According to theoretical calculations, the number of Ru_{CUS}-O bonds per square nanometer was increased with the trend of (110) < (111) < (101) < (001), which is consistent with experimentally estimated activity over 2h. In addition to some detailed investigations on OER catalytic process, RuO_2 single crystals or thin films electrodes were also employed as a model system to catalyze other reactions, such as CO oxidation, Cl_2 evolution, NH_3 oxidation, methanol oxidation, etc.[62, 63, 65, 69] Exner et al. have studied a full kinetics of Cl_2 evolution at a RuO_2 (110) model electrode using DFT, which started from the stable reaction surface of RuO_2(110)-(1OHbr1Obr+2Oot), and then computed the kinetics energy barriers.[65] On basis of the energy profiles, they found that Volmer-Heyrovsky mechanism is the most favorable, which involves adsorption and discharge of a chloride anion (Cl^-) on the on-top oxygen site (O_{ot}, capping all Ru_{CUS})

to form O_{ot}-Cl species, named as Volmer step, and subsequently the direct recombination of the O_{ot}-Cl species and Cl^- from electrolytes and Cl_2 release, denoted as Heyrovsky step. Over's group, based on DFT calculation, investigated the reaction mechanism of NH_3 oxidation, as shown in **Figure 3**k, which includes successive dehydrogenation of adsorbed NH_3 by co-adsorbed oxygen and the final recombination of adsorbed N and O to produce adsorbed NO that is released at higher temperatures. Among them, the desorption of NO was considered as a rate-determining step.[69]

Notably, much efforts have been devoted to Ru-based single crystals and thin films, but it is still largely under-represented relative to polycrystalline nanomaterials. Therefore, more efforts are required in this aspect of the development of Ru-based catalysts.

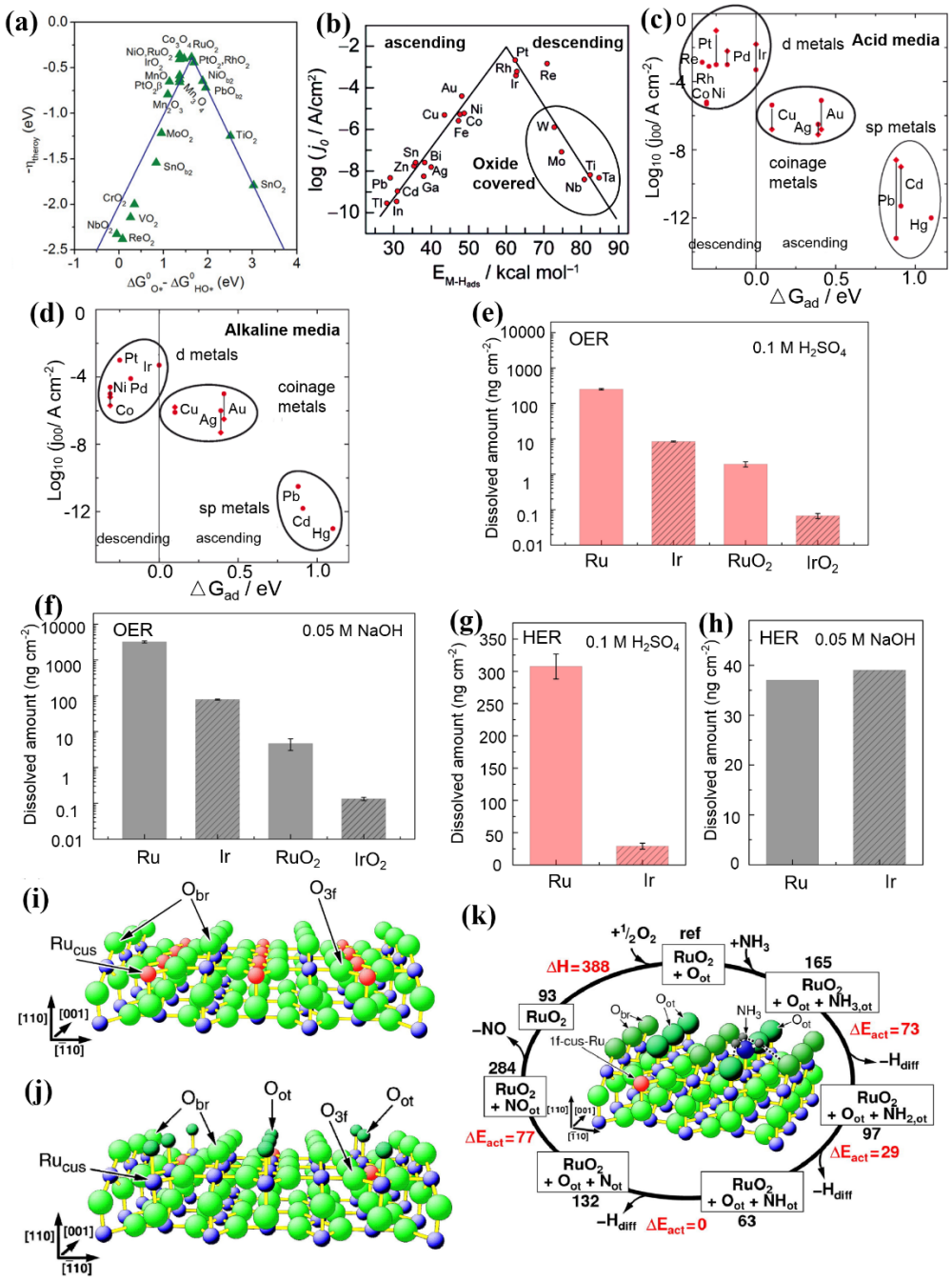

Figure 3. "Volcano"-shaped relationships **a)** between OER activity and binding energy of ΔG_{*O}-ΔG_{*OH} in some metal oxides, or **b)** based on HER activity and M-H bond energy for several metal elements, or **c**, **d)** between HER activity and adsorption energies of several metal elements in acidic media **(c)** and alkaline media **(d)**. a) Reproduced with permission.[43] Copyright 2011, Wiley-VCH. b) Reproduced with permission.[48] Copyright 2010, American Chemical Society. c, d) Reproduced with permission.[52] Copyright 2014, Beilstein. **e**, **f)** Comparison of dissolved metal amount for Ru, Ir, RuO_2 and IrO_2 samples in different electrolytes of 0.1 M H_2SO_4 **(e)** and 0.05 M NaOH **(f)** during the OER process. **g**, **h)** Comparison of dissolved metal amount for Ru and Ir samples in different electrolytes of 0.1 M H_2SO_4 **(g)** and 0.05 M NaOH **(h)** during HER process. Reproduced with permission.[57] Copyright 2016, Elsevier. **i**, **j)** Ball-stick model of the clean RuO_2(110) surface (**i**)

and oxygen-adsorbed RuO_2(110) surface (**j**). Big and small balls indicated the O and Ru atoms, respectively. O_{br} and O_{3f} represent the bridge-bonded and 3-fold (bulk-coordinated) surface oxygen atoms, respectively. O_{ot} refers to on-top adsorbed O atoms. (**k**) Illustration of the microscopic mechanism reaction steps for the NH_3 oxidation over RuO_2 (110) surface. Reproduced with permission.[69] Copyright 2009, Elsevier.

3. RECENT ADVANCES IN RU-BASED ELECTROCATALYSTS TOWARDS WATER SPLITTING

Currently, Ru-related materials including Ru metal, Ru oxides, Ru phosphides, sulfides, or selenides, and other Ru-related compounds have been widely explored as OER/HER electrocatalysts. This section summarizes some recent advances of Ru-related materials and further discusses them with more detailed classifications. In order to make a more comprehensive understanding and comparison among these Ru-based samples as OER/HER catalysts, **Table 1** and **2** list the obtained OER and HER performance evaluation parameters, respectively.

Table 1 Summary of representative Ru-based electrocatalysts toward OER.

Materials	Electrolytes	Loading (mg cm^{-2})	Overpotential (mV) at 10 mA cm^{-2}	Tafel slope (mV dec^{-1})	Stability (V or mA cm^{-2}@h)	Reference
RuO_2 nanosheet	0.5 M H_2SO_4	0.102	260@ 10 mA mg^{-2}	54	Not given	[20]
$Ru_{60}Co_{40}/Ru_{40}Co_{60}$	0.1 M $HClO_4$	0.03 mg_{Ru} cm^{-2}	200 mA/mg_{Ru} at 1.48V	Not given	Not given	[97]
Co-RuIr	0.1 M $HClO_4$	0.051	235	66.9	10 mA cm^{-2} @ 25 h	[101]
$Pt@Ru_{cuboctahedral}$	0.1 M $HClO_4$	0.015	1.31 V vs. NHE @ onset potential	Not given	Initial 10 mA cm^{-2}@ ~2.78 h	[105]
Pd-Ru core-shell (0.5 nm shell)	0.1 M $HClO_4$	0.0127 mg_{Ru} cm^{-2}	230	Not given	Not given	[106]
Pd-Ru branched NPs	0.1 M $HClO_4$	0.408	225	61	1.48 V@ 2h	[107]
Au-Ru branched NPs	0.1 M $HClO_4$	0.408	220	62	Not given	[108]
$Ru@IrO_x$	0.05 M H_2SO_4	0.051	282	69.1	1.55 V@ 24h	[24]
Ru_2Ni_2 SNs	0.1 M KOH	0.1	357	Not given	Not given	[124]
	1 M KOH		~310	Not given	Not given	

S-400-H	1 M KOH	0.285	204	56	1.456 V@ ~5.56h	[125]
RuO_2@C@SiO_2	3 M H_2SO_4	Not given	270-280	Not given	10 mA cm^{-2} @ 100 h	[155]
RuO_2 NR	1 M NaOH	0.357	278	78.3	Not given	[150]
Amorphous RuO_2	0.1 M $HClO_4$	Not given	1.1 V vs Ag/AgCl @onset potential	30	Not given	[158]
crystalline RuO_2	1 M KOH	0.52	230	Not given	10 mA cm^{-2} @ 24 h	[167]
IrO_2-RuO_2@Ru (3:1)	0.5 M H_2SO_4	0.379	281	53.1	1.6 V@ 2h	[193]
Co-doped RuO_2 NWs	0.5 M H_2SO_4	Not given	200	Not given	Not given	[28]
	1 M KOH	Not given	304	Not given	Not given	
Cu-doped RuO_2 (S-300)	0.5 M H_2SO_4	0.275	188	43.96	10 mA cm^{-2} @ 8 h	[210]
$Cr_{0.6}Ru_{0.4}O_2$ (550)	0.5 M H_2SO_4	0.283	178	58	10 mA cm^{-2} @ 10 h	[211]
1D-RuO_2-CN_x	0.5 M H_2SO_4	0.214	250	52	1.57 V@ 50h	[14]
	0.5 M KOH		260	56	1.6 V@ 23h	
	0.1 M PBS		356	160	1.6 V@ 7h	
RuO_2/N-C	1 M KOH	0.306	280	56	1.5 V@ 18h	[233]
$Y_2Ru_2O_7$	0.1 M $HClO_4$	0.051	190 @ onset potential	55	1 mA cm_{oxide}^{-2} @ 8 h	[237]
$Y_2[Ru_{1.6}Y_{0.4}]O_{7-d}$	0.1 M $HClO_4$	0.051	180 @ onset potential	37	Not given	[238]
$Y_{1.85}Zn_{0.15}Ru_2O_{7-\delta}$	0.5 M H_2SO_4	0.204	291	36.9	1 mA cm^{-2} @ 8 h	[239]
$[STO]_1[SRO]_1$	0.1 M KOH	Not given	360@ 2 μA cm^{-2}	Not given	1.87 V@ 24h	[244]
Ruthenate nanosheets	0.1 M $HClO_4$	0.2	255	38	10 mA cm^{-2} @ 6 h	[247]
NiFeRu-LDH	1 M KOH	Not given	225	32.4	10 mA cm^{-2} @ 10 h	[262]
$Ni_{1.25}Ru_{0.75}P$	1 M KOH	0.284	340	Not given	1.57 mA cm^{-2} @ 20 h	[264]

Table 2 Summary of representative Ru-based electrocatalysts toward HER.

Materials	Electrolytes	Loading (mg cm^{-2})	Overpotential (mV) at 10 mA cm^{-2}	Tafel slope (mV dec^{-1})	Stability (V or mA cm^{-2}@h)	Reference
Ru/C_3N_4/C	0.1 M KOH	0.204	79	Not given	-0.05V@50h	[17]
4H/fcc Ru NTs	1 M KOH	0.034	23	29.4	Not given	[26]
hcp-Ru@NC	0.5 M H_2SO_4	0.280	27.5	37	-0.0275V@ ~5.56h	[19]
Ru ND/C	1 M KOH	0.177	43.4	49	-0.05V@2.5h	[75]
Ru nanosheet	0.5 M H_2SO_4	0.102	20 @ 10 mA mg^{-2}	46	Not given	[20]
PtRu@RFCS-6h	0.5 M H_2SO_4	0.354	19.7	27.2	-10 mA cm^{-2}@48h	[13]
RuCo@NC (S-4)	1 M KOH	0.275	28	31	Not given	[90]

NiRu@N-C (S-2)	0.5 M H_2SO_4	0.273	50	36	-10 mA cm^{-2}@10h	[91]
	1 M KOH		32	64	-10 mA cm^{-2}@10h	
Co-substituted Ru	1 M KOH	0.153	13	29	-10 mA cm^{-2}@20h	[94]
Mo@Ru-3	0.5 M H_2SO_4	0.275	30.5	36.4	-0.0305 V@10h	[92]
Pd@Ru NRs	1 M KOH	0.255	30	30	-0.031 V@12h	[103]
	0.5 M H_2SO_4		37	33	Not given	
Ru@Pt	0.5 M H_2SO_4	0.204	Not given	~30	Not given	[104]
Ru-MoO_2 (S-2)	0.5 M H_2SO_4	0.285	55	44	-0.08V@12h	[110]
	1 M KOH		29	31	Not given	
	0.5 M PBS		~100	Not given	Not given	
$Cu_{2-x}S$@Ru NPs	1 M KOH	0.23	82	48	-0.05V@12h	[111]
	0.5 M H_2SO_4		129	51	Not given	
Ni@Ni_2P-Ru	0.5 M H_2SO_4	0.283	51	35	-10 mA cm^{-2}@6.25h	[112]
	1 M KOH		Not given	41	-10 mA cm^{-2} @ ~11.1h	
Ru/MoS_2/CP	1 M KOH	1	13	60	-0.015V@12h	[120]
Ru_2Ni_2 SNs	0.1 M KOH	0.1	39.3	25	Not given	[124]
	1 M KOH		40	23.4	Not given	
S-400-H	1 M KOH	0.285	28	35	-0.036V@~11.1h	[125]
Ru-HPC	1 M KOH	0.2	22.7 @ 25 mA cm^{-2}	33.9	Initial 5 -mA cm^{-2} @10h	[137]
	0.5 M H_2SO_4		61.6	66.8	Not given	
Ru@GnP	1 M KOH	0.25	22	28	Initial -15 mA cm^{-2} @30h	[140]
	0.5 M H_2SO_4	0.75	13	30	Initial -15 mA cm^{-2} @30h	
Ru@NG-4	1 M KOH	0.857	40	76	-0.1V@10h	[139]
	1 M H_2SO_4		60	41	Not given	
Ru@CN-0.16	1 M KOH	Not given	32	53	Initial -12 mA cm^{-2} @45h	[135]
	0.5 M H_2SO_4		~126	Not given	Not given	
	1 M PBS		~100	Not given	Not given	
Ru@C_2N	1 M KOH	0.285	17	38	Not given	[27]
	0.5 M H_2SO_4		13.5	30	Not given	
Ru-NC-700	0.1 M KOH	0.2	47	14	Not given	[144]
	1 M KOH		12	Not given	Not given	
	0.5 M H_2SO_4		29	28	Not given	
hydrous RuO_2	1 M KOH	0.52	60	Not given	-10 mA cm^{-2} @ 24 h	[167]
$Ir_{0.80}Ru_{0.20}O_y$	1 M NaOH	Not given	< 50 mV	31.5	-10 mA cm^{-2} @ ~2.78 h	[200]
Ni-doped RuO_2 NWs	0.5 M H_2SO_4	Not given	78	Not given	Not given	[28]
	1 M KOH	Not given	52	Not given	Not given	

1D-RuO_2-CN_x	0.5 M H_2SO_4	0.214	93	40	-0.15 V@ 70h	[14]
	0.5 M KOH		95	70	-0.1 V@ 10h	
	0.1 M PBS		356	135	-0.4 V@ 10h	
RuO_2/N-C	1 M KOH	0.306	40	44	-0.04 V@ 20h	[233]
Sr_2RuO_4	1 M KOH	0.232	61	51	-10 mA cm^{-2} @ 10 h	[29]
RuP_2@NPC	0.5 M H_2SO_4	1	38	38	-0.038 V@ 11h	[251]
	1 M KOH		52	69	-0.052 V@ 10h	
	1 M PBS		57	87	-0.057 V@ 10h	
RuP (L-RP)	1 M KOH	0.093	18	34	-10 mA cm^{-2} @ 200 h	[30]
	0.5 M H_2SO_4		19	37	-10 mA cm^{-2} @ 200 h	
	1 M PBS		95	54	-10 mA cm^{-2} @ 200 h	
s-RuS_2/S-rGO	1 M KOH	0.464	25	29	-10 mA cm^{-2} @ 100 h	[260]
	0.5 M H_2SO_4		69	64	Not given	
	1 M PBS		93	41	Not given	
NiFeRu-LDH	1 M KOH	Not given	29	31	-10 mA cm^{-2} @ 10 h	[262]

3.1. Ru metal

3.1.1. Phase and morphological control. Crystallized Ru metal is highly active for HER, which typically consists of two crystalline structures, either a hexagonal close packed (hcp) or an unusual face-centered cubic (fcc) structure.[17, 70, 71] Identifying which is a more active phase toward HER not only provides effective guidance to develop and design excellent HER catalysts but also is helpful to unravel the catalytic mechanism. Zheng et al presented an interesting finding of anomalous fcc Ru lattice structure (**Figure 4**a) as a super HER electrocatalyst.[17] In the preparation route, a certain amount of dicyandiamide solid powder was uniformly dispersed in $RuCl_3$ aqueous solution. After being dried by employing a rotary evaporator and a freeze-dryer, the collected solid was further annealed at 600 °C for 1 h under argon atmosphere to obtain the resultant Ru-graphitic carbon nitride complex supported on carbon ($Ru/C_3N_4/C$). Of note, due to the existence of Ru catalyst, most of the dicyandiamide precursor did not follow the rational reaction path of polycondensation to achieve the periodic g-C_3N_4

matrix but was converted to nitrogen-doped carbon. More importantly, with the aid of g-C_3N_4 as support, the growth of the anomalous fcc Ru lattice structure was induced. The as-synthesized Ru sample with unusual fcc structure displayed the superior HER activity than that of Ru/C control sample with only a sole hcp phase in both alkaline and acidic electrolytes (**Figure 4**b). Moreover, it performed 2.5-folds higher HER rates than that of Pt in the alkaline aqueous solution (**Figure 4**c). Further combined density functional theory (DFT) calculations revealed that the enhanced activity of Ru/C_3N_4/C could be ascribed to its suitable adsorption energies to some pivotal reaction intermediates and reaction kinetics during the HER process **(Figure 4**d-f). Later, Zhang's group employed the Au nanowires (NWs) as sacrificial templates which were then etched by copper ions (Cu^{2+}) in dimethylformamide (DMF) solution to produce hierarchical 4H/fcc Ru nanotubes (NTs) as high-performance HER electrocatalysts.[26] Although *fcc* Ru manifested more outstanding HER activity than *hcp* Ru, Ru metal with hcp crystalline structure generally tended to be formed via the facile synthetic procedure. According to the Kitagawa and co-workers' report, the formation of multiply twinned Ru particles is mainly based on the "nanosized" effect, which improves the difficulties of sample preparation.[72] Consequently, most of metallic Ru catalysts still exhibited hcp crystalline structure.[19, 73, 74] For instance, Li and co-workers developed hcp-Ru nanocrystal coated with the N-doped carbon thin layer (hcp-Ru@NC) via a simple thermal annealing route with $RuCl_3$, dopamine (DA) and cetyltrimethylammonium bromide (CTAB) as raw materials.[19] Briefly, polydopamine (PDA) was first formed by quick self-polymerization of DA in a phosphate buffer

solution, which was then dispersed with the aid of CTAB in the ambient environment. Due to the strong complexation reaction between metal ions and the -NH_2 group, PDA could largely absorb the added Ru^{3+} ions, followed by the reduction to Ru metal at 80 °C. Lastly, by adjusting the annealing temperature ranged from 400 °C to 800 °C, the Ru metal with different crystallinity was obtained. Interestingly, it was the first time to find that the HER performance of hcp-Ru has a large dependence on its crystallinity and this sample with fully crystallized hcp-Ru displayed the most prominent HER performance in 0.5 M H_2SO_4. In addition, Ru nanodendrites with the mixed fcc/hcp structure were also fabricated as a super HER electrocatalyst in alkaline condition.[75] Relative to crystallized form, amorphous phase is expected to exhibit better catalytic behavior. In Tee et al's previous study, ultrathin amorphous Ru film loaded on fluorine-doped tin oxide (FTO) glass was prepared by a spin coating technology and subsequently underwent thermal treatment in various temperatures to optimize the obtained products. [76] Further electrocatalytic results revealed that the amorphous Ru after 250-°C calcining treatment with short-range ordered structure showed an optimal and stable catalytic activity.

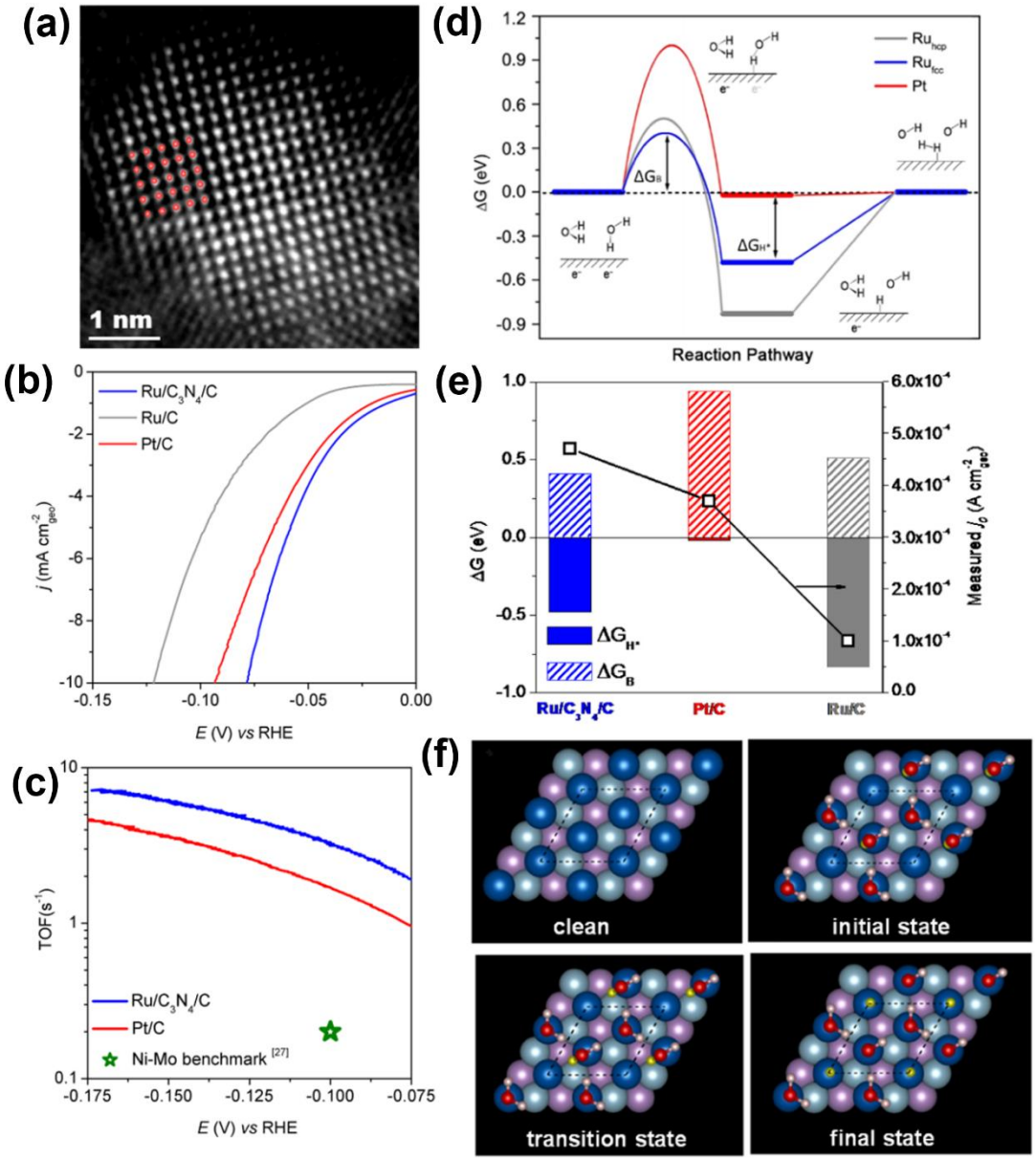

Figure 4. a) HAADF-STEM images of Ru with fcc structure. **b)** Polarization curves of the $Ru/C_3N_4/C$, conventional Ru/C, and benchmark Pt/C samples toward HER in 0.1 M KOH. **c)** TOF values as a function of operation potential over the designed $Ru/C_3N_4/C$ and commercial Pt/C. **d)** Computed HER free-energy diagram in alkaline electrolytes on three model surfaces of Ru_{fcc}, Ru_{hcp}, and Pt. **e)** The hydrogen-adsorption free energy value and water-dissociation free energy barrier of the three models obtained from **d**, as well as the measured exchange current density values (j_0). **f)** Atomic configurations model for water-dissociation step on Ru_{fcc} surface. Color: pink, the bottom layer of Ru; light blue, the middle layer of Ru; deep blue, the top layers of Ru; white and red, H and O atoms in a single H_2O molecule, respectively; yellow, the dissociated H atom. Reproduced with permission.[17] Copyright 2016, American Chemical Society.

In addition to crystal structure regulation, maximizing the surface area and engineering the number of surface active sites also play a crucial role in the

enhancement of activity for an electrocatalyst.[34] Many researchers made lots of efforts to fabricate porous frameworks or nanostructures of Ru metal via multiple synthesis routes. For example, Huang's group and Zhang's group have produced porous Ru nanodendrites and Ru nanotubes using Cu metal and Au nanowires as sacrificial seeds, respectively, and remarkable electrocatalytic activity for hydrogen generation was reported.[26, 75] Kong and coworkers demonstrated a facile solvothermal process for synthesizing two-dimensional (2D) ultrathin Ru nanosheets as HER catalysts (**Figure 5**a-b), and further oxidation allows for the production of its 2D oxide derivative for accelerating OER.[20] Such a solvothermal process underwent at 180 °C for 18 h with Ru acetylacetonate and urea being dissolved in a mixture solution of isopropanol and deionized water. It is noticeable, however, that RuO_2 nanoparticles were achieved when replacing Ru acetylacetonate with $RuCl_3$ as metal sources. It is likely that Ru metal was produced by self-decomposition of Ru acetylacetonate, where Ru^{3+} received electrons from the acetylacetonate ligands or their derivatives, so as to be reduced. Relative to its powder counterpart, Ru nanosheets showed the significantly enhanced acidic HER activity with reduced overpotentials at 10 mA cm^{-2} by ~10 mV and decreased Tafel slopes, and its area-specific current density was also increased by 1.62-fold at -0.10 V vs RHE (**Figure** 5c-d). On the basis of DFT results, this might be attributed to the smaller absolute value of the Gibbs free energy change for hydrogen(/ΔG_{H*}/) in 2D Ru structure (**Figure 5**e). Lastly, a home-made water electrolyzer was built up with Ru nanosheets and its oxide derivative as cathode and anode, respectively. To reach a current density of 10 mA cm^{-2}, a potential of about 1.53V was required in 0.5 M H_2SO_4

(**Figure 5**f).

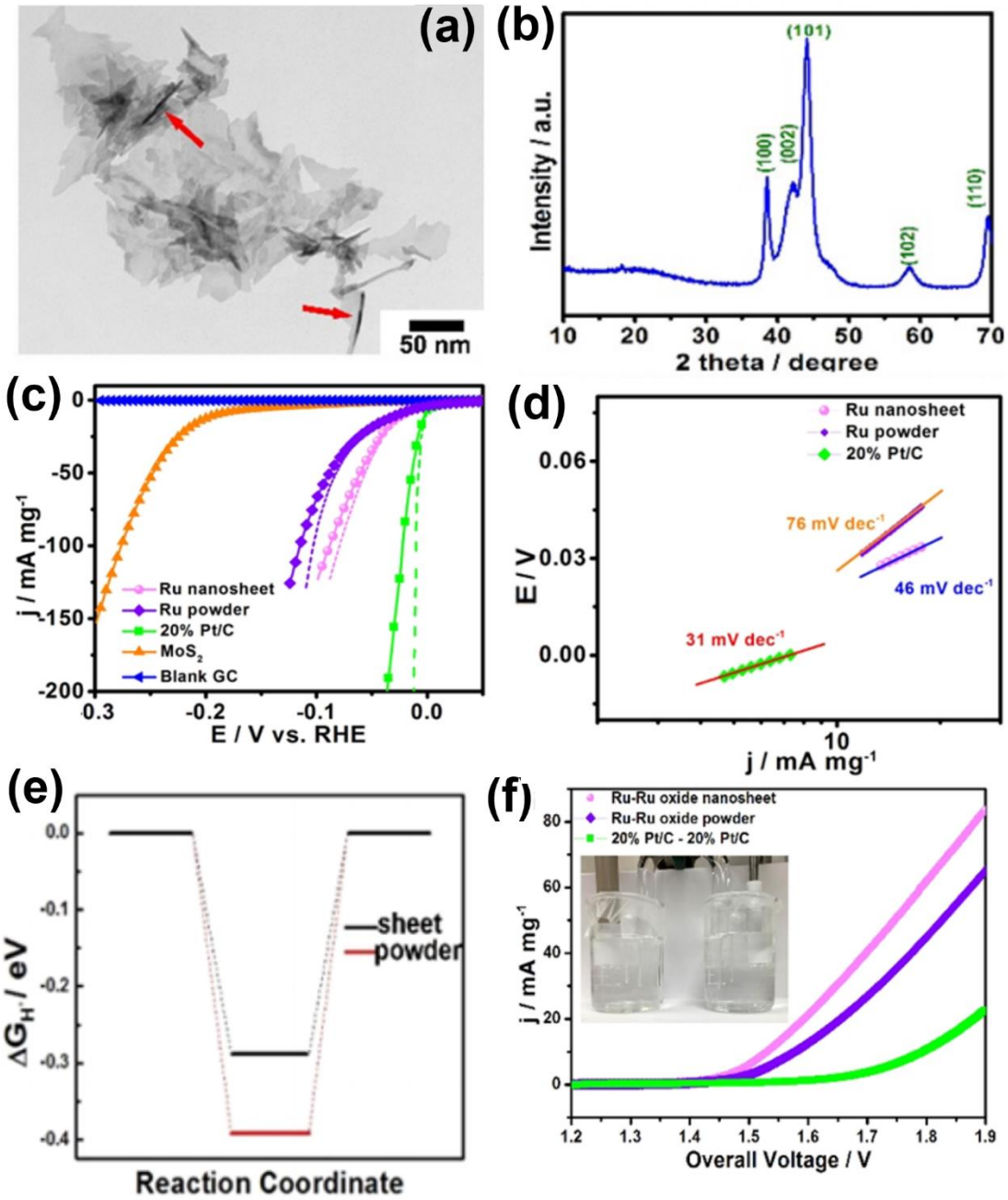

Figure 5. a) TEM image and **b)** XRD pattern of as-made 2D ultrathin Ru nanosheets. **c)** HER polarization curves and **d)** the corresponding Tafel plots of Ru nanosheet, Ru powder and Pt/C. **e)** Calculated Gibbs free energy for hydrogen adsorption on Ru nanosheet and powder surfaces. **f)** Overall water-splitting activity for Ru-Ru oxide nanosheet, Ru-Ru oxide powder, and Pt/C-Pt/C. Reproduced with permission.[20] Copyright 2016, American Chemical Society.

Additionally, deliberately developing 3D binder-free electrodes with controlled Ru loading can also endow them with adequately exposed active sites, thus leading to super

electrocatalytic performance. These Ru-based 3D electrodes can be realized by using impregnation method or deposition approach to integrate Ru nanoparticles or form Ru film on the different conductive substrate, such as Ni foam, FTO, carbon fiber, Si nanowires and Ti_2AlC, etc.[76-81] The anti-corrosion ability of supports is of pivotal importance for utilization of 3D electrodes. Jovic et al summarized the corrosion behavior of some MAX phases according to previous studies and firstly selected Ti_2AlC as substrates to electrodeposit Ru layers (Ru/Ti2AlC).[81] Expectedly, the Ru/Ti2AlC electrode is highly active for HER.

Since Ru metal is extremely unstable in electrocatalytic OER process,[82, 83] very little effort was devoted to designing various pure monometallic Ru as high-performance OER electrocatalysts. Nevertheless, many researchers focused more on its stability issues, which have been concretely discussed in the above section. Very recently, the novel branched Ru nanoparticles with exposed low-index facets were developed and featured obvious prolonged stability and higher activity for OER in acidic media when compared to the polycrystalline counterpart. Such results were attributed to that the low-index facets with lower energy surfaces mitigate the Ru dissolution.[84]

3.1.2. Alloys engineering. It has been shown that alloying hetero metal elements is an effective route to modify the surface chemical properties of the host metal derived from the formation of heteroatom bonds and the alteration of the lattice parameters and charge distributions.[13, 85, 86] Accordingly, it could contribute to the remarkably boosted electrocatalytic performance (activity or stability). For Ru-other noble metal alloy, Ru-

Ir, Ru-Pd, Ru-Au, and Ru-Pt alloys have been successfully fabricated as HER catalysts.[13, 87-89] By picking Ru-Pt alloy as an example, Xing's group explored the effects of Pt doping in Ru binary alloy by the successful synthesis of Ru nanoparticles alloyed with a trace amount of Pt and partially embedded in porous carbon spheres (PtRu@RFCS) based on a polycondensation reaction between resorcinol-formaldehyde (RF) and resin in the presence of metal ions, as depicted in **Figure 6**a.[13] During the production process, as the polymerization between RF and resin occurred, metal precursor were added into the gel solution, which triggered the further condensation reaction due to the strong interaction between metal precursor and functional groups (e.g.,$^{-}CH_2^{+}$) on the resin surface. Noteworthily, it was observed that the addition times of metal ions significantly regulated the embedded depth of the resulting metal nanoparticles (**Figure 6**b). The HRTEM images revealed that some isolated Pt nanoclusters were obtained on the surfaces of the PtRu alloy nanoparticles for this PtRu@RFCS-6h sample, in contrast to the pure PtRu alloy phase in PtRu/RFCS (**Figure 6**c-d). The PtRu@RFCS-6h hybrid gave better HER catalytic performance than Ru@RFCS-6h and PtRu/RFCS, and even partially outperformed Pt/C, with a low overpotentials of 19.7 mV at a current density of 10 mA cm^{-2}, small Tafel slope of 27.2 mV dec^{-1}, high exchange current density of 1.57 mA cm^{-2}, and a turnover frequency of 4.03 H_2 s^{-1}(**Figure 6**e-g) in 0.5 M H_2SO_4. Through integrating the analysis from the view of HER thermodynamics and kinetics with reported DFT calculations on different metal surfaces, the improved HER electrocatalytic performance after Pt doping might come from this weakened binding

strength between metal and hydrogen atoms (M-H) and promoted rapid hydrated proton dissociation (**Figure 6**h).

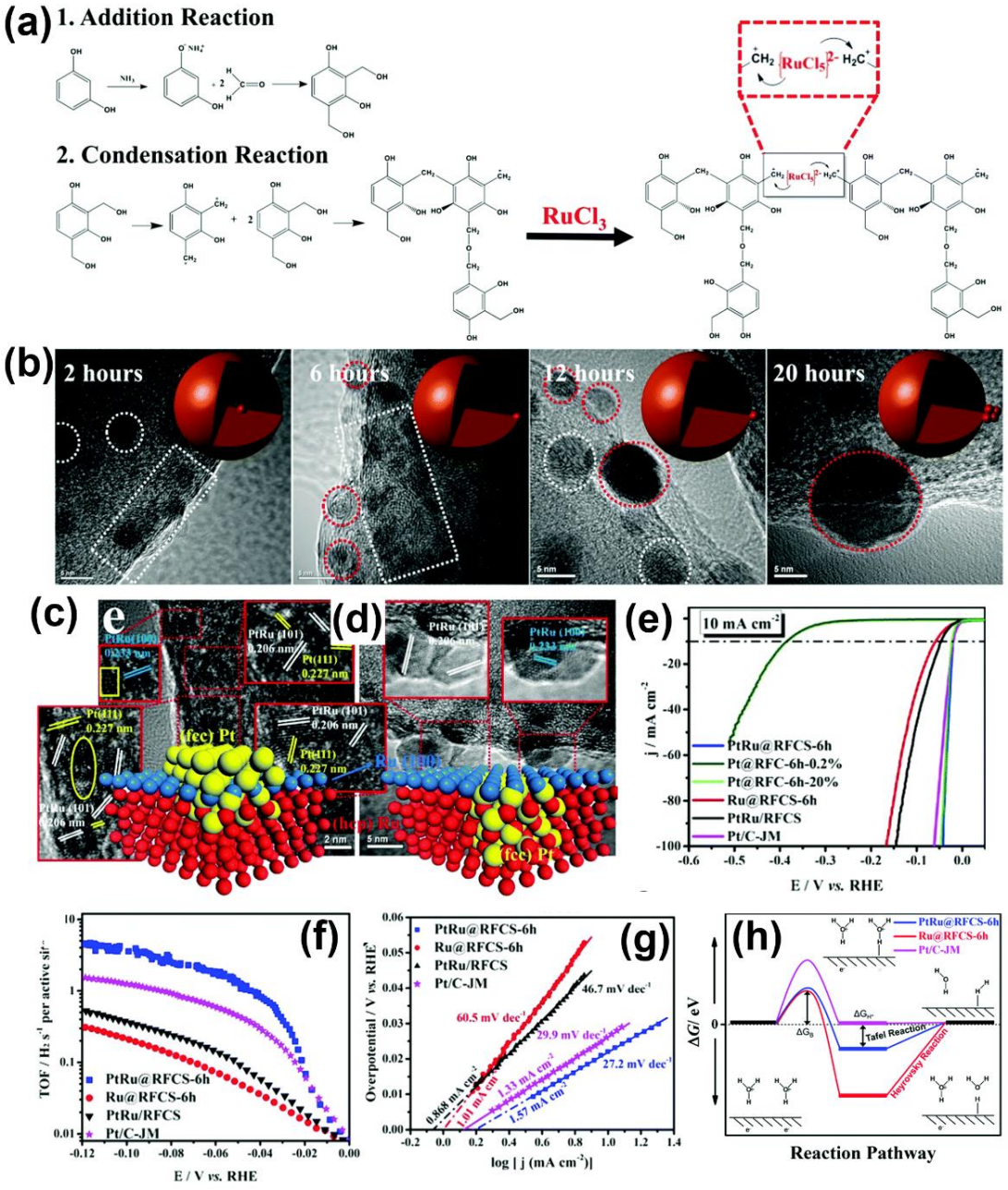

Figure 6. a) Schematic synthesis of Ru@RFCS. **b)** HRTEM images of a series of Ru@RFCS samples with different addition time of metal ions. **c**, **d)** HRTEM images and corresponding atomic configuration structure for as-obtained PtRu@RFCS-6h **(c)** and PtRu/RFCS **(d)**. **e)** HER polarization curves, **f)** TOF values, and **g)** Tafel plots of PtRu@RFCS-6h hybrid, Ru@RFCS-6h, PtRu/RFCS, and commercial Pt/C electrocatalysts under acidic conditions. **h)** Free energy diagram of HER in alkaline electrolytes for Ru@RFCS-6h hybrid, Ru@RFCS-6h, and commercial Pt/C. Reproduced with permission.[13] Copyright 2018, Royal Society of Chemistry.

Besides, of note, forming alloys from noble metals and non-precious metals such as transition metals (TM, eg. Co, Ni, Fe, Mo, W, etc) not only guarantee the high activity but also bring about the balance of good cost-competitiveness, which have been widely investigated.[90-92] As a much cheaper alternative to Ru, Co metal is largely inferior to Ru for hydrogen production. According to electronic structure and lattice constant of metal, Co and Ru can form d orbit overlap when alloying. Meanwhile, the Ru atoms could enter Co lattice, in contrast, Co atoms may also incorporate into Ru lattice, so that to tune the M-H bond strength and provide much more active sites toward HER.[93] Recently, an effort has been put forward to enhance the HER activity of Co metal by alloying with a small number of Ru atoms, and the Co-Ru nanoalloys were encased in nitrogen-doped graphene shells (RuCo@NC) (**Figure 7**b).[90] The catalysts were prepared by adopting a metal-organic frameworks (MOFs)-assisted strategy, where $Co_3[Co(CN)_6]_2$ MOF was first formed by self-assembly of organic ligands (CN^- groups) and metal ions or clusters through coordination bonds, and then after introducing a certain amount of Ru^{3+} ions into this MOF via an ion-exchange reaction, the collected solid powders underwent thermal decomposition under nitrogen atmosphere at 600 °C for 4 h, as shown in **Figure 7**a. The optimal RuCo@NC sample with controlled Ru-doping amount (which was named as S-4) exhibited a most obvious increase in HER performance relative to the undoped counterparts(S-0) and even better than the commercial Pt/C catalysts in basic solutions (**Figure 7**c-d). The DFT results suggested that more electrons could be transferred from RuCo alloy core to graphene layer compared with pure Co metal core, so as to obtain the enhanced C-H bond and

thus significantly lower ΔG_{H^*}, eventually boosting HER performance (**Figure 7**e-g). Soon afterward, a similar study reported that NiRu nanoalloy encapsulated in nitrogen-doped carbon (NiRu@N-C) was employed as efficient HER electrocatalysts in the pH-universal electrolytes.[91] It is worth mentioning that in a very recent work, cobalt-substituted ruthenium nanosheets displayed an unprecedented high electrocatalytic activity for basic HER with ultralow overpotential at the current density of 10 mA cm^{-2} (13 mV) and Tafel slope value (29 mV dec^{-1}) as well as robust stability (**Figure 8**a-d).[94] Further structural identification was carried out by aberration-corrected high-angle annular dark-field scanning transmission electron microscopy (HAADF-STEM) and X-ray absorption fine structure (XAFS) measurements, which showed the atomically isolated Co in Ru lattice. Through theoretical calculations in **Figure 8**e-h, the prominently decreased energy barrier of water dissociation after single Co atom substitution account for the top-level HER catalytic activity. Based on Brewer-Engel valence-bond theory, it is well-known that unpaired d-band electrons help to form chemisorptive bonds with H atoms, thus leading to improved HER catalytic activity.[95] Ru, as the right-half of TMs elements, possessed unpaired d electrons, meanwhile, Mo belongs to the left-half in the TM elements region with a half-filled d orbital ($4d^5s^1$), thus alloying Ru with Mo can create more d electrons. Zhang et al developed the Mo-doped hcp Ru alloy catalyst and observed that such structural tailor could greatly improve the HER performance of Ru metal and bring the extraordinary HER catalytic activity.[92] Apart from the binary alloy materials, much attention is also attracted to the ternary alloys because the introduction of a third metal element creates more changes

to tailor the electronic structure of host metal. Accordingly, some trimetallic alloys of Pt-Ru-Cr, Pt-Ru-Fe, Pt-Ru-Co, and Ru-Mo-Co, etc, have been successfully developed.[93, 95, 96]

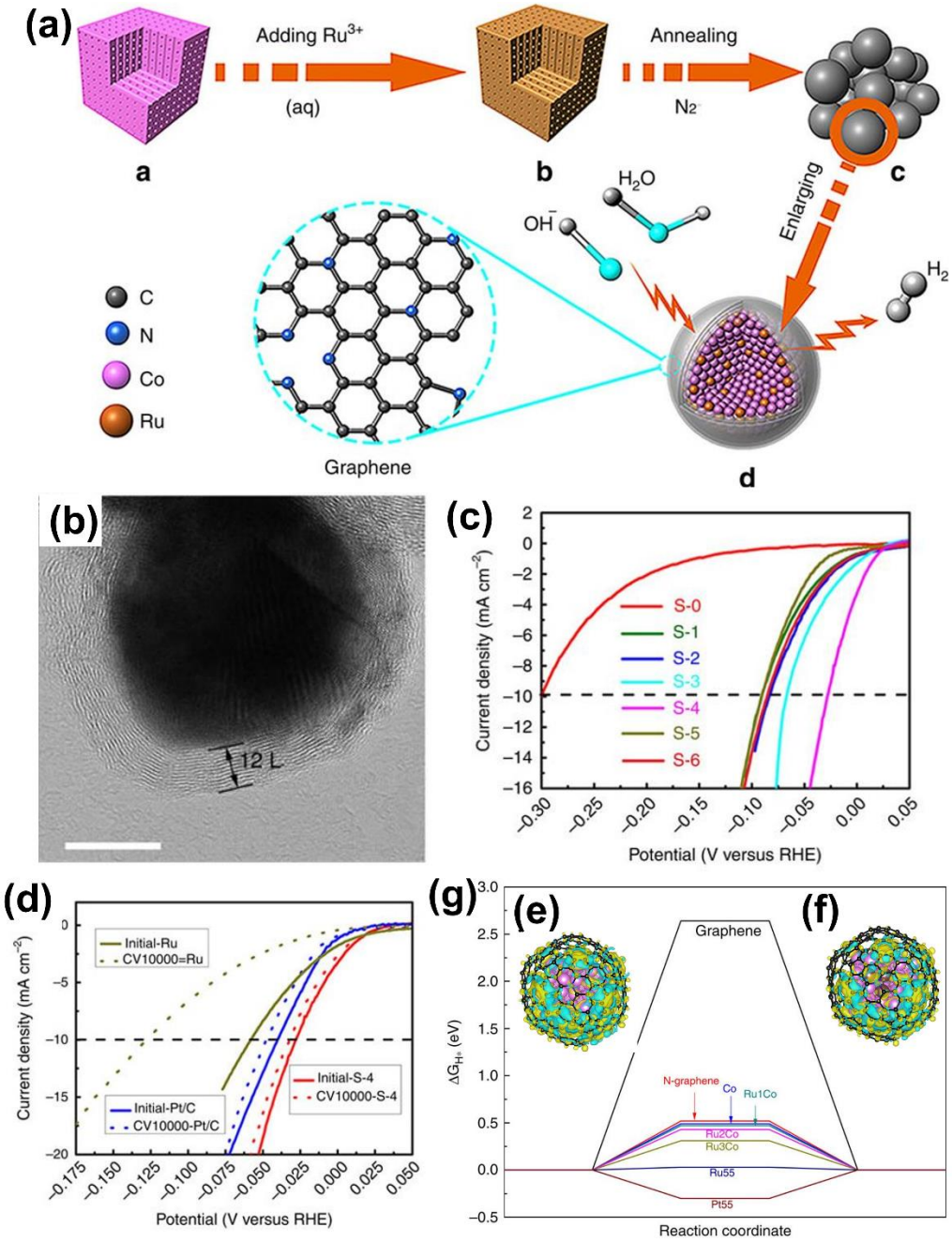

Figure 7. a) The preparation process of RuCo@NC. **b)** The TEM image of RuCo@NC. **c**, **d)** LSV curves of RuCo@NC hybrids with different Ru-doping amount **(c)**, S-4, pure Ru and Pt/C **(d)** toward HER in alkaline solutions. **e**, **f)** Charge density distribution for Co **(e)** and Co_3Ru models **(f)** from DFT calculation, where the decreased and increased charge density can be suggested by cyan and yellow areas, respectively. **g)** Calculated Gibbs free energy for hydrogen adsorption on different models. Reproduced with permission.[90] Copyright 2017, Nature Publishing Group.

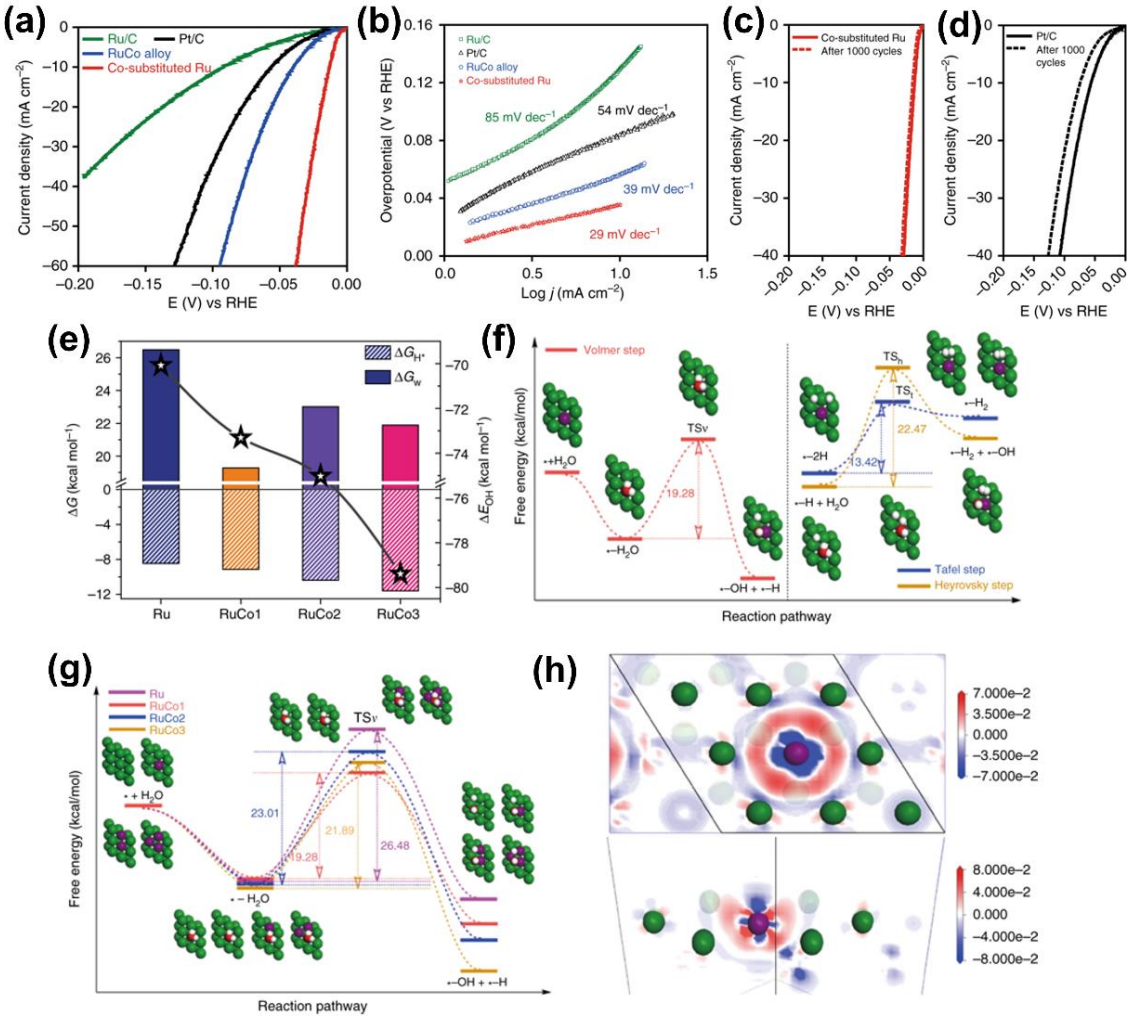

Figure 8. a) HER polarization curves, and **b)** the corresponding Tafel plots of different samples in 1 M KOH. **c**, **d)** Stability tests for Co-substituted Ru **(c)** and Pt/C **(d)** based on 1000 cycles. **e)** Gibbs free energy for hydrogen adsorption (ΔG_{H^*}), the energy barrier of water dissociation (ΔG_w) and OH binding energy (ΔE_{OH}) for various Co-substituted Ru samples. **f)** Free-energy diagrams for three different HER reaction steps including Volmer, Tafel, and Heyrovsky on $RuCo_1$ model. **g)** HER free-energy diagrams for Volmer reaction step on various Co-substituted Ru sample surfaces. **h)** Top-view and side-view images of electron configuration change after the substitution of a single Co atom. These green, purple, red and white balls represent Ru, Co, O, and H atoms, respectively. Reproduced with permission.[94] Copyright 2018, Nature Publishing Group.

Except for exploring Ru-M alloy materials as HER electrocatalysts, it has been confirmed that some introduced TMs in Ru binary or ternary alloy can significantly enhance the OER electrocatalytic activities and stability of these Ru-involving materials.[83, 97-101] Strasser's group synthesized various binary Ru-M (M = Co, Ni, Cu, Cr, Re, Pd, Ir) alloy samples by varying their compositions and displayed their OER

electrocatalytic behavior in acidic media.[97] On the basis of Ru mass loading, $Ru_{60}Co_{40}$ and $Ru_{40}Co_{60}$ catalysts exhibited the highest mass activity of about 200 mA/mg_{Ru} at a potential of 1.48 V vs RHE, whereas only 100 mA/mg $_{Ru}$ was observed for the pure Ru catalyst. A while ago, Shan et al. found that Co-doped RuIr alloy delivered significantly ameliorated OER activity and stability under acidic conditions due to appropriate oxygen-intermediates binding behavior together with a lowered metal dissolution relative RuIr alloy.[101] Additionally, in the work, the prominent HER catalytic properties for Co-doped RuIr alloy were also observed. Thus, an electrolyzer voltage of just 1.52 V in 0.1 M $HClO_4$ was required to yield a 10 mA cm^{-2} current density for overall water splitting to attain oxygen and hydrogen.

3.1.3. Core-shell hybrids construction. In a Ru-M bimetallic system, the core-shell structure was also developed to boost catalytic activity and stability of the monometallic counterpart for both OER and HER.[102-106] Luo et al. fabricated mesoporous Pd@Ru nanorods with well-defined core-shell nanostructure (mesoporous Pd@Ru NRs) as HER electrocatalyst in alkaline condition.[103] The overpotential of Pd@Ru NRs at 10 mA cm^{-2} was much smaller than that of pure Ru and Pd as well as solid Pd@Ru NRs. Benefiting from the Ru/Pd (111) like interface structures in mesoporous Pd@Ru NRs, a lower Gibbs free energy barrier for water dissociation was obtained so that they showed improved HER activity. Wang et al. reported that Ru@Pt core-shell nanoparticles showed higher HER activity than that of the conventional strain-free RuPt alloy.[104] The obvious HER enhancement in Ru@Pt core-shell nanoparticles could be attributed to a highly compressive strained Pt surface as a result of regulating fcc Ru-

induced interfacial lattice mismatch. For OER process, due to the extreme instability of Ru metal as mentioned above, much attention was paid to enhance the stability in M-Ru core-shell structure relative to pure Ru metal.[105, 106] As demonstrated by AlYami et al., Pt@Ru core-shell nanocrystal with an atomic layer Ru cuboctahedral shell exhibited slightly improved OER activity but dramatically enhanced stability in comparison to pure Ru.[105] They referred that the greatly stable low index facets of the cuboctahedral shell may increase the structural integrity and largely inhibit rearrangement or segregation of Ru from Pt core during easy oxidation/reduction process, so as to enhance the stability. Tilley's group found that Ru metal shell could be stabilized by Pd core to strengthen the OER stability while retaining the high activity similar to pure Ru.[106] Such enhancement of OER stability could be originated from more metallic Ru in Pd-Ru core-shell nanoparticles when compared with Ru nanoparticles. Furthermore, the same group also fabricated Pd-Ru or Au-Ru nanoparticles with core-branch structure and this class of catalysts presents more potential in improved OER stability and activity owing to exposed low index Ru facets.[107, 108]

3.1.4. Building advanced heterostructures. Generally, the rational engineering of Ru metal and other components (e.g. metal, oxides, sulfides, phosphides, etc, named as Ru/A) into heterostructured composites is highly useful in boosting their electrocatalytic performance (activity or stability) due to the synergy between different components.[24, 109-129] For example, Ru-MoO_2 nanocomposites were well constructed by in-situ carbonizing the Ru modified Mo-based MOF at 700 °C for 3 h to offer remarkable HER catalytic performance under pH-universal conditions.[110] The

synergism, induced by the strong electronic interactions between MoO_2 and Ru nanoparticles, endows higher electrical conductivity, optimal water adsorption energy, and faster charge transfer ability of the nanocomposite, and then an enhanced HER activity was achieved. Yoon and his coworkers fabricated the cactus-like hollow $Cu_{2-x}S$@Ru nanoplates (NPs) with heterojunctions, which showed widths of about 116 nm and hollow interiors (**Figure 9**b and c).[111] Shown in **Figure 9**a is the synthetic route, where Ru^{3+} ions initially undergo cation exchange with Cu^{+} ions from the $Cu_{1.94}S$ NPs, and then are thermally reduced. Further heteroepitaxial growth of Ru atoms leads to cactus-like nanostructures, that accompanied with the dissolution of the $Cu_{1.94}S$ NPs, thus forming the hollow nanostructure. The as-obtained hollow $Cu_{2-x}S$@Ru NPs deliver excellent catalytic activities with an overpotential as low as 82 mV at 10 mA cm^{-2} and a small Tafel slope of 48 mV dec^{-1} in 1 M KOH electrolyte (**Figure 9**d and e) because of moderate water dissociation kinetics triggered by the high interface density between the metal and metal sulfide, and more exposed active sites in hollow structure. Besides, Liu et al. unveil the Ru modulation effects in a multi-heterogeneous system made up of Ni metal, nickel phosphides (Ni_2P), and Ru metal (Ni@Ni_2P-Ru).[112] Benefiting from the Ru incorporation that accelerates the sorption behavior of H to obtain the optimal adsorption free energy of hydrogen (ΔG_H) and regulates phosphatization degree of Ni via a Ru-Ni coordination effect to produce Ni@Ni_2P-Ru heterostructures with improved conductivity, the Ni@Ni_2P-Ru hybrids achieved improved HER performance with a low overpotential, small Tafel slope, and large exchange current density, as well as excellent stability in both 0.5 M H_2SO_4 and 1 M KOH solutions. Very recently,

Qiao's group reported the synthesis of a hetero-structured Ru@IrO_x material with highly strained ruthenium as core and a partially oxidized iridium as the shell (**Figure 9**f and g). The Ru@IrOx nanomaterials were fabricated by employing a sequential polyol route, where ruthenium (III) acetylacetonate was first reduced to Ru colloids in an ethylene glycol (EG) solution with poly-(vinylpyrrolidone) (PVP) as a stabilizer under refluxing conditions (198 °C, 3 h). Subsequently, iridium (III) chloride hydrate was added into colloidal Ru suspension, and the system was heated rapidly to 130 °C and then slowly to 198 °C under refluxing conditions, eventually achieving the coating of IrO_x shells on Ru cores. It was found that such structure well modified the electronic structure of both core and shell, specifically, increased valence of the iridium shell and decreased valence of the ruthenium core (**Figure 9**h and i), which eventually created a positive synergy and thus led to the enhanced OER activity and stability in 0.5 M H_2SO_4 when compared to $RuIrO_x$.[24] Notably, Ru dissolution is always the critical issue of stability of Ru-based materials. In this work, the current density at 1.55 V vs RHE for Ru@IrO_x sample declined slowly to about 90% of initial value after a 24-h long-term testing with extremely low Ru dissolution and relatively low Ir dissolved concentration of about 2.0 ppb, while $RuIrO_x$ only retained nearly 20% of its initial performance within a 1-h measurement, together with Ru and Ir dissolved amounts of nearly 30 and 4 times, respectively, larger than that obtained in the case of Ru@IrO_x (**Figure 9**j-l). Furthermore, a stable hybrid of isolated single ruthenium atoms firmly immobilized on the surface of cobalt-iron layered double hydroxides (Ru/CoFe-LDHs) were constructed to boost the OER activity and stability in alkaline electrolytes when

compared to pure CoFe-LDHs and commercial RuO_2.[126] Benefiting from synergetic electron coupling by creating Ru-O-Fe/Co bonds, oxidation states of single-atomic Ru maintained below +4 even at a high potential, thus enabling Ru/CoFe-LDHs to have exceptional oxygen-evoluting ability including very low overpotential of 198 mV at 10 mA cm^{-2} and super stability at the large current density of nearly 200 mA cm^{-2} over 24 h, simultaneously.

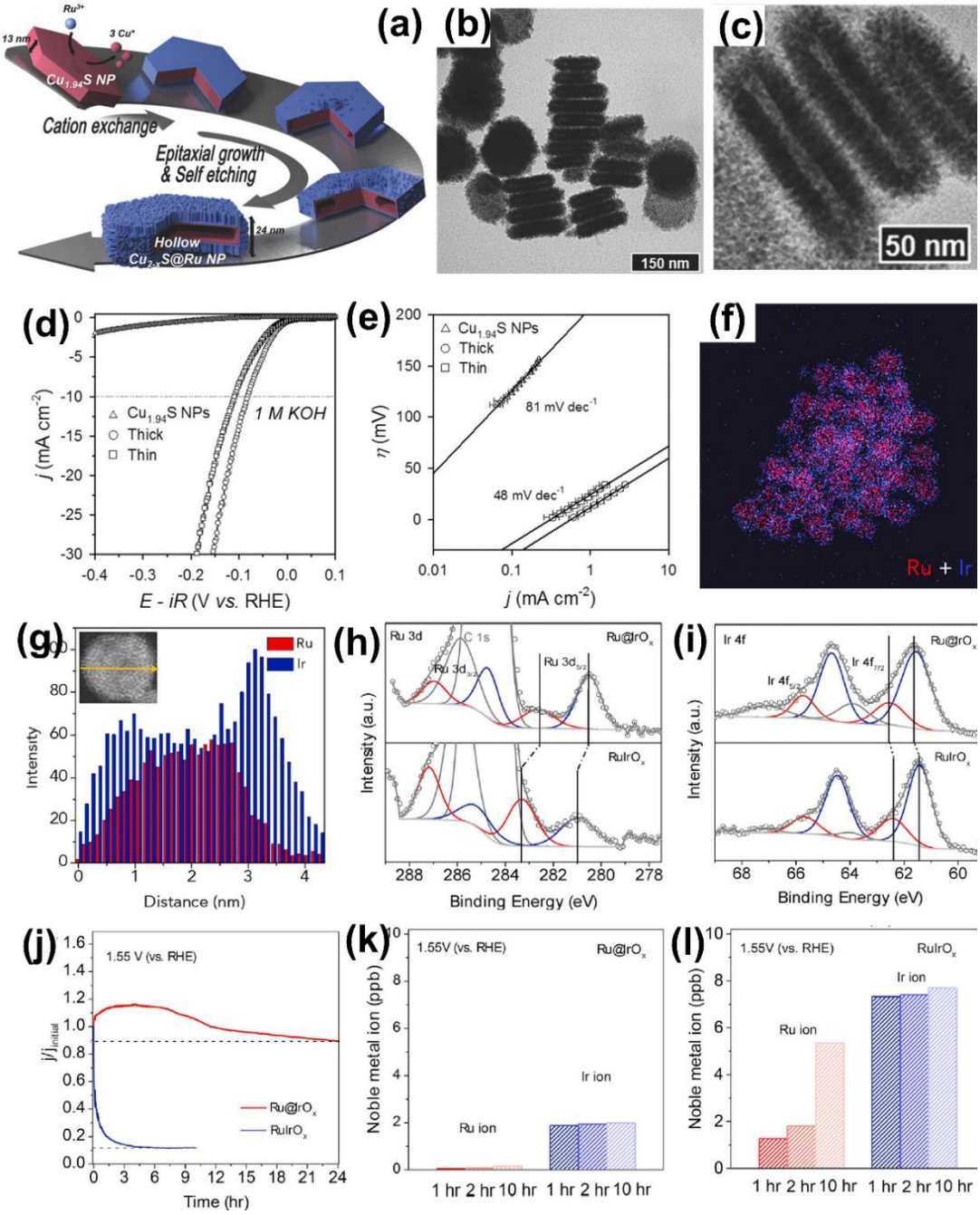

Figure 9. a) Schematic illustration of preparing $Cu_{2-x}S$@Ru nanoplates. **b, c)** Representative TEM images of $Cu_{2-x}S$@Ru nanoplates. **d)** LSV and **e)** Tafel results of OER in 1 M KOH over thick and thin hollow $Cu_{2-x}S$@Ru NPs and $Cu_{1.94}S$ NP. Reproduced with permission.[111] Copyright 2017, Wiley-VCH. **f)** Overlapped EDX elemental mapping of Ru and Ir, and **g)** EDX line profile for Ru@IrO_x nanocrystals. Comparison of **h)** Ru 3d and **i)** Ir 4f XPS spectra of Ru@IrO_x and $RuIrO_x$ samples. **j)** The chronoamperometry curves of Ru@IrO_x and $RuIrO_x$ catalysts fixed at a constant potential of 1.55 V. **k**, **l)** Ru and Ir ions dissolved concentration for Ru@IrO_x **(k)** and $RuIrO_x$ **(l)** catalysts after various reaction times. Reproduced with permission.[24] Copyright 2019, Elsevier.

In alkaline electrolytes, the HER process consists of the dissociation of water and

the subsequent associative desorption of hydrogen.[116] However, most HER catalysts only perform well for the latter, and the overall alkaline HER was significantly restricted by the difficult cleavage of H-OH bonds.[116] Several pioneering works proposed the novel concepts that a synergistic interplay between water dissociation and hydrogen sorption for superior alkaline HER activity could be generated by employing multi-phase composites with heterostructure as catalysts.[116-118] As the most typical case, Subbaraman and his co-workers illustrated that the alkaline HER catalytic activity of Pt can be largely boosted by modifying with $Ni(OH)_2$, which played the crucial role as an OH^- adsorption promoter so that to expedite water dissociation.[118] The similar phenomenon has also been observed in Ru/A (oxides, sulfides, phosphides, etc) heterostructure systems.[119-122, 127] Liu et al. developed Ru/$Y(OH)_3$ nanohybrid as outstanding HER catalysts in alkaline media, in which $Y(OH)_3$ supports accelerated water dissociation.[119] Qiao's group directly grew defect-rich MoS_2 nanosheets on carbon paper via a facile 180-°C hydrothermal method and then decorated MoS_2 nanosheets with Ru nanoparticles by an impregnation-calcination process (Ru/MoS_2/CP) (**Figure 10**a and b).[120] When generating hydrogen in alkaline condition, there is an interfacial synergistic effect between Ru and MoS_2 in such Ru/MoS_2/CP sample, whereby Ru metal promotes the cleavage of H-OH bonds and nearby MoS_2 with rich defects allows for favorable hydrogen adsorption/desorption (**Figure 10**c). Thereby, the as-designed Ru/MoS_2 sample exhibited considerable activity with the overpotential of only 13 mV at 10 mA cm^{-2}, which was much better than the single component (Ru or MoS_2) and even outperformed Pt/C (**Figure 10**d).

Several Ru/A heterostructured composites were also applied to overall water splitting.[123-125] In Huang's study, ruthenium-nickel sandwiched nanoplates (Ru-Ni SNs) were prepared by a colloid chemistry method, in which ruthenium(III) acetylacetonate, nickel(II) acetylacetonate, and PVP were uniformly dissolved in benzyl alcohol with the aid of ultrasonication, and then the system was heated at 170 °C for 5 h in an oil bath.[124] TEM and HR-TEM images revealed an interesting morphology of two hexagonal Ru rings caped on the two ends of a Ni pillar in Ru-Ni sandwiched structure (**Figure 10**e-g). By adjusting the molar ratio of Ru and Ni metal sources, Ru_2Ni_1, Ru_2Ni_2 and Ru_2Ni_3 SNs with similar morphologies were obtained. Among them, Ru_2Ni_2 SNs are most active for both OER and HER in alkaline media and is much higher than that of benchmarks Pt/C (**Figure 10**h and i). An electrolyzer prototype with Ru_2Ni_2 SNs as both cathodic and anodic catalysts offered a considerable catalytic activity for water splitting along with high stability (**Figure 10**j and k). Yang et al. reported the ultrafine Ru and Cu-doped RuO_2 complex embedded in an amorphous carbon substrate (S-400-H) as promising bifunctional catalysts toward both OER and HER in alkaline aqueous solutions.[125] In such composite S-400-H, ultrafine Ru acted as the main HER active sites while ultrasmall Cu-doped RuO_2 displayed the improved OER activity when compared with ultrasmall RuO_2 and also outperformed the commercial RuO_2. DFT results confirmed that Cu doping tailored d-band center, so as to change the electronic distribution around Ru active centers in RuO_2, eventually enhancing OER activity of RuO_2. The unique microstructures and composition enabled the S-400-H to be catalysts on both cathode and anode for full water electrolysis with

a current density of 10 mA cm^{-2} at 1.47 V as well as excellent stability for 40000 s.

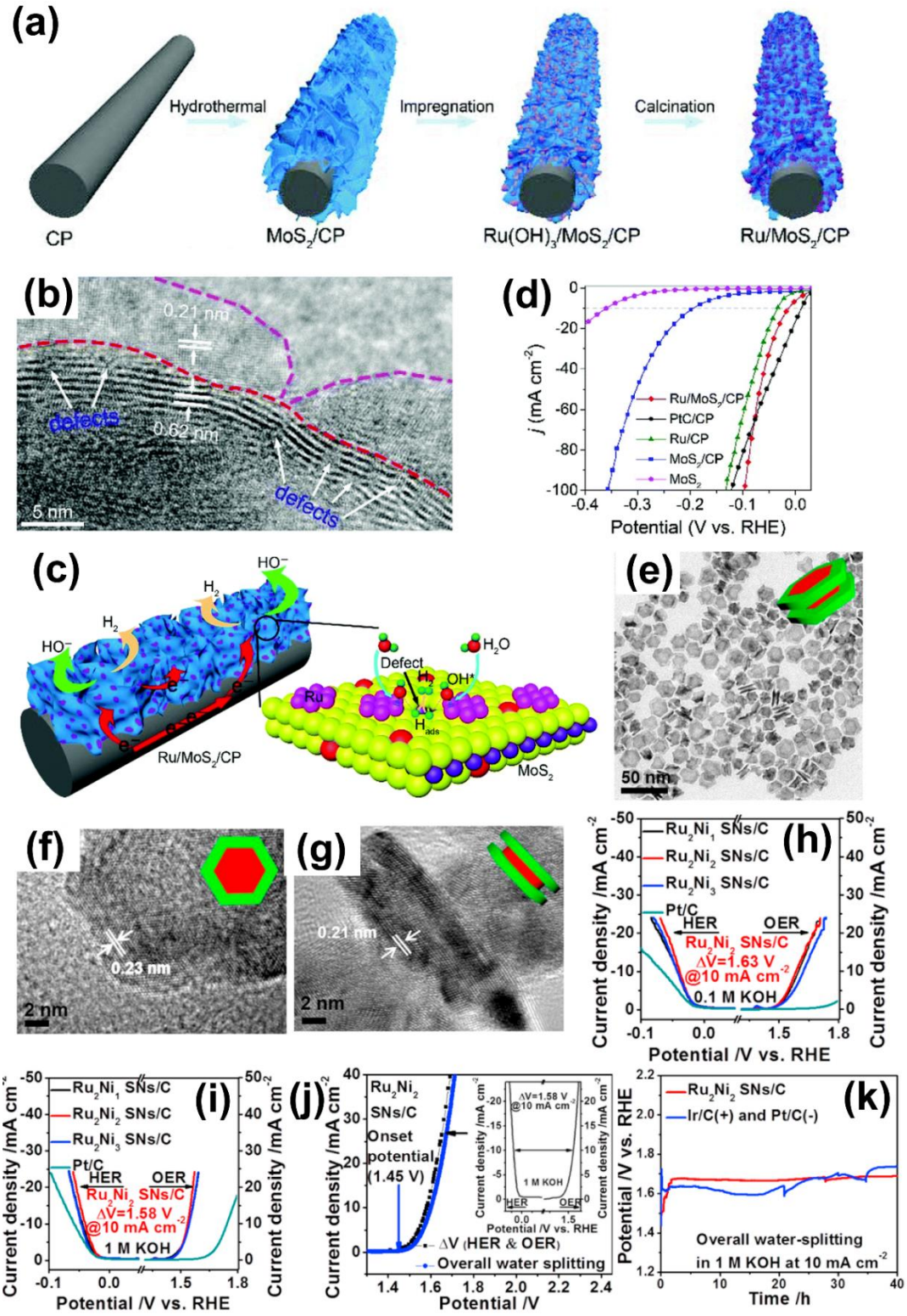

Figure 10. a) The synthetic route of Ru/MoS_2/CP. **b)** HRTEM images of Ru/MoS_2/CP. **c)** Schematic illustration showing an interfacial synergistic effect between MoS_2 and Ru toward HER in alkaline media. **d)** Polarization curves of Ru/MoS_2/CP and other control samples for alkaline HER. Reproduced with permission.[120] Copyright 2017, Royal Society of Chemistry. **e-g)** Obtained TEM

and HRTEM images of Ru_2Ni_2 SNs from a different view. **h**, **i)** HER and OER activity results based on LSV curves for various Ru-Ni SNs/C, and commercial Pt/C in 0.1 M KOH **(h)** and 1 M KOH **(i)**. **j)** Polarization curves of Ru_2Ni_2 SNs in a two-electrode water splitting system under alkaline conditions, Insert is the separated OER and HER polarization curves. **k)** Chronopotentiometry test at 10 mA cm^{-2} for Ru_2Ni_2 SNs/C and Ir/C-Pt/C. Reproduced with permission.[124] Copyright 2018, Elsevier.

3.1.5. Ru-C composites design. Apart from the above-mentioned composites of Ru metal with other metals, phosphides, and oxides, etc, Ru metal can also be loaded on various functional carbon substrates, generating Ru-C hybrids, which have been extensively reported as extraordinarily high-activity HER electrocatalysts in the pH-universal electrolytes.[74, 130-140] In these composites, carbon-based supports, including reduced graphene oxide (RGO), carbon nanotubes (CNTs), carbon nanosheet, porous carbon, XC-72 Vulcan carbon, etc., show lots of merits, which are summarized as below.[74, 130-135] First, carbon materials generally have super conductivity, that decreases the electrical resistance among active species.[131] Then, carbon substrates with the ultrahigh specific area can avoid the agglomeration of Ru nanocrystals and accordingly obtain uniform and highly-dispersed fine Ru particles.[135] Third, abundant porous structure can facilitate mass diffusion, particularly accelerate the transportation of electrolytes and release of H_2 product.[136, 137] Last but not least, the formed interfacial interactions between carbon and metal efficiently tune the electronic configuration of active sites.[137, 138] All of these may lead to more active sites and excellent catalytic activity.

In general, Ru-C composites are fabricated by using two classes of strategies of “in situ produced carbon” and “as-formed carbon”. The former is mainly derived from the high-temperature calcination treatment of a mixture of Ru salts and organic

molecules.[135-139, 141] During the annealing process, metal species catalysis and thermal decomposition enable organic linkers to be successfully transferred into various carbon nanostructures, e.g., carbon nanosheets, irregular porous carbon, or CNTs, etc. For instance, Zhang et al. reported the synthesis of a novel ruthenium/nitrogen-doped carbon (Ru/NC) catalyst using polyaniline as a carbon precursor and $RuCl_3$ xH_2O as the metal source, and the micro-morphology of the resultant samples could be controlled by the pyrolysis temperature ranged from 800 ºC to 1000 ºC.[134] In a recent published work, Shao-Horn's group developed ruthenium-decorated hierarchical porous carbon (Ru-HPC) based on a bimetallic metal-organic frameworks strategy (**Figure 11**a), in which 1, 3, 5-benzenetricarboxylic acid (H_3BTC) was employed as the organic ligand, and Cu^{2+} and Ru^{3+} were used as metal sources. After self-assembly by coordination bonds between metal ions and H_3BTC, CuRu-MOF was achieved. Then, the pyrolysis was carried out at 700 ºC for 2h, in which the organic ligand would transfer into nitrogen-doped carbon and metal ions were reduced to metal Ru and Cu. After that, the resulting Cu was removed by $FeCl_3$ and thus functioned as pore templates.[137] **Figure 11**b-d display that ultrafine Ru nanoparticles were anchored on carbon substrate with a hierarchically porous structure for Ru-HPC sample and the formation of hierarchical structures could stem from removal of Cu, as confirmed by N_2 adsorption/desorption isotherms. Toward hydrogen production, Ru-HPC showed highly excellent catalytic activity with a low overpotential of 22.7 mV to reach 25mA cm^{-2}_{geo} 1 M KOH (**Figure 11**e) and robust stability (**Figure 11**f). By contrast, the "as-formed carbon" strategy utilizes well-defined carbon supports and Ru salts, and then usually undergo a low-

temperature reduction process to attain Ru-C hybrids.[74, 140] As reported by Baek's group, a robust mechanochemically assisted synthesis method was proposed to produce this composite of uniform Ru nanoparticles loaded on the graphene nanoplatelets (Ru@GnP) (**Figure 11**g).[140] By ball-milling commercial copious graphite with dry ice, they developed edge-carboxylic-acid functionalized graphene nanoplatelets (CGnP), which easily adsorbed Ru ions on their surface. Then sodium borohydride ($NaBH_4$) was added into above Ru ions-contained CGnP dispersions to in situ reduce Ru ions into Ru metal. Finally, further calcination was conducted to remove excessive carboxylic acid groups, so that to form the resulting Ru@GnP hybrid. Hu et al. also demonstrated that by directly grinding the mixture of metal precursor ($RuCl_3$), sodium borohydride ($NaBH_4$), sodium hydroxide (NaOH), and commercial XC-72 Vulcan carbon in an agate mortar at an ambient temperature, highly dispersed Ru nanoparticles supported on carbon (Ru/C) were successfully achieved.[74] All of the above mentioned Ru-C materials, when used as HER electrocatalyst, showed superior catalytic activity.

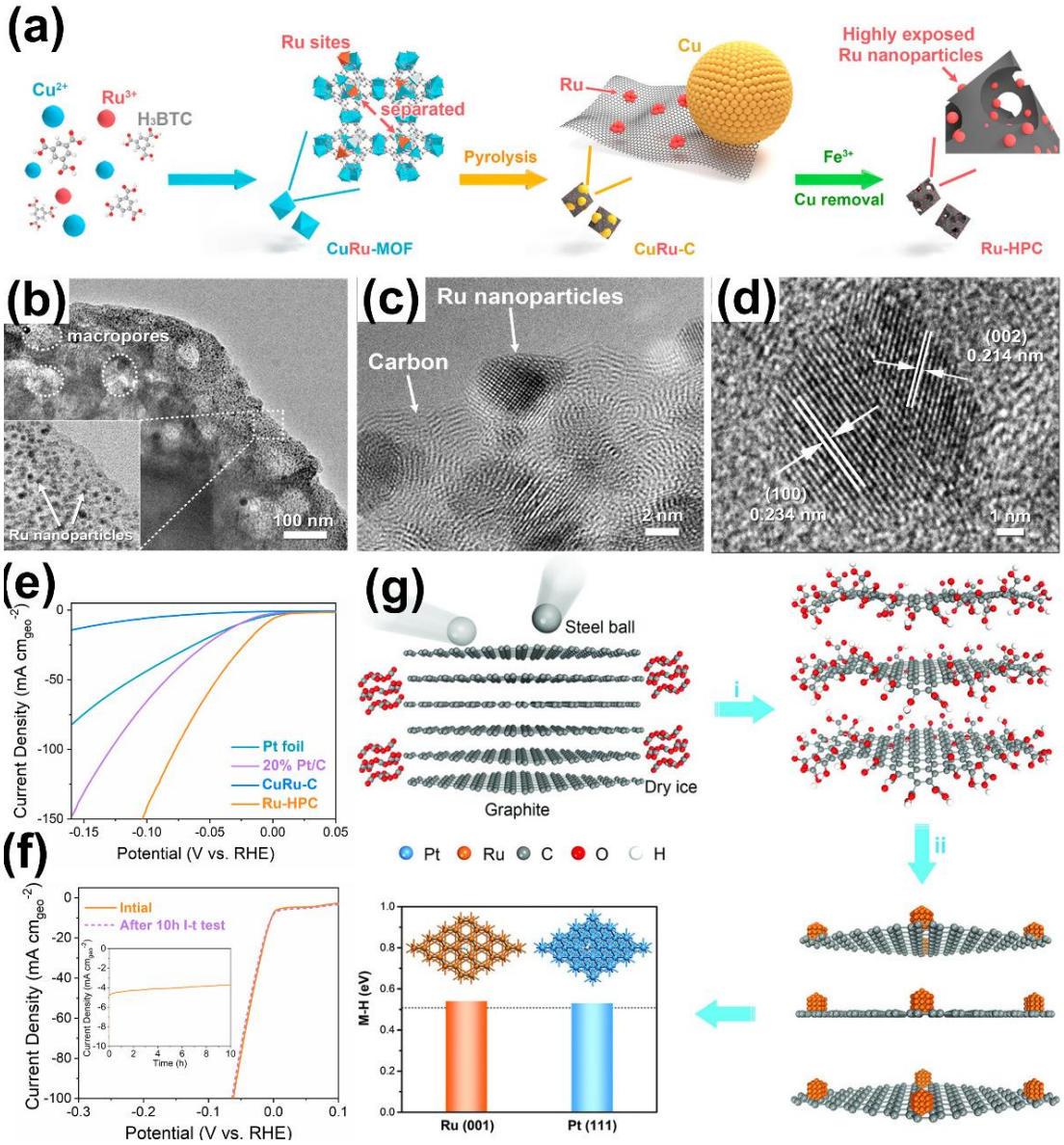

Figure 11. a) A schematic diagram to describe the synthesis of Ru-HPC. **b)** TEM and **c**, **d)** HRTEM images of the Ru-HPC. **e)** HER Polarization curves of the designed Ru-HPC, CuRu-C, 20% Pt/C, and Pt foil in alkaline media. **f)** HER Polarization curves of Ru-HPC before and after 10 h continuous current-time measurement in alkaline electrolytes. Insert images showed the 10 h continuous current-time test of Ru-HPC. Reproduced with permission.[137] Copyright 2019, Elsevier. **g)** Schematic illustration of the preparation of Ru@GnP electrocatalyst. Reproduced with permission.[140] Copyright 2018, Wiley-VCH.

The nanosized effect of Ru crystal for Ru-C composites on HER performance could be controlled by changing the mass ratio of carbon precursors and metal sources, which was realized by Barman's study.[139] In that work, the researcher designed various N-doped graphene-supported ultra-small Ru nanocrystals composites (Ru@NG-x) on

the basis of different mass ratio (x) of dicyanamide and $RuCl_3xH_2O$ as raw materials. According to high-resolution TEM (HRTEM) images, Ru nanocrystals in Ru@NG-10 have sizes of 4-5 nm. In contrast, the average sizes of Ru nanocrystals in Ru@NG-2 and Ru@NG-4 samples are about 2 nm. The electrochemical tests revealed that the HER performance of three electrocatalysts recorded in both acid and alkaline conditions followed a trend of Ru@NG-10 < Ru@NG-2 ≈ Ru@NG-4, strongly corresponding to the order of the Ru nanocrystals sizes: Ru@NG-10 (4-5 nm > Ru@NG-2 ≈ Ru@NG-4 (~2 nm). Additionally, the effect of confinement space for Ru nanoparticles encapsulated by carbon shell on HER catalytic activity was also studied by Chen and his coworkers.[142] They found that the fully-encapsulated Ru catalyst (F-Ru@PNC) showed higher catalytic activity than the semi-encapsulated Ru catalyst (S-Ru@PNC), and both of them were also superior to Ru nanoparticles supported on PNC (Ru/PNC). Subsequent DFT calculation results elucidated that the charge transfer between the Ru nanoparticles and the carbon layer was affected by the different confined spaces, so as to generate different HER activities.

Among Ru-C composites, N-rich organic precursors after the carbonization help to form Ru-N-C hybrids and the synergy between metal-embedding and N-doping can enhance the catalytic activity.[27, 132, 135] Based on a recent report by Li's group, owing to metal-N_4 species with more thermodynamically robust stability, precious metal nanoparticles had a large tendency to be thermally stable single atoms in an inert atmosphere when mobile precious metal atoms were anchored to the defects of N-doped carbon.[143] Inspired by these findings, several researchers have proposed various

strategies to design different Ru-N-C composites for efficient hydrogen generation. As a good case, Baek's group first reported the production of ultrafine Ru-dispersed and nitrogenated two-dimensional porous carbon (Ru@C_2N) by a coupled two-step room-temperature reaction: (1) C_2N structure was first formed through the polycondensation of Hexaaminobenzene (HAB) and hexaketocyclohexane (HKH) in N-methyl-2-pyrrolidone (NMP); (2) $RuCl_3$, as a Ru precursor, was subsequently reduced by $NaBH_4$ reducing agent.[27] As a result, Ru@C_2N showed a high specific surface area of 400.1 m^2 g^{-1} and a Ru content of about 28.7 wt.%. Such a Ru@C_2N catalyst enabled the unprecedented HER activity with the low overpotentials to reach 10 mA cm^{-2} (13.5 mV in 0.5 M H_2SO4; 17.0 mV in 1.0 M KOH), and small Tafel slopes (30 mV $decade^{-1}$ in 0.5 M H_2SO_4; 38 mV $decade^{-1}$ in 1.0 M KOH), which beat most of reported electrocatalysts and is even better than Pt/C. Meanwhile, the superior catalytic activity toward HER of Ru@C_2N to control samples of Co@C_2N, Ni@C_2N, Pd@C_2N, and Pt@C_2N with the similar synthesis verified the promotion by Ru metal, and a poisoning study with SCN^- revealed highly dispersed Ru nanoparticles as the dominant active sites. According to further theoretical calculations, the intrinsic origin of such high HER activity for Ru@C_2N is from a favorable Ru-H binding energy. Later, Wang and coworkers also introduced highly uniform Ru nanoparticles on N-doped carbon hybrids (Ru@CN) through the calcination of a solid mixture of melamine, D-glucosamine hydrochloride (GAH), and $RuCl_3$ at 800 °C for 6h, and confirmed it as an efficient HER electrocatalyst in pH-universal conditions.[135] The outstanding HER activity can be attributed to factors such as the high specific area, rich zero-valence Ru, good

conductivity, and large active site density. More recently, Chen's group designed one-dimensional Ru, N-codoped carbon nanowires by employing tellurium (Te) nanowires as sacrificial templates, as illustrated in **Figure 12**a (The resulting product was named as Ru-NC-T, where T represents the pyrolysis temperature.).[144] According to several advanced material characterizations like TEM, HAADF-STEM, XAS, and EELS, it was found that in addition to Ru nanoparticles, Ru single atoms embedded within the carbon matrix (RuC_xN_y) were also achieved **(Figure 12**b-i). When served as HER electrocatalysts in 1 M KOH, the optimized Ru-NC-700 delivered a super catalytic activity with an η_{10} of only 12 mV, which is markedly superior to Pt/C (about 49 mV) (**Figure 12**j) and much better than almost all of Ru-involving catalysts performed in alkaline electrolytes. Based on a series of controlled experiments, they argued that such unprecedent activity was greatly originated from RuC_xN_y species with minimal contributions from Ru nanoparticles. Furthermore, DFT calculations also confirmed that a much lower hydrogen binding energy for RuC_xN_y was obtained relative to Ru nanoparticles, especially RuC_2N_2 functioned as the most active catalytic site (**Figure 12**k).

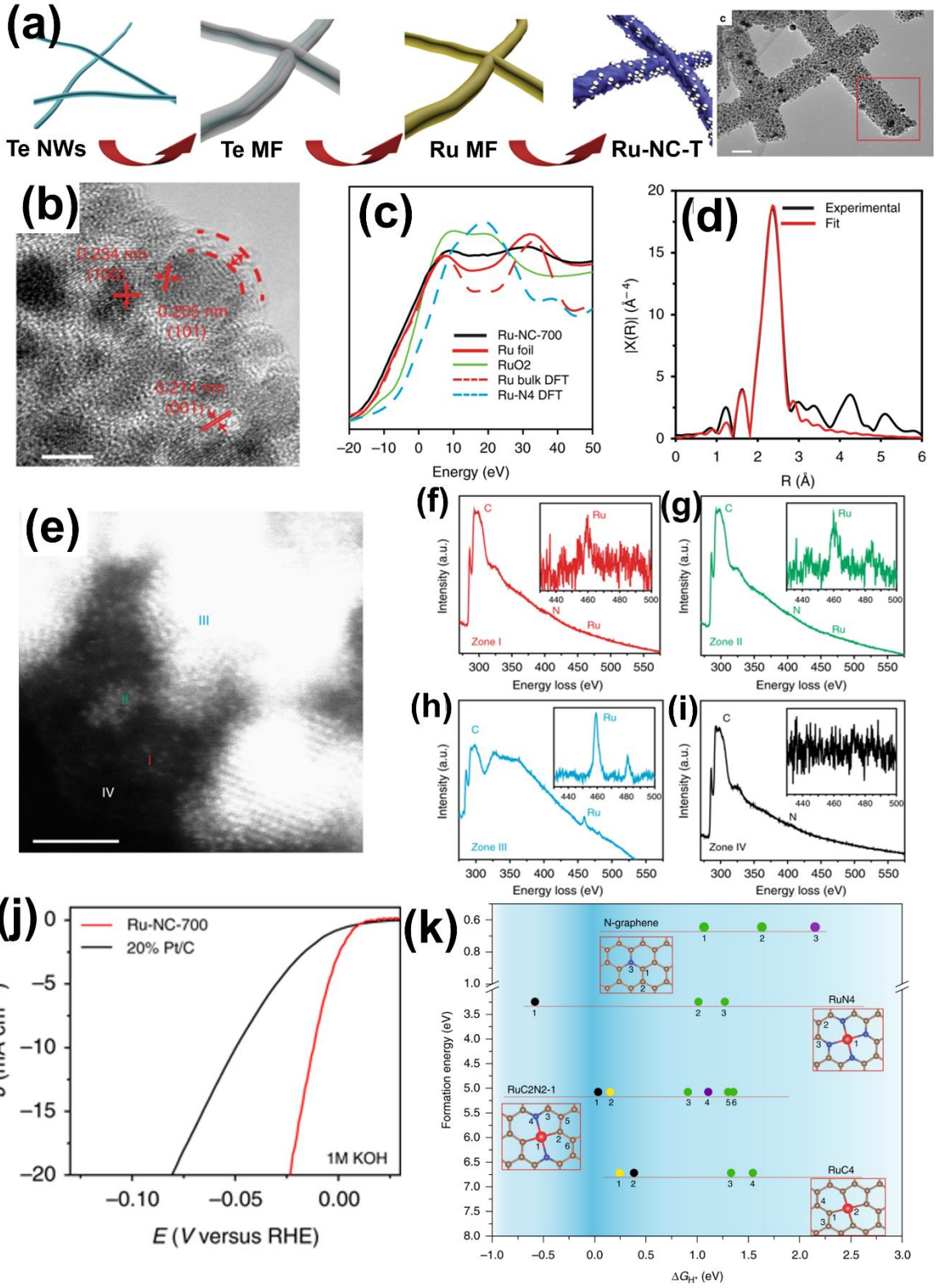

Figure 12. a) The synthesis process of the Ru-NC-T sample based on Te nanowires as sacrificial templates. The image at right is the HRTEM image of Ru-NC-800 sample. **b)** The HRTEM image of Ru-NC-800. **c)** XANES results for Ru-NC-700, solid lines and dash lines represent experimental data and simulated data from DFT calculations, respectively. **d)** Fourier-transformed EXAFS data for Ru-NC-700. **e)** HAADF-STEM images of Ru-NC-700 and **f-i)** EELS spectra of zones (I)-(IV) in **e**, which is corresponding to Ru single atoms, Ru nanoclusters, Ru nanoparticles, and metal-free

carbon. **j)** HER polarization curves of Ru-NC-700 and 20% Pt/C under alkaline conditions. **k)** Energy diagram of different RuC_xN_y structures based on DFT calculations. Reproduced with permission.[144] Copyright 2019, Nature Publishing Group.

3.2. Ru oxides

3.2.1. RuO_2. RuO_2 is extremely active to accelerate O_2 evolution, and up to now, it has been generally recognized as the benchmark toward OER electrocatalysts in both acidic and alkaline electrolytes.[14, 43, 54, 56, 145-150] As compared in acidic condition, the utilization of higher-pH electrolytes enables numerous transition metals to be employed as electrode catalysts, owing to their high anti-corrosion behavior in alkaline condition. Accordingly, plenty of efficient and low-cost electrocatalyst alternatives to RuO_2 were developed in the alkaline solution.[151] In contrast, superior acidic OER catalysts still rely on few acid-resisting noble metals such as Ir and Ru, thus RuO_2-based materials as acidic OER catalysts were more widely investigated compared with those in alkaline electrolytes. Nevertheless, no matter operating in an acid or alkaline environment, RuO_2 exhibited a fast-fading activity toward OER, even though its initial catalytic behavior is high,[58, 82, 152] which has been discussed in detail in the second part. When comparing RuO_2 with IrO_2, which is another OER state-of-art standard, RuO_2 have better OER activity than IrO_2 while the stability of RuO_2 is much inferior to that of IrO_2.[14, 54, 153] Interestingly, Danilovic et al. discovered that the most active precious metal oxide toward OER in acidic condition is actually the least stable one, which is primarily dominated by density of surface defects along with the nobility of metal oxides.[153] Consequently, to enable the practical operation, the improvement of long-term stability for RuO_2-related catalysts without affecting its electrocatalytic activity is highly

essential, and of course, it is more eager to simultaneously enhance its activity and stability. However, still, numerous previous studies only focus on the OER activity but neglect the corrosion issue.

For extensively reported RuO_2 materials as OER electrocatalysts, the obtained performance varies drastically, which have a large dependence on various synthetic strategies and experimental conditions that contributed to different morphologies, particle sizes, crystallinity, crystal facet and degrees of hydration, etc.[20, 147, 127, 154-167]

Particle size and morphology control: For the sake of maximizing the mass utilization efficiency of Ru metal and creating more active sites per mass, it is most logical to reduce the particle size and design a novel nanostructure. Several predecessors controlled the particle sizes by changing pyrolysis temperature.[147, 154] Among them, Xu's group found that the specific/mass activities for OER were decreased when increasing particle sizes,[154] while Ma et al. emphasized that the particle size and the degree of crystallinity jointly affect the OER catalytic behavior, thereby existing an optimum calcining temperature.[147] Paoli et al. employed the magnetron sputtering method to produce well-defined and mass-selected RuO_2 nanoparticles and demonstrated a tentative maximum in acidic OER mass activity for the particles with the size of about 3-5 nm.[54] Nevertheless, as experimentally evidenced by Reier et al.,[82] anodic-oxidized Ru nanoparticles at the diameter of around 4 to 6 nm were more unstable than the corresponding bulk one. Thus, it seems to exist both positive and negative relationship with the particle size on activity and stability, respectively.

RuO_2 thin film patterned on conductive substrates is effective to increase the

number of active centers, and sometimes enhance the long-term stability.[155-157] DeSario et al. proposed a versatile deposition method to obtain the ultrathin RuO_2 film on various 3D substrates (SiO_2 or carbon-coated SiO_2 paper).[155] The as-prepared RuO_2@SiO_2 or RuO_2@C@SiO_2 electrode showed very high OER activities on the basis of area and mass in the acid electrolyte (10 mA cm^{-2} at an overpotential of 270-280 mV or 20-60 mA mg^{-1} at an overpotential of 330 mV). More significantly, such high performance was achieved with a catalyst loading roughly 300-580 times less than that of bulk RuO_2. Of note, at the constant density current of 10 mA cm^{-2}, a stable activity for over 100 h was also observed. According to Kibsgaard et al., the surface structure of RuO_2 thin film was further optimized via constructing highly ordered mesopores, which significantly boosted the OER geometric activity along with unaffected specific activity under acidic condition.[118] Additionally, various other nanoarchitecture, such as nanorods, nanowires, and nanosheets also attracted great attention.[14, 20, 28, 150] Recently, one-dimensional RuO_2 nanorods with a length-width ratio of ~4.37 were fabricated via a facile hydrothermal-calcination route.[150] This OER catalyst afforded the low operating potential of 1.508 V vs. RHE to reach a 10 mA cm^{-2} current density in 1 M NaOH, which exceeded that required for commercial RuO_2. Such results might be caused by higher surface area that create more active sites. As well, the negligible change before and after 500 continuous cycles confirmed the robustness of this RuO_2.

Crystallinity and crystal facet engineering: The crystallinity and Miller index of crystal face for catalysts renders the control in the local structure of the surface

adsorption sites, which is usually significant in determining OER catalytic behavior.[61, 149, 158-160] For example, Nakato et al. identified the fact that amorphous RuO_2 delivered a smaller Tafel slope and lower onset potential than that of the rutile crystalline one in an acidic electrolyte.[158] Such higher OER activity could result from lower local structural distortion energy due to larger structural flexibility in the amorphous sample. Stoerzinger et al. demonstrated that RuO_2 (100) facet was more active and stable than the (110) facet for OER under alkaline condition, which was partially due to richer coordinatively undersaturated metal sites on the (100) surface.[149] Roy et al. systematically studied the impacts of RuO_2 crystallographic orientations on OER catalytic activity and stability.[61] In this case, they prepared three thin films with different orientations of (111), (101), and (001), and single-crystal (110), as well as commercial nanoparticles. When acting as OER electrocatalysts in 0.05 M H_2SO_4, the initial activities, from the view of the current density at 1.6 V vs RHE, followed this trend: (001) > (101) > particles > (110) > (111). However, in stark contrast to pioneering works, their stability was not related to the activity. Additionally, several other related works were published, such as analyzing the effect of crystallographic orientations on Ru redox during OER under different pH conditions, or evaluating the function of different crystal facets with different water coverage on H_2O deprotonation degree and adsorption free energies.[159, 160] Strikingly, owing to the highest thermodynamic stability on RuO_2 (110) crystal face, more attention was drawn on some properties of this surface during oxygen evolution. Several DFT-based investigations unraveled that the surface peroxo species of Ru-O-O-Ru, produced by the neighboring Ru-O bonds, could be the

reaction intermediates.[148, 161] It should be noted that local structural distortion could be triggered by generation of the peroxo bonds, thereby influencing the intermediate stabilization. Based on Sabatier principle, a catalyst is most efficient when the stability of intermediates is neither too weak nor too strong.[162] Besides, Shao-Horn's group identified the structural changes on the surface of single-crystal RuO_2 (110) as a function of applied potential during an acidic OER process via *in-situ* X-ray scattering measurements and DFT calculations (**Figure 13**a and b), and they proposed that the deprotonation of -OH species which stabilized the -OO group was a rate-determining step.[22] Inspired by this research, Kuo and his co-workers further correlated the pH-dependent electroabsorption energies of adsorbed hydroxide and oxide intermediate (OH_{ad} and O_{ad}), with OER catalytic behavior for RuO_2 (110).[162]

Other control: Oxidation treatment for RuO_2 nanoparticles could play a key role in OER activity and stability. The thermally oxidized RuO_2 offered more superior stability to the electrochemically-grown oxides, yet somewhat lower activity.[163-165] A possible explanation behind this behavior was the different density of surface defects.[153] Paoli et al. revealed that as-deposited Ru particles presented better OER activity but much easier corrosion in comparison with the RuO_2 nanoparticles obtained by a thermal oxidation process.[54] Later, in 2016, Stephens's group further compared the OER performance of as-deposited, O_2-plasma treated and thermally oxidized Ru nanoparticles, and found a reversed trend of activity and stability, in which the thermally oxidized material was the most stable, followed by the plasma treated one, and then the as-deposited one **(Figure 13**c-e).[166] In addition, the impact of degrees of

hydration on OER catalytic behavior was corroborated by Lee et al.[167] The hydrous RuO_2 provided higher stability and yet lower activity for OER than the corresponding anhydrous one.

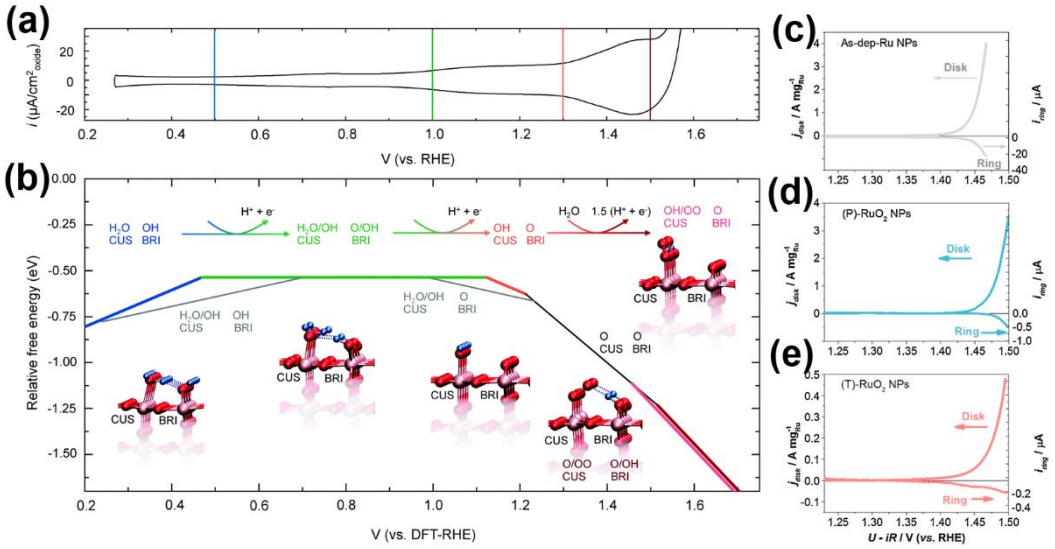

Figure 13. a) The reference CV curve on the surface of single-crystal RuO_2 (110) in Ar-saturated 0.1 M $HClO_4$ electrolytes. **b)** Relative Gibbs adsorption-energy diagram calculated from DFT for the most stable adsorbate species at various electrochemical operation potential. Reproduced with permission.[22] Copyright 2017, Royal Society of Chemistry. **c-e)** Disk and ring current densities as a function of applied potential between 1.0 and 1.5 V for as-deposited **(c)**, O_2-plasma treated **(d)** and thermally oxidized **(e)** Ru nanoparticles in 0.05 M H_2SO_4. Reproduced with permission.[166] Copyright 2016, Elsevier.

RuO_2 also offered a moderately high HER activity according to several pioneering works.[167-175] The first study about applying RuO_2 as HER electrocatalysts was reported by Trasatti's group.[168] Since then, some researchers, like Chabanier et al. Burke et al. Rochefort et al., etc,[170-173] further studied the HER properties of RuO_2 in alkaline or acidic media, in which it had been revealed that structural transformation, namely, the lattice expansion in rutile RuO_2, took place during the HER activation process. Rosen's group carried out a series of in-depth X-ray diffraction (XRD) and X-ray photoelectron

spectroscopy (XPS) investigation for fresh RuO_2 electrodes and that after producing hydrogen for a different time. This study demonstrated that hydrogen evolution triggered the structural transformation from RuO_2 to a new ruthenium oxyhydroxide phase, $RuO(OH)_2$ (**Figure 14**), and then it is over time reduced to zero-valence Ru.[174] Subsequently, Karlsson et al. re-evaluated this data from Rosen' group.[175] The XPS results in the former study was employed to confirm the generation of a new $RuO(OH)_2$ phase while it might be caused by carbon contamination in the surface of the electrode. However, the overall conclusion about structural changes was nearly consistent, which also agreed with other studies. Besides, according to a previous study from Lee and his co-workers, the hydrous RuO_2 nanoparticles for highly efficient hydrogen generation were constructed via an aqueous-phase synthetic strategy.[167] Benefiting from the hydrated surface structure and good conductivity, the hydrous RuO_2 nanoparticles presented a low overpotential and high current densities under alkaline condition, which was superior to the corresponding crystalline one after annealing treatment and even better than Pt/C. Meanwhile, the obtained crystalline RuO_2 showed excellent OER performance, suggesting the bifunctionality of RuO_2. These findings inspired the building of an alkaline water electrolyzer using hydrous and crystalline RuO_2 nanoparticles as cathodic and anodic catalysts, respectively, and the overpotential of 273 mV without iR correction was needed to deliver the current density of 10 $mAcm^{-2}$, surpassing that of the couple of Pt/C and IrO_2 (~343 mV).

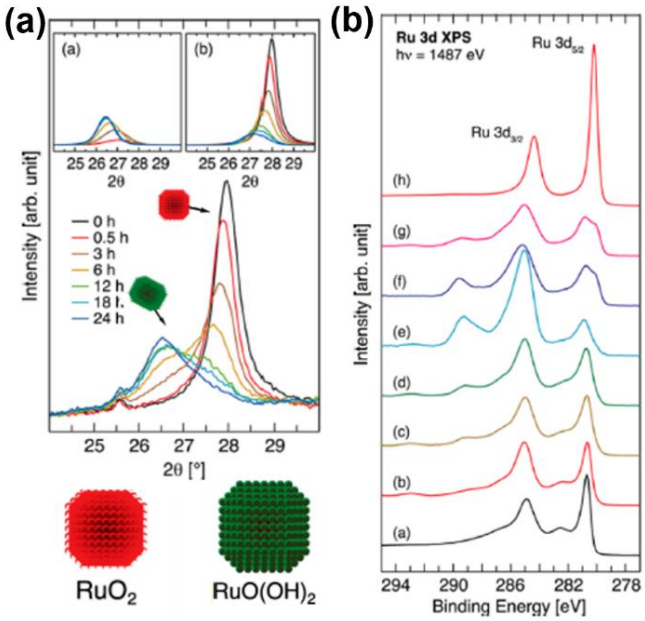

Figure 14. a) XRD patterns and **b)** Ru 3d XPS spectra of the RuO_2/Ni electrodes toward hydrogen generation for a different time. Color: red, RuO_2; green, $RuO(OH)_2$. Reproduced with permission.[174] Copyright 2014, American Chemical Society.

3.2.2. RuO_2-based mixed oxides. The electrocatalytic behavior of RuO_2 may be often modified by forming mixed metal oxides.[125, 176-205] In general, doping of other metal components can tune the electronic structure of RuO_2, and thus increase or stabilize catalytic active sites, in turn improving OER or HER performance, especially in most concerned OER stability. Therefore, in the following parts, more attention was paid to discuss the influence of metal components incorporation in RuO_2-based mixed oxides on OER or HER activity and stability, and distinguished various as-formed phase structures, such as a single phase or mixed phases.

Ru-Ir oxides: Ru-Ir oxides have been demonstrated to offer considerable activity and stability toward OER.[176-185] Especially, its dilution with stable IrO_2 significantly weakened corrosion effect during the OER process.[176, 179, 182, 186] According to Kotz et al., it was found that the corrosion rate was lowered to 4% of the original data by doping

only a small number of IrO_2 (20%).[176] On basis of various synthetic routes, including sputtering, hydrolysis, Adams' fusion method, etc,[176-181, 187, 188] the obtained Ru-Ir oxide materials generally showed a solid solution phase, in which Ir^{4+} atoms were uniformly mixed with Ru^{4+} atoms in the RuO_2 crystal lattice because of a similar atomic radius (0.077 nm for Ir^{4+} and 0.076 nm for Ru^{4+}), while sometimes the separate RuO_2 and IrO_2 phases might be present.[189-192] Mamaca et al. produced the Ru-Ir oxides mixture nanoparticles via thermal decomposition and unveiled that the presence of IrO_2 undoubtedly worked against Ru dissolution to improve stability and yet increased the overpotential compared to RuO_2.[182] Li et.al prepared the $Ir_xRu_{1-x}O_2$ solid solution with nanorods morphology and found the "best" performance for the $Ir_{0.2}Ru_{0.8}O_2$ sample.[191] Further OER mechanism of $Ir_xRu_{1-x}O_2$ solid solution obtained by hydrolysis synthesis was investigated by Sunde's group.[184] Integrating experiment with theoretical analysis, the pH and potential-dependent OER activity trends could be well described by mononuclear reaction mechanism with the third or fourth step as a rate-determining step for RuO_2 or IrO_2, respectively. In 2017, Xing's group successfully explored a novel nanostructure of RuO_2@Ru nanoparticles discontinuously covered by IrO_2 (IrO_2-RuO_2@Ru) through a combined hydrolysis-pyrolysis approach.[193] Benefiting from the large specific surface area, fast charge transfer, and the synergetic effect between IrO_2 and RuO_2@Ru (**Figure 15**a and b), the optimal IrO_2-RuO_2@Ru (3:1) was rationalized to be most active and stable for catalyzing water oxidation (**Figure 15**c and d). Moreover, for the sake of further balancing the cost and performance (activity and stability), a third type of inert metal was introduced into Ru-Ir oxides, such as Ta, Ce,

Mo, and Co, etc.[186, 194-198] Audichon et al. suggested that although Ce doping reduced the total amount of active sites, the good oxygen mobility in a ceria crystal helped to enhance the catalytic activity per active site, thereby assuring a high efficiency of such ternary oxide toward OER.[198]

Relative to Ru-Ir oxides extensively as OER electrocatalysts, they have aroused less attention on catalyzing HER.[178, 199, 200] In 2018, $Ir_xRu_{1-x}O_y$ nanowires after the cathodic activation have been manifested to be quite active for hydrogen generation (**Figure 15**e).[200] XPS and XRD results disclosed a transformation of the surface oxides to the metal alloy through continuous cathodic activation (**Figure 15**f and g), which was mainly responsible for the enhanced HER activity with a favorable hydrogen adsorption energy (**Figure 15**h).

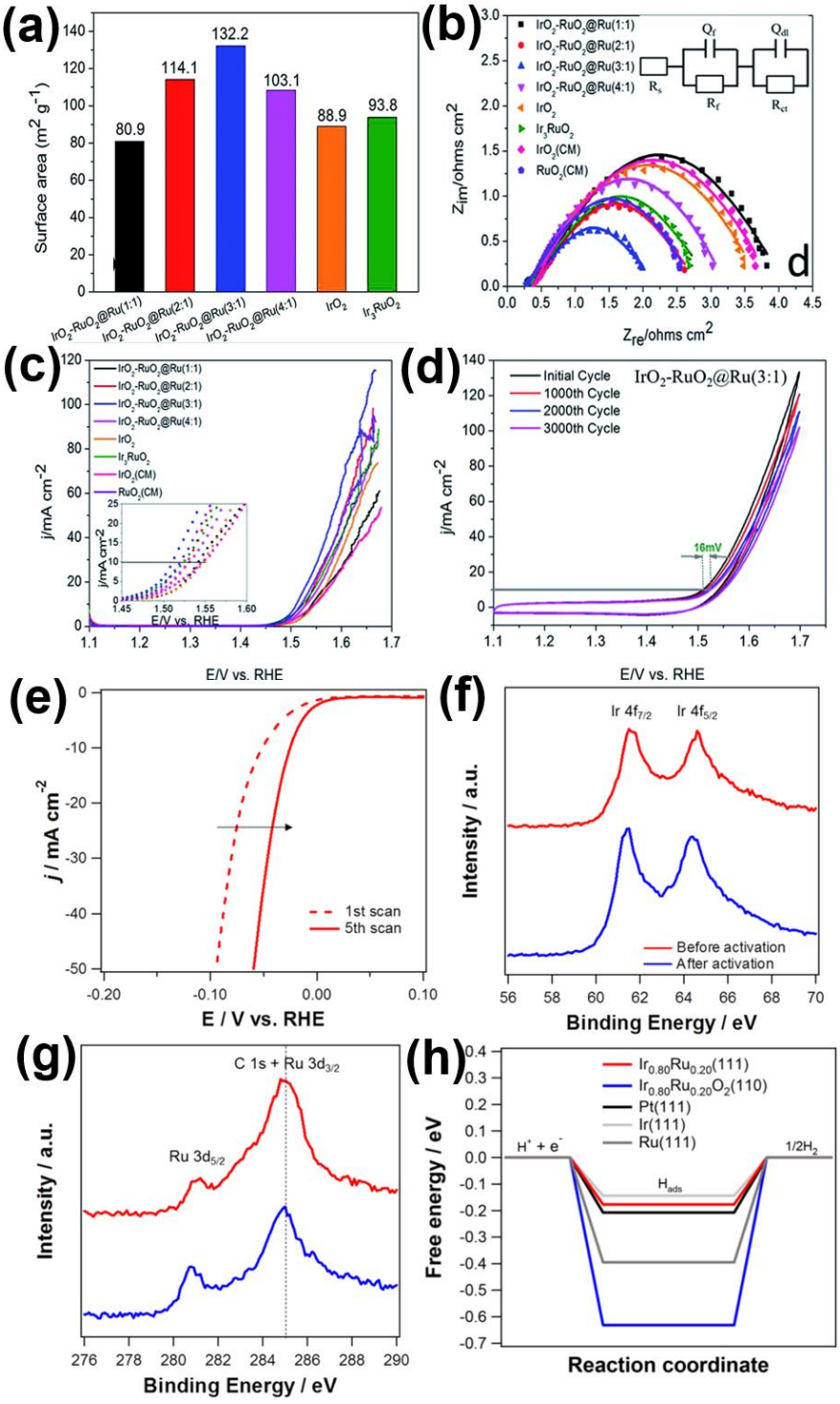

Figure 15. a) BET specific surface areas, **b)** EIS results at 1.55 V, and **c)** acidic OER polarization curve of various IrO_2-RuO_2@Ru electrocatalysts and other control samples. **d)** Accelerated durability tests based on cyclic potential sweeps with different cycles for the optimal IrO_2-RuO_2@Ru (3:1) sample. Reproduced with permission.[193] Copyright 2017, Royal Society of Chemistry. **e)** The first and fifth LSV curves toward HER in alkaline media for $Ir_{0.8}Ru_{0.2}O_y$ nanowires. **f)** Ir 4f and **g)** Ru 3d XPS results before and after cathodic activation. **h)** Hydrogen-adsorption free-energy plots for HER on various catalysts surface. Reproduced with permission.[200] Copyright 2018, American Chemical Society.

Other heteroatoms-doped RuO_2: Additionally, the OER activity and stability of pristine RuO_2 can be greatly improved by incorporating several alien metal atoms into rutile RuO_2 crystal lattice, including Cu, Zn, Sn, Fe, Co, Ni, etc.[28, 125, 201-209] Petrykin et al. illustrated partial substitution of Ru atoms in RuO_2 by Zn atoms induced a lattice distortion, which in turn offered more active OER catalytic activity.[202] According to Chen's group, Cu atoms were successfully introduced into RuO_2 via directly pyrolyzing Ru-exchanged Cu-based MOF derivative.[207] Relative to undoped counterpart, the as-designed catalyst showed remarkably enhanced OER activity in acidic electrolytes (the low overpotential of 188 mV at a current density of 10 mA cm^{-2}) and super stability. Theoretical calculation analysis disclosed that doping low-valent Cu into RuO_2 led to increased O vacancy, so as to trigger the generation of unsaturated Ru cations on the surface, and a p-band center of O more near Fermi level was also achieved, thus resulting in the enhanced performance. Furthermore, DFT calculations confirmed that doping of other divalent metals, such as Ni, Co, Fe, and Mn, also enabled the shift of adjacent O p-band center closer to Fermi level, and was expected to improve OER performance. Nevertheless, the easy oxidation of Ni, Co, Fe, and Mn led to various unfavorable structures. Recently, Huang's group employed a facile wet-chemical route to develop transition metal (M = Fe or Co or Ni)-doped RuO_2 networked nanowires (NWs) as a novel electrocatalyst toward water splitting.[28] They found that both OER and HER were markedly boosted after M doping under all pH conditions, and Co-doped RuO_2 NWs possessed the highest OER activity, followed by the corresponding Ni-doped one and then Fe-doped one, while the HER activities among them have a

different sequence of Ni doping > Co doping > Fe doping. As evidenced from first-principles calculations, such activity trends were originated from the balanced adsorption free energy of the intermediates (*OH for OER and *H for HER) in oxygen/hydrogen-evolution process, with a volcano-like relationship. Afterward, the as-prepared Co-doped and Ni-doped RuO_2 NWs efficiently functioned as anodic and cathodic catalysts in a home-made water electrolyzer, respectively, delivering superior activity and stability over the Ir/C-Pt/C couple under both acidic and alkaline conditions. Apart from less cation doping, in a most recent study by Lin and his co-workers, a MOF-derived Cr-Ru oxide solid solution material (**Figure 16**a) with low Ru content ($Cr_{0.6}Ru_{0.4}O_2$) was fabricated for catalyzing oxygen generation.[208] In the synthesis procedure (**Figure 16**a), a small amount of $RuCl_3$ was first loaded into the pores of Cr MOF (MIL-101) via an impregnation method, and then the resulting composites were further pyrolyzed at high temperature in air. The obtained $Cr_{0.6}Ru_{0.4}O_2$ exhibited unexceptionable acidic OER performance with an ultralow overpotential of 178 mV at 10 mA cm^{-2} and long-term stability for 10000-cycles CV test or 10 h chronopotentiometry measurement, much surpassing that of RuO_2 (**Figure 16b** and c). According to XAS measurements and DFT calculation, the electronic state of RuO_2 were profoundly modulated by Cr incorporation, rendering a lower electron density at Ru sites, the shortened Ru-O bond length, and shifted O p-center closer to Fermi level (**Figure 16**d-g), thus directly contributing to higher OER activity, while the decreased occupation at the Fermi level was the main reason for the enhanced stability, corresponding to the previous work. Analogous Ru-based solid solutions were also

formed when mixing RuO_2 with SnO_2 or TiO_2 with similar structure to RuO_2.[203, 212-214] Additionally, except for the cation incorporation, Kadakia and his co-workers demonstrated that F doping into $Sn_{0.8}Ru_{0.2}O_2$ solid solution could optimize the shift of d-band center toward RuO_2, which consequently contributed to a RuO_2-like OER activity with only 20% precious metal loading.[213]

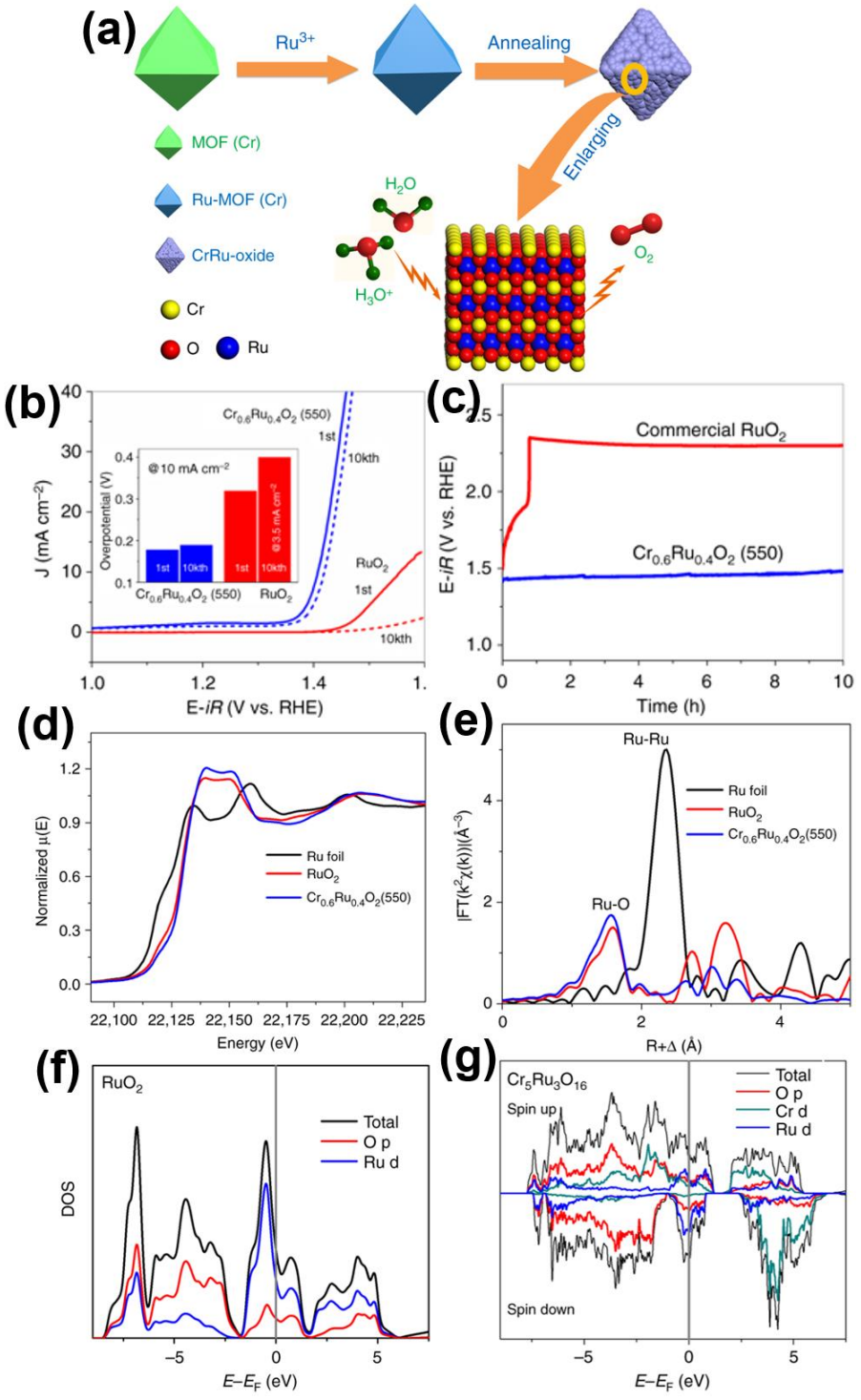

Figure 16. a) Schematic synthesis of MOF-derived $Cr_{0.6}Ru_{0.4}O_2$ solid solution. **b)** LSV curves toward OER before and after 10,000 potential cycles for as-made $Cr_{0.6}Ru_{0.4}O_2$ (550) and RuO_2 electrocatalysts in acidic solutions. The insert is the comparison of overpotentials at the current density of 10 mA cm^{-2} from LSV curves in **b**. **c)** Chronopotentiometry measurement of as-made $Cr_{0.6}Ru_{0.4}O_2$ (550) and commercial RuO_2 samples at a static current density of 10 mA cm^{-2} for 10 h. **d)** XANES spectra of Ru K-edge and **e)** Fourier-transformed EXAFS spectra of Ru edge for Ru foil, RuO_2, and $Cr_{0.6}Ru_{0.4}O_2$ (550). **f**, **g)** Density of states (DOS) plots of RuO_2 **(f)** and $Cr_5Ru_3O_{16}$ **(g)**. Reproduced with permission.[211] Copyright 2019, Nature Publishing Group.

Oxides mixture: Furthermore, to enhance the stability of RuO_2 under OER conditions, coupling RuO_2 with several inert or stable oxide components also tends to be an appealing strategy.[181, 215-220] For instance, Scott's group found that Nb_2O_5 addition stabilized the RuO_2 during the oxygen-evoluting process.[220] Also, insertion of Mn_xO_y enables the considerable enhancement of both OER activity and stability of RuO_2, which maybe result from the disrupted RuO_2 crystallinity, a modification in the electronic state of Mn, and cracked morphology.[221] Recently, Kumar et al. prepared the PdO-RuO_2 compound by a modified Adams fusion method, as acidic OER catalysts with extraordinary stability for 100 h in PEM water electrolysis.[222] In addition to the above-mentioned oxides, such improved impact could be extended to other oxide components such as Ta_2O_5, ZrO_2, WO_3, MnO_x, or Co_3O_4, etc.[178, 186, 215, 216, 218, 223-225] RuO_2-related oxides mixture were also verified to be efficient toward HER.[226-228] Li et al. constructed a composite electrocatalyst composed of RuO_2-NiO composites nanorod arrays morphology *in suit* grown on Ni foam via a facile hydrothermal approach.[227] NiO could promote water dissociation and favor the generation of hydrogen intermediates, and such binder-free integrated structure brought about much large surface area, fast charge transfer, and enhanced mechanical stability. Therefore, the RuO_2-NiO/Ni foam delivered an exceptional HER electrocatalytic performance.

3.2.3. RuO_2/carbon support composites. Several studies have unveiled that integrating RuO_2 with conductive carbon-related support, such as carbon nanotubes (CNTs), and various *in-situ* formed carbon matrix, could improve the OER or HER electrocatalytic activity, and even reduce the degradation of RuO_2 under OER

conditions.[14, 125, 229-235] Park et al. fabricated a unique composite catalyst of small RuO_2 nanoparticles with the size of about 17 nm encapsulated in carbon substrate, and observed their enhanced activity and stability toward OER in comparison with carbon-free RuO_2 nanoparticles.[235] Yuan et al. hybridized ultrasmall RuO_2 nanoparticles with N-doped carbon framework (RuO_2/N-C) by using a newfangled molecule-assisted strategy, where 1,10-Phenanthroline (Phen) molecules, simultaneously as carbon and nitrogen sources, can coordinate with Ru^{3+} ions to form Ru-Phen complexes, and through subsequent annealing in N_2 atmosphere at 700 °C for 2 h, the RuO_2/N-C hybrid was obtained (**Figure 17**a).[233] Benefiting from the space confinement impact, the RuO_2 nanoparticles in the as-prepared RuO_2/N-C hybrid were highly dispersed and ultrasmall with an average size of only ~1.7 nm (**Figure 17**b and c), which helped to generate more exposed active sites. Compared with pure RuO_2, the RuO_2/N-C catalyst offered better OER and HER activity in 1 M KOH aqueous solution with the overpotentials of 280 and 40 mV at 10 mA cm^{-2}, respectively (**Figure 17**d and e). More significantly, these activities presented negligible attenuation after 1000 cycles-CV test (**Figure 17**f and g). By experimental analysis and DFT calculations (**Figure 17**h and i), ultrasmall size of RuO_2 and high conductivity of N-doped carbon support, along with a synergy between them from strong interaction, conjointly contributed to the above-mentioned remarkable performance. In addition, a hybrid nanostructure of one-dimensional (1D) RuO_2 nanowires grown on carbon nitride, named as (1D-RuO_2-CN_x), was elaborately designed by Barman's group.[14] Based on the XRD, HR-TEM, XPS results, and some electrochemical tests results, such as EIS and ECSA, it was concluded that strong

coupling between 1D RuO_2 and CN_x support enabled favorable electron transfer, thus leading to high activity and structural stability for OER and HER. It's also found that 1D morphology provided numerous catalytic active sites and highly crystalline RuO_2 is good for stability. Consequently, the as-obtained 1D-RuO_2-CN_x exhibited superior activity to catalyze oxygen and hydrogen release with considerable durability under a wide range of pH conditions.

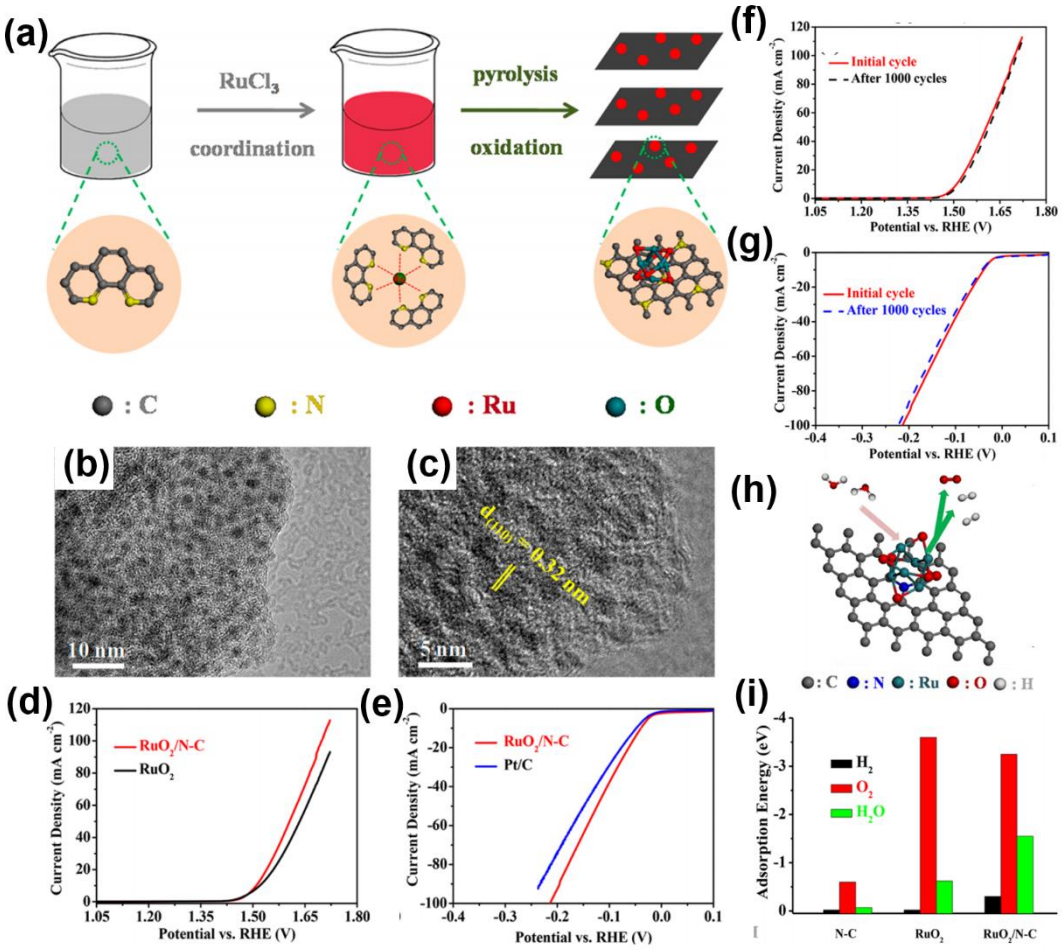

Figure 17. a) Schematic Illustration depicting the preparation route of the RuO_2/N-C hybrid. **b)** TEM and **c)** HRTEM images of the RuO_2/N-C catalyst. **d)** OER polarization curves of RuO_2/N-C and commercial RuO_2 in 1 M KOH solution. **e)** HER polarization curves of RuO_2/N-C and commercial Pt/C in 1 M KOH solution. **f**, **g)** LSV curves of the obtained RuO_2/N-C sample toward OER **(f)** and HER **(g)** for the initial one and that after 1000 cycles. **h)** Atomic model diagram revealing the water electrolysis on RuO_2/N-C electrocatalyst. **i)** Comparison of adsorption energies of H_2, O_2, and H_2O on the surface of N-C, RuO_2, and RuO_2/N-C samples. Reproduced with permission.[233] Copyright 2018, American Chemical Society.

3.2.4. Other Ru-based oxides. Pyrochlore or perovskite-type oxides ($A_2B_2O_7$ or ABO_3) have also sparked tremendous attention as OER/HER catalysts due to their robust chemical and structural stability.[21, 236-245] Besides, the partial substitution of A or B site by other elements provided more opportunities to regulate the catalytic behavior.[246] In particular, $Y_2Ru_2O_7$ is the most reported pyrochlore-structure material for oxygen production, especially in acidic environment.[236-239] Yang's group first put forward pyrochlore $Y_2Ru_2O_7$ with largely enhanced OER performance in strong acidic electrolytes over the benchmark RuO_2.[237] The low onset potential of around 1.42 V and a large current density of 2.23 mA cm^{-2} at 1.5 V were achieved for $Y_2Ru_2O_7$, and such prominent activity was still retained after 10000 continuous cycles (**Figure 18**a). By contrast, the onset potential of RuO_2 was 1.47 V, 50 mV higher than $Y_2Ru_2O_7$, and its current density at 1.5 V was less than one-sixth of that of $Y_2Ru_2O_7$ **(Figure 18**a). Moreover, a severe activity loss was obtained for RuO_2 after 10000 cycles (**Figure 18**a). XAS data revealed that $Y_2Ru_2O_7$ had a lower Ru oxidation state and a significantly different Ru-Ru bond in comparison with RuO_2 (**Figure 18**b and c), that led to the improved activity. As suggested by theoretical calculation results, the formation of pyrochlore oxide could decrease the overlapped Ru 4d-orbital and O 2p-orbital band center energy (**Figure 18**d-f), and thus the Ru-O bond in $Y_2Ru_2O_7$ structure was more stable than that in RuO_2, eventually contributing to the more superior stability. Besides, in order to further boost the oxygen-evolving performance of $Y_2Ru_2O_7$ under an acidic condition, a novel pyrochlore oxide with Ru ions being partially substituted by Y ions and porous morphology, fabricated via using a mature sol-gel method along with

perchloric acid as the porogen, was proposed by the same group.[238] In the sol-gel process, metal ions were mixed with citric acid (CA) chelates to obtain metal complexation. Such complexation reaction results in the formation of three-dimensional structures and minimizes cation segregation, so as to obtain the high purity and excellently control the powder composition. XRD and HR-TEM analysis confirmed the successful formation of pure pyrochlore structure, and the rich porous structure was also observed by SEM, TEM, and BET results (**Figure 18**g and h). In 0.1 M perchloric acid electrolyte, the designed $Y_2[Ru_{1.6}Y_{0.4}]O_{7-\delta}$ delivered a significantly enhanced OER activity with a low onset potential of only 1.41 V, Tafel slope of 37 mV dec^{-1}, and high TOF of 560 s^{-1} at the potential of 1.5 V, in comparison with $Y_2Ru_2O_7$ and RuO_2 (**Figure 18**i). By some advanced characterization approaches, such as XAS, they demonstrated that abundant oxygen defects with the mixed valences of $Ru^{4+/5+}$ in this $Y_2[Ru_{1.6}Y_{0.4}]O_{7-\delta}$ sample gave rise to an optimal energy band structure, and combining with the large surface area from the porous properties, resulted in the large OER enhancement. Subsequently, Feng et al. also optimized the OER activity by partial substitution of Zn for A-site Y in $Y_2Ru_2O_7$.[239] Noteworthily, the origin of this enhancement is analogous to Yang's group. Other Ru-related pyrochlore oxides, such as $Pb_2Ru_2O_{6.5}$, $Bi_2[Ru_{2-x}Bi_x]O_{7-y}$, $Sm_2Ru_2O_7$, $Bi_{2.4}Ru_{1.6}O_7$, $(Na_{0.33}Ce_{0.67})_2(Ir_{1-x}Ru_x)_2O_7$, etc., were also reported as promising OER candidates.[240-243]

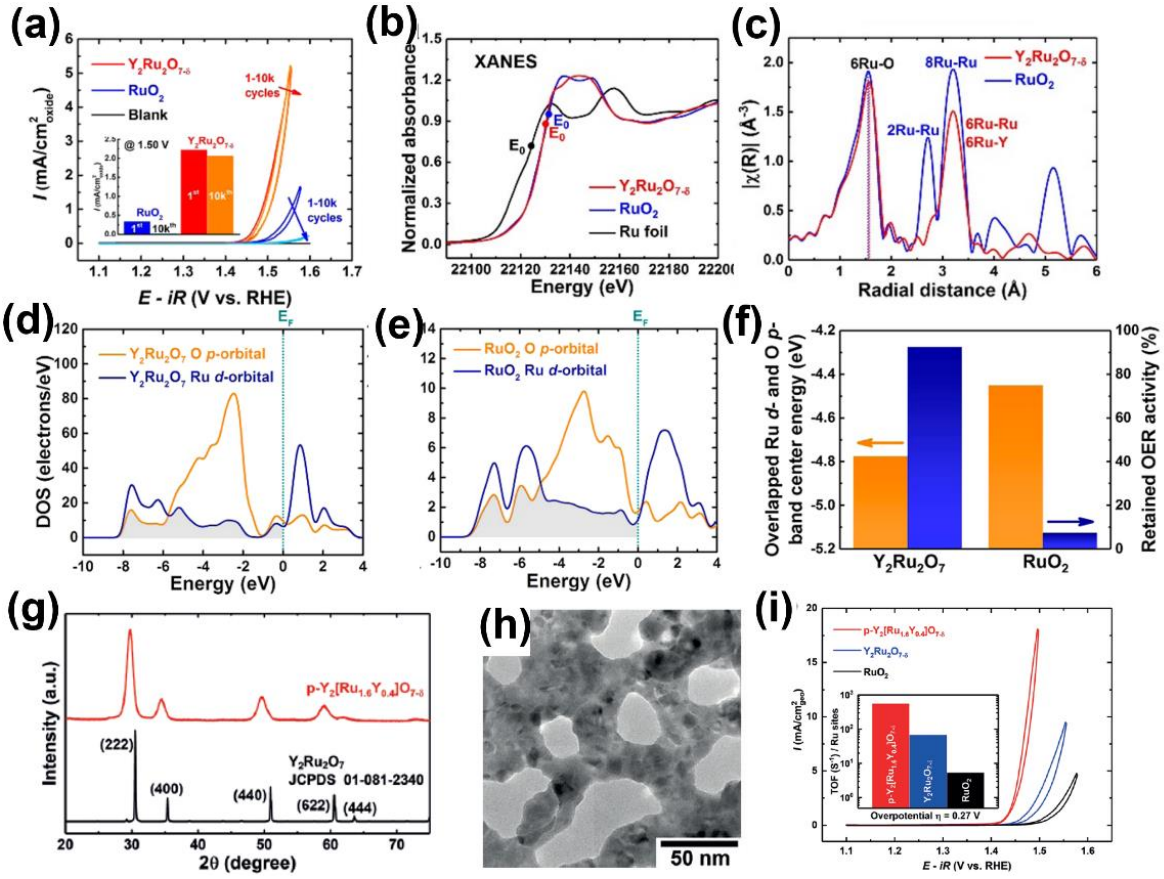

Figure 18. a) CV curves of the 1st and 10 000th cycles of $Y_2Ru_2O_{7-\delta}$ and RuO_2 for OER in strong acid solution, in which the insert is a comparison of current densities at the applied potential of 1.5 V vs RHE. **b)** XANES data of Ru K-edge and **c)** Fourier-transformed EXAFS results of Ru edge for $Y_2Ru_2O_{7-\delta}$, RuO_2 and Ru foil. **d**, **e)** Computed DOS results of Ru 4d and O 2p orbitals for the two samples of $Y_2Ru_2O_{7-\delta}$ **(d)** and RuO_2 **(e)**. **f)** Comparison of overlapped Ru 4d-band and O 2p-band center energy and residual activity after stability test for $Y_2Ru_2O_{7-\delta}$ and RuO_2 catalysts, respectively. Reproduced with permission.[237] Copyright 2017, American Chemical Society. **g)** XRD patterns and **h)** TEM images of porous $Y_2[Ru_{1.6}Y_{0.4}]O_{7-\delta}$ obtained at room temperature. **i)** CV curves toward OER for porous $Y_2[Ru_{1.6}Y_{0.4}]O_{7-\delta}$, $Y_2Ru_2O_{7-\delta}$ and RuO_2 electrocatalysts in O_2-saturated 0.1 M $HClO_4$. Insert displayed the comparison of the corresponding TOFs of these samples at the overpotential of 0.27 V. Reproduced with permission.[238] Copyright 2018, Wiley-VCH.

In 2014, according to Chang et al., different oriented $SrRuO_3$ thin films were constructed as OER electrocatalysts in alkaline solution.[21] The experimental results disclosed that the OER activities increased in the sequence of (001) < (110) < (111), inversely proportional to their stability. Such activity and stability results were dominated by the transformation of stable but inactive Ru^{4+} to unstable but active $Ru^{n>4+}$ which was induced by the OER operating potential. Later, Akbashev and his co-

workers designed a perovskite heterostructure with an ultrathin $SrRuO_3$ layer covered with an ultrathin $SrTiO_3$ layer. It was found that the OER-insert $SrTiO_3$ was activated by such little $SrRuO_3$ (one unit cell) and the ultrathin $SrTiO_3$ (two unit cells) helped to suppress corrosion of OER-active $SrRuO_3$.[244] A while ago, our group also demonstrated that layered Ruddlesden-Popper oxide, Sr_2RuO_4, is highly efficient for HER in alkaline solution.[29] To drive the 10 mA cm^{-2}, it needed a low overpotential of only 61 mV, which was significantly smaller than that of perovskite-type $SrRuO_3$ (101 mV) and RuO_2 (95 mV) samples. More significantly, relative to RuO_2, the TOF value for $SrRuO_3$ exhibited more than a 10-fold improvement. On basis of theoretical and experimental analyses, such superior performance was possibly due to a synergy between the rock-salt layer and perovskite layer in this unusual layered structure, where water dissociation was first accelerated by the SrO-terminated surface in the former, and subsequently the apical oxygen site in the latter promoted favorable H intermediate adsorption and H_2 evolution.

Very recently, hexagonal ruthenate nanosheets were synthesized by exfoliating the proton exchanged $NaRuO_2$.[247] From representative TEM images in **Figure 19**c, translucent nanosheets were observed, indicating the ultrathin thickness. When employing such nanosheets as OER electrocatalysts in acidic medium, it manifested significant activities with a small overpotential of ~255 mV and Tafel slope of 38 mV dec^{-1} as well as the robustness in the harsh environment, outperforming the rutile-structure RuO_2 (**Figure 19**a and b). Moreover, no obvious oxidation and morphology change occurred after a prolonged stability test. Further DFT calculations corroborated that the edges of nanosheets were the highly active region for OER (**Figure 19**d and e).

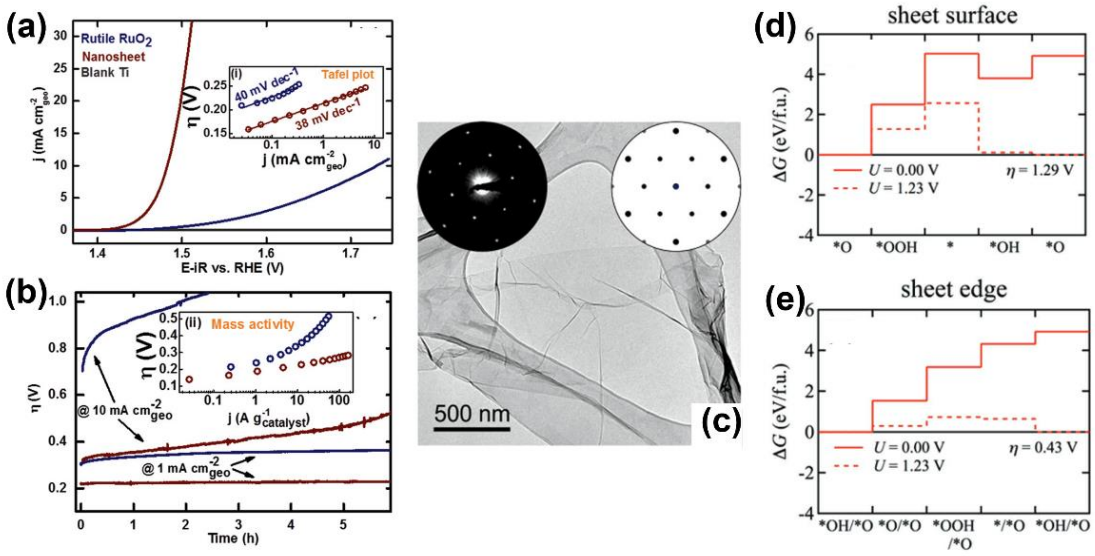

Figure 19. a) OER polarization curves and the corresponding Tafel plots (insert), and **b)** chronopotentiometry durability tests and mass activity (insert) of hexagonal ruthenate nanosheets and rutile-structure RuO_2 in 0.1 M $HClO_4$ electrolytes. **c)** The TEM image of the ultrathin nanosheet. **d)** Free energy diagram of the overall OER pathways at the 3f site of the ruthenate nanosheet surface and **e)** at the Ru_{cus} site of the ruthenate nanosheet edge. Reproduced with permission.[247] Copyright 2019, Wiley-VCH.

3.3. Ru phosphides, sulfides, or selenides

3.3.1. Ru phosphides. Owing to the analogous operation mechanism between the hydrodesulfurization (HDS) reaction and HER, transition metal phosphides (TMPs), which were highly efficient for HDS, have attracted a considerable attention in electrocatalytic hydrogen generation recently.[9] Pioneering works have demonstrated that cobalt phosphides (CoP_x), nickel phosphides (NiP_x), iron phosphides (FeP_x), molybdenum phosphides (MoP_x), etc, showed the excellent HER catalytic behavior, but they were far from satisfactory when comparing with the state-of-art Pt/C.[16, 248-250] In particular, in recent three years, ruthenium phosphides (RuP_x), a novel material for HER, has been widely investigated, which offered a Pt-like or even Pt-outperformed performance in the aqueous solutions with almost all pH values.[30, 251-253]

In 2017, Mu's group first corroborated that a RuP_2-based composite was an extremely active and pH-universal HER electrocatalyst.[251] In this study, RuP_2 nanoparticles encapsulated by N, P co-doped carbon (RuP_2@NPC) were fabricated by facile one-pot pyrolysis with phytic acid (PA), melamine, and ruthenium chloride as precursors. **Figure 20**a describes the synthetic procedure, where RuPA complexes were first formed via cross-linking PA and ruthenium ions, and then were annealed with melamine at 900°C for 2 h under an inert atmosphere. When working as an electrocatalyst for hydrogen production, this composite presented a Pt-like activity, delivering the current density of 10 mA cm^{-2} at the low overpotentials of 38, 52, and 57 mV in acidic, alkaline and neutral media, respectively (**Figure 20**b-d). Besides, superior stability was also demonstrated with unobservable activity loss after 2000 cyclic voltammetry measurements. Other ruthenium phosphides phases, such as RuP and Ru_2P, also showed the remarkable HER performance.[30, 253-255] For instance, our group designed the RuP nanoparticles by a low-temperature phosphatization strategy and identified it as a super HER electrocatalyst in a wide range of pH.[30] Of note, it was found that large RuP nanoparticles offered surprisingly higher intrinsic activity and stability than the small one, which could be attributed to the stabilization of P species because of the lowered surface energy for large particles. Liu et al. reported the preparation of ultrafine Ru_2P nanoparticles loaded on reduced graphene oxide nanosheets and described their HER performance in both 1 M KOH and 0.5 m H_2SO_4 electrolytes.[254] To evaluate the effects of P atomic amount in RuP_x on the HER catalytic behavior, several researchers controllably produced morphologically equivalent RuP

and RuP_2 samples, and all of them found that RuP performed better than RuP_2.[256, 257] Chang et al. proposed that such enhancement was due to higher conductivity and more catalytically active sites in RuP relative to RuP_2, while, by applying theory calculation, Ge et al. confirmed that RuP with a higher charge density at the Ru site was more favorable for the H chemisorption, so as to display higher HER activity than RuP_2.[256, 257] Furthermore, some mixed RuP_x phases were also developed as highly efficient HER catalysts. Chi and his co-workers introduced a composite of Ru_2P and RuP_2 mixture wrapped in N, P dual-doped carbon nanospheres (RuP_x@NPC).[258] According to TEM images, the as-obtained sample had a core-shell hollow structure with an ultrathin carbon layer, of only about 30 nm, and ultrasmall RuP_x nanoparticles with an average diameter of ~ 4 nm were homogeneously distributed on carbon matrix. Such structure provided a large surface area, inhibited aggregation and stack of ultrafine RuP_x nanoparticles, and regulated electronic structure, thereby leading to outstanding HER performance.

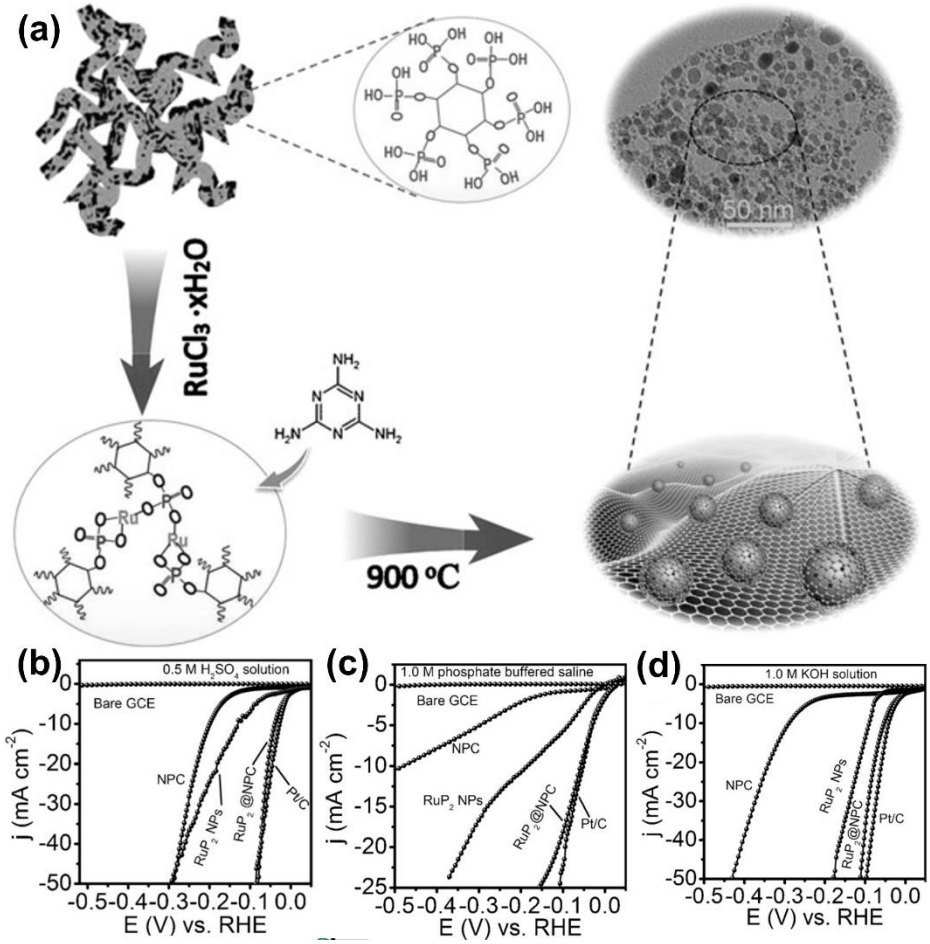

Figure 20. a) The schematic synthesis route of RuP_2@NPC catalyst. **b-d)** LSV curves of RuP_2@NPC and other control samples for HER in 0.5 M H_2SO_4 **(b)**, 1 M PBS **(c)**, and 1 M KOH **(d)** aqueous solution. Reproduced with permission.[251] Copyright 2017, Wiley-VCH.

3.3.2. Ru sulfides and selenides. Furthermore, several ruthenium chalcogenides (RuS_x or $RuSe_x$) have been also explored as promising HER electrocatalysts.[259, 260] For example, Wang et al. created a hybrid of crystalline $Ru_{0.33}Se$ nanoparticles deposited on TiO_2 nanotube arrays ($Ru_{0.33}Se$/TNA), which offered extraordinary HER electrocatalytic activity in alkaline solution, yielding a current density of 10 mA cm^{-2} at a small overpotential of 57 mV.[259] Our group successfully synthesized spherical RuS_2 on S-doped reduced graphene oxide (s-RuS_2/S-rGO) with remarkable HER performance in all-pH conditions by using a facile solvothermal process and subsequent

low-temperature heat treatment.[260] Especially, the s-RuS_2/S-rGO hybrid exhibited a low overpotential of 25 mV to reach 10 mA cm^{-2} and a small Tafel slope of 29 mV dec^{-1}, as well as robust 100-h stability in 1 M KOH electrolyte. To unveil the intrinsic origins for such superior alkaline HER activity, the HER reaction pathways on both RuS_2 and benchmark Pt were studied via using DFT calculations. According to these results, RuS_2 showed a comparable water dissociation ability and adsorption free energy of hydrogen intermediates ($\triangle G_{H^*}$) to Pt, confirming its excellent activity toward HER. Besides, Further hybridization with carbon substrate enabled s-RuS_2/S-rGO with the increased surface area, improved charge transport, and a strong coupling effect between RuS_2 and S-rGO, thus greatly promoting the HER catalytic activity. Apart from Ru phosphides, sulfides and selenides, a recent work by Li et al. compared the HER activities among different metal diborides (MB_2), and demonstrated RuB_2 as the most active one among them due to a suitable *d*-band center and a large density of efficient active centers .[261]

3.4. Other Ru-related derivative catalysts

3.4.1. Ru dopants. Ruthenium (Ru), as heteroatom dopants, have been introduced into many host materials, such as NiFe-layered double hydroxide (NiFe-LDH), nickel phosphide (Ni_2P), molybdenum carbide (Mo_2C), titanium dioxide (TiO_2), iridium oxide (IrO_2) etc.[262-269] Driven by the chemical synergism between the Ru dopant and host compound, some chemical properties and electronic structures for the original materials are engineered and optimized, thereby which are promising to show the enhanced electrocatalytic activity toward OER or HER. Liyanage and his co-workers confirmed

that doping Ru atoms into Ni_2P could activate the electron of Ni and accelerate the oxidation of Ni, so as to lower the OER kinetic reaction barrier, eventually enhancing the OER activity of Ni_2P.[264] Chen et al. found that the incorporation of Ru into NiFe-LDH might promote the electrochemical hydrogen production in 1 M KOH electrolyte, substantially reducing the overpotential from 188 mV to 29 mV at a current density of 10 mA cm^{-2}, which also outperformed that of Pt/C and most of the as-reported electrocatalysts (**Figure 21**a and b).[262] According to control experiments and DFT calculations, such enhancement should be ascribed to the decrease of water dissociation energy barrier in the Volmer step after Ru introduction (**Figure 21**c and d), thereby accelerating its HER process. Besides, due to the remained high OER performance after Ru doping from NiFe-LDH, the obtained NiFeRu-LDH was simultaneously utilized as both anodic and cathodic catalysts in an alkaline electrolyzer, which offer the small cell voltage of 1.52 V to attain 10 mA cm^{-2}, much superior to the benchmark couple of Pt/C and Ir/C (**Figure 21**e). Nong et al. further prepared the Ru-doped TiO_2 via a one-step corroding route with perovskite $SrTi_{1-x}Ru_xO_3$ as the precursor.[266] Based on physical characterizations like X-ray photoelectron spectroscopy (XPS) and electron paramagnetic resonance spectroscopy (EPR), it was the first time to observe that the Ru ion was pentavalent while partial Ti received one electron from Ru and became Ti^{3+} in the Ru-doped TiO_2 sample, and such electron structure brought about the appropriate Gibbs free energies for hydrogen adsorption in an HER process, thus achieving better HER performance relative to undoped counterpart.

3.4.2. Ru-based molecule metallopolymer. Last but not least, some researchers also have reported Ru metal-organic molecule polymers as promising OER or HER catalysts and proposed that the structural and electronic properties of the metal active sites can be effectively tuned by various organic ligands.[270-274] In 2009, Yoshida et al. found that $[Ru(tmtacn)(R_2bpy)(OH_2)]^{2+}$ (tmtacn = 1,4,7-trimethyl-1,4,7-triazacyclononane; R_2bpy = 4,4'-disubstituted-2,2'-bipyridines, R=H, Me, and OMe) was active toward OER, and R_2bpy with stronger electron-donating ability lead to a superior O_2-evolving activity.[270] Such molecule chemistry not only reduce the usage of Ru metal but also offer more possibilities for the stabilization of Ru metal. Millet's group developed two different ruthenium-based molecular complexes of [Ru(tpy)(bpy)(OH)] (tpy was 2,2'-6',2''-terpyridine and bpy was 2,2'-bipyridine) and [Ru(tpy)(bpm)(OH)] (bpm was 2,2'-bipyrimidine) (**Figure 21**f) as acidic OER electrocatalysts. They exhibited a significant electrochemical activity and sustained sufficient stability under highly oxidative conditions.[271] For hydrogen-generating behavior, Udachyan et al. reported the synthesis of thin film Ru ions involving triazine-trithiolate polymers chemically bounded on the copper substrate.[272] When being regarded as HER electrocatalysts in acidic electrolytes, this metallopolymer presented excellent activity, such as low overpotential of around 150 mV to reach 10 mA cm^{-2}, high exchange current density, and large double-layer capacitance, along with long-term stability. Such high HER performance could be mainly ascribed to the protonation ability of redox active Ru metal centers and the uncoordinated ligand centers (N and S).

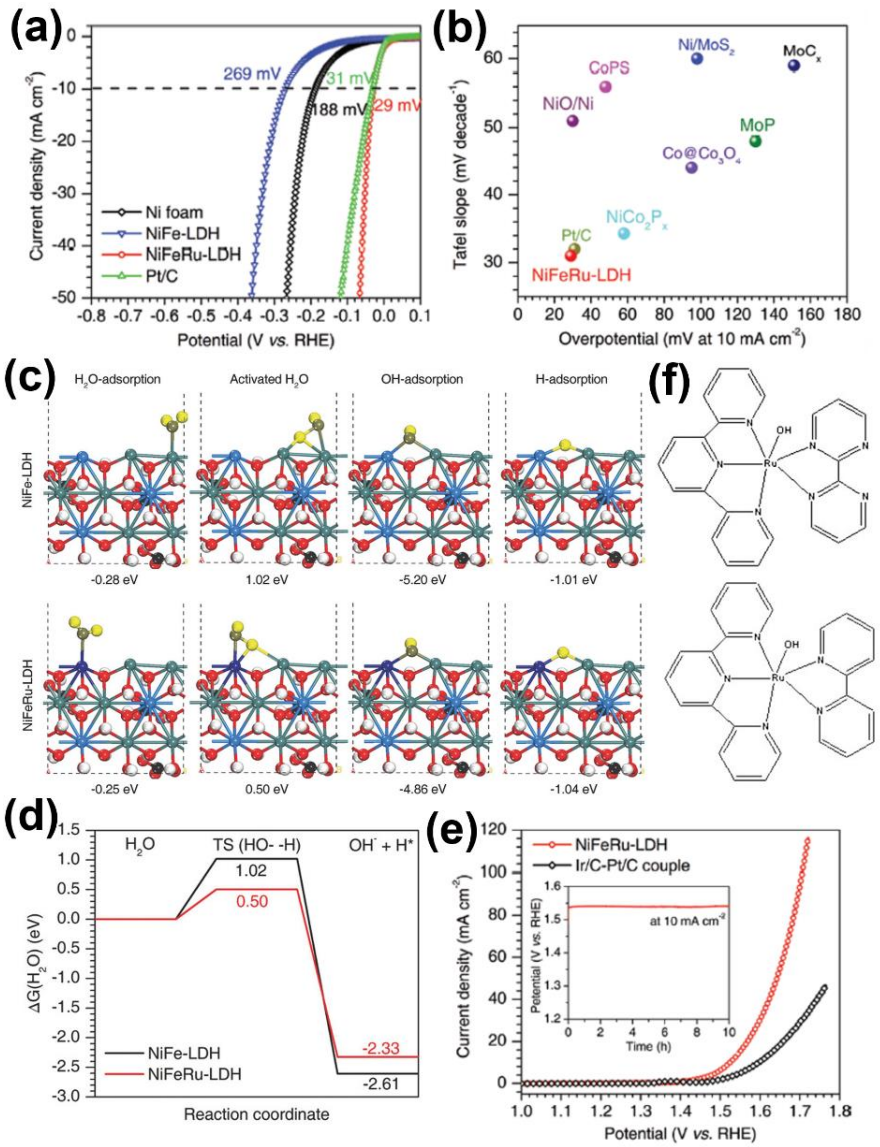

Figure 21. a) HER polarization curves of NiFeRu-LDH, NiFe-LDH, Ni foam, and benchmark Pt/C in alkaline solution. **b)** Comparison of overpotentials at 10 mA cm^{-2} and Tafel slopes for the designed NiFeRu-LDH and many reported state-of-the-art catalysts toward HER in 1 M KOH. **c)** Computed free energies of H_2O adsorption, H_2O activation, OH intermediate adsorption, and H intermediate adsorption on NiFe-LDH and NiFeRu-LDH surface. **d)** Comparison of adsorption free-energy diagrams for the first water-splitting step (Volmer) on the surface of NiFeRu-LDH and NiFe-LDH. **e)** Overall water-splitting activity based on LSV curves for NiFeRu-LDH and Ir/C-Pt/C, and Chronopotentiometry tests of NiFeRu-LDH electrocatalysts at the current density of 10 mA cm^{-2} over 10 h. Reproduced with permission.[262] Copyright 2018, Wiley-VCH. **f)** Chemical structure of [Ru(tpy)(bpy)(OH)] (left) and [Ru(tpy)(bpm)(OH)] (right). Reproduced with permission.[271] Copyright 2013, Elsevier.

4. EVALUATING THE OVERALL WATER SPLITTING OF RU-BASED ELECTROCATALYSTS WITH OTHERS

According to the above-mentioned discussion, numerous Ru-based electrocatalysts with bifunctionality have been explored and demonstrated their outstanding overall catalytic behavior toward water electrolysis, as summarized in **Table 3**, most of which are obviously superior to that of various other representative bifunctional materials for overall water splitting in **Table 4**. Especially, the cell voltage to achieve a current density of 10 mA cm^{-2} in the water-splitting electrolyzer, and the operating stability including chronoamperometry or chronopotentiometry were compared.

Table 3 Summary of representative Ru-based electrocatalysts toward overall water splitting.

Materials (Cathode-Anode)	Electrolytes	Loading (mg cm^{-2})	Overall voltage (V) at 10 mA cm^{-2}	Stability (V or mA cm^{-2}@h)	Reference
Ru nanosheet-RuO_2 nanosheet	0.5 M H_2SO_4	Not given	1.53	1.53 V @ 7000s	[20]
Ru_2Ni_2 SNs	1 M KOH	3	1.45@ onset potential	10 mA cm^{-2} @40h	[124]
S-400-H	1 M KOH	0.285	1.47	1.475 V @~11.1h	[125]
Ru-HPC-p-RuO_2	1 M KOH	0.4	1.53	1.7 V @2h	[137]
hydrous RuO_2-crystalline RuO_2	1 M KOH	0.52	1.503	Not given	[167]
IrO_2-RuO_2@Ru (3:1)-Pt/C	0.5 M H_2SO_4	1	1.489	Not given	[193]
Ni-doped RuO_2 NWs-Co-doped RuO_2 NWs	0.5 M H_2SO_4	Not given	1.537	1.537 V @12h	[28]
	1 M KOH	Not given	1.542	1.542 V @12h	
1D-RuO_2-CN_x	1 M KOH	Not given	1.59@ 20 mA cm^{-2}	1.53 V @3h	[14]
RuO_2/N-C	1 M KOH	0.5	1.507	1.55 V @12h	[233]
L-RP/C-L-RO/C	1 M KOH	8	1.49	10 mA cm^{-2} @50h	[30]
s-RuS_2/S-rGO- RuO_2/C	1 M KOH	5	1.54@ 20 mA cm^{-2}	20 mA cm^{-2} @24h	[260]
NiFeRu-LDH	1 M KOH	Not given	1.52	10 mA cm^{-2} @10h	[262]

Table 4 Summary of other representative bifunctional electrocatalysts toward overall water splitting.

Materials (Cathode-Anode)	Electrolytes	Loading (mg cm^{-2})	Overall voltage (V) at 10 mA cm^{-2}	Stability (V or mA cm^{-2}@h)	Reference
CoP@a-CoOx plate/C	1 M KOH	5	1.66	10 mA cm^{-2} @30h	[16]
Pt/C-IrO_2/C			1.59		
Pt-CoS_2/CC	1 M KOH	Not given	1.55	10 mA cm^{-2} @20h	[275]
Pt-NiFe LDH-ht	1 M KOH	0.205	1.505	20 mA cm^{-2} @8h	[276]
Ir_6Ag_9NTs/C	0.5 M H_2SO_4	13.3 μg_{Ir} cm^{-2}	1.55	5 mA cm^{-2} @30h	[277]
IrW/C	0.5 M H_2SO_4	30 μg_{Ir} cm^{-2}	1.48	10 mA cm^{-2} @8h	[278]

	1 M KOH		1.50 @ onset potential	Not given	
	1 M PBS		1.55 @ onset potential	Not given	
SNCF-NRs	1 M KOH	3	1.68	10 mA cm^{-2} @ 30h	[279]
$FeNi_3N$/NF	1 M KOH	Not given	1.62	10 mA cm^{-2} @ 400h	[280]
Ir/MoS_2/CF	1 M KOH	Not given	1.57	Not given	[281]
Co_3Se_4	1 M KOH	2.6	1.59	100 mA cm^{-2} @28h	[282]
FeB_2	1 M KOH	Not given	1.57	10 mA cm^{-2} @24h	[283]
$Co_{0.9}S_{0.58}P_{0.42}$	1 M KOH	Not given	1.59	10 mA cm^{-2} @ 10h	[284]
MoP/NF	1 M KOH	Not given	1.62	10 mA cm^{-2} @20h	[285]
Ni/Mo_2C-PC	1 M KOH	2	1.66	1.74 V @ 10h	[286]

5. CONCLUSION AND PROSPECTIVE

Overall, this review highlights the recent advances of some major kinds of Ru-related materials toward OER, HER, or overall water electrolysis in pH-universal electrolytes. **Tables 1**, **2**, and **3** compare their electrocatalytic performance. RuO_2, due to the optimal bonding force to oxygen intermediate species, has been regarded as the most active OER catalysts in both alkaline and acidic electrolytes. However, owing to dissolution from the excessive oxidation at a high overpotential of above 1.4 V during the OER process, RuO_2 was extremely unstable. Currently, many traditional metal-based oxides or hydroxides with low cost and abundant reserves, such as perovskite oxides, NiFe hydroxides, etc., offered super OER activity and stability in alkaline solutions, which was totally comparable to or even superior to RuO_2. Thus, considering both the performance and economy at the same time, RuO_2, as the alkaline OER electrocatalysts, may not be the best choice. Nevertheless, in acidic solutions, the development of traditional metal-based electrocatalysts was largely limited by acid-dissolution properties, and thus the excellent OER electrocatalysts in acidic media still relied on few acid-resisting Ru or Ir-based noble metals. Although RuO_2 suffered from unstable

issues, the stability and activity could be further largely enhanced on the basis of further structure optimization and design for RuO_2, which were extensively reported in many studies. Therefore, RuO_2-based materials as acidic OER catalysts can be regarded as a good choice. When referring to metallic Ru, it shows greater potential in hydrogen generation in the electrolytes with a wide pH range. Previous DFT results have revealed pure Ru metal has a moderate hydrogen-adsorption free energy value (slightly larger than that of benchmark Pt), suggesting the outstanding HER performance in acidic media. However, in alkaline electrolytes, the dissociation of water first occurred in the HER process, and thus the overall alkaline HER was significantly affected by the difficult cleavage of H-OH bonds. According to the previous study, the pure Ru metal has a lower water dissociation free energy barrier in comparison with Pt, indicating the superiority of Ru metal toward alkaline HER. Besides, more significantly, most of HER catalysts only perform well in acidic media due to the limitation of difficult water dissociation. Thus, in a word, Ru is a good choice in pH-universal electrolytes. Furthermore, through various tuning methods to optimize the electronic structure of Ru, including phase and morphology control, doping, building hybrids, forming phosphides or sulfide, etc., the HER performance can be significantly improved. In the main part, we pay more attention to these proposed guidance and design strategies for developing highly efficient electrocatalysts and optimizing electrocatalytic performance. With different synthetic routes, diversified morphologies with a large specific area (eg. nanorods, nanosheets, nanofilm, nanoparticles with various sizes, mesoporous structure, etc.) were obtained, thereby augmenting catalytic active sites. The phase structure, like

hcp Ru and fcc Ru, as well as amorphous form, or crystal facets and thermal treatment ways were also tuned to optimize HER and OER activity, respectively. Besides, introducing alien metal atoms like Ir, Pt, Co, Ni, Mo, Cu, Sn, etc. into Ru metal and RuO_2, or Ru as dopants, incorporated into other host matrixes (eg. Mo_2C, TiO_2, Ni_2P, MoS_2, etc.) could modulate the lattice parameters and electronic structure, so as to aggrandize their catalytic properties. Furthermore, the constructed hybrid structures by assembling Ru/RuO_2 with another component can strengthen the catalytic behavior (activity or stability) owing to the synergy between the coupling components. Among them, several bifunctional heterostructures catalysts toward efficient OER and HER enable the simple fabrication of a water electrolyzer system. Integration with conductive carbon substrates can lead to satisfied conductivity and inhibit metal aggregation, offering more exposed active sites. Despite the universality of these strategies in improving both OER and HER activity, it should be noted that pure Ru or RuO_2 could be easily oxidized to soluble RuO_4 under OER condition and thus was extremely unstable. Accordingly, in order to alleviate this issue, these above-mentioned modulation methods for OER were applied to slow down Ru dissolution and enhance stability. Pyrochlore-type oxides are demonstrated to be highly stable for OER. Last but not the least, in recent years, lots of novel materials based on Ru phosphides, sulfides, selenides, borides or metal-organic molecule polymers show promising applications in catalyzing OER/HER due to special Ru active centers.

Despite such significant progress, several challenges for the field are still available, and there is still a big room for flourishing, as outlined below. (1) *Expected bifunctional*

catalytic behavior. Typically, Ru oxides-based materials have been intensively exploited as OER catalysts, while Ru metal or Ru phosphides, sulfides and selenides-related catalysts have greater potential in hydrogen generation. Only very limited Ru-involving materials can efficiently catalyze both OER and HER at the same time, and ideal bifunctional electrocatalysts are still yet to be achieved. Thus, to simplify construction of an electrolyzer and reduce its manufacturing costs, more efforts are still needed to develop bifunctional electrocatalysts toward both OER and HER, for instance fabricating more composites via integrating different OER-active components with HER-active materials or exploring more novel regulation strategies to activate the other relatively inert reaction (eg. HER for RuO_2, OER for RuP, RuS_2, etc.), eventually realizing bifunctionality. (2) *Stability issues.* Apart from activity, stability is another crucial requirement for practical applications. For Ru oxides or Ru metal, numerous works have demonstrated their improved stability during the OER process, but they are still far from sufficient. Therefore, a further thorough understanding of the activity degradation via exploiting multiple novel and combined techniques is highly urgent, which would give a scientific guideline for the design of efficient and durable electrocatalysts. Especially, the optimization of pyrochlore or perovskite-type oxides offered more possibilities due to their flexible and robust structure. (3) *Advanced Characterization techniques.* Though extensive Ru-based materials have been reported as good OER or HER catalysts, in-depth identification of the underlying mechanism including the authentic catalytic active sites, dopant interactions, and the synergistic effect between different components is still lacking, which is a challenging task.

Therefore, the development of some advanced in-situ techniques such as Operando X-ray absorption spectroscopy (XAFS), in-situ XRD, TEM, and Raman, etc. is necessary to detect the real-time and atomic-level changes of the valence state, structure, composite, morphology, defects, etc., consequently revealing the real active sites and intermediates, and deepening the understanding about the role of each component in these materials. In such in-situ techniques, particularly XAFS analysis offer a suitable investigation means, which is able to capture the dynamic electronic structure and local coordination environment of the catalyst during the reaction. Additionally, closely linking the experimental works with the mathematical efforts based on the first-principles density functional theory (DFT) calculations will better unveil the electrochemical process in Ru-based materials. (4) *Wide pH applicability.* Despite that Ru-based catalysts are mostly applicable to a broad range of pH for separated OER or HER, to date, almost all known Ru-related materials for HER-OER bifunctional catalysis are commonly operated in alkaline or acidic (PEM) electrolyzers. Nevertheless, such electrolyzers were restrained by plenty of inherent drawbacks, such as relatively high energy consumption, expensive installation/maintenance, severe causticity, etc. In order to avoid these problems, neutral electrolytes are more desirable. Consequently, exploring effective and stable catalysts in neutral media should be actively pursued. (5) *Highly desired practical application:* To push these electrocatalysts toward industrial applications in practical water electrolysis, aside from aforementioned aspects, several other significant breakthroughs are also of vital need, including: further minimizing the noble Ru loading while keeping perfect water-

splitting behavior; developing a scalable and simple electrocatalyst synthetic approach to enable mass production; and constructing free-standing catalysts with 3D hierarchical structure, which gets rid of obstacle of the binder on charge transfer and brings about more active sites.

In a word, along with the continuous development and inputs in material science and thorough comprehending of Ru-related materials and even others, we believe more significant opportunities for many efficient electrocatalysts and their commercial utilization in energy-related systems will certainly be provided on a larger scale in the coming future.

AUTHOR INFORMATION

Corresponding Author

*E-mail: bsmengni@polyu.edu.hk (Meng Ni).

*E-mail: shaozp@njtech.edu.cn (Zongping Shao).

Notes

The authors declare no competing financial interest.

ACKNOWLEDGMENTS

M. Ni thanks the funding support (Project Number: PolyU 152214/17E) from Research Grant Council, University Grants Committee, Hong Kong SAR.

REFERENCES

(1) Chu, S.; Majumdar, A. Opportunities and Challenges for A Sustainable Energy Future. *Nature* **2012**, *488*, 294-303.

(2) Chu, S.; Cui, Y.; Liu, N. The Path Towards Sustainable Energy. *Nat. Mater.* **2017**, *16*, 16-22.

(3) Yu, J.; Chen, G.; Sunarso, J.; Zhu, Y.; Ran, R.; Zhu, Z.; Zhou, W.; Shao, Z. Cobalt Oxide and Cobalt-Graphitic Carbon Core-Shell Based Catalysts with Remarkably High Oxygen Reduction Reaction Activity. *Adv. Sci.* **2016**, *3*, 1600060.

(4) Seh, Z. W.; Kibsgaard, J.; Dickens, C. F.; Chorkendorff, I. B.; Norskov, J. K.; Jaramillo, T. F. Combining Theory and Experiment in Electrocatalysis: Insights into Materials Design. *Science* **2017**, *355*, 4998.

(5) Katsounaros, I.; Cherevko, S.; Zeradjanin, A. R.; Mayrhofer, K. J. J. Oxygen Electrochemistry as A Cornerstone for Sustainable Energy Conversion. *Angew. Chem. Int. Ed.* **2014**, *53*, 102-121.

(6) Zeng, K.; Zhang, D. Recent Progress in Alkaline Water Electrolysis for Hydrogen Production and Applications. *Prog. Energ. Combust.* **2010**, *36*, 307-326.

(7) Zou, X. X.; Zhang, Y. Noble Metal-Free Hydrogen Evolution Catalysts for Water Splitting. *Chem. Soc. Rev.* **2015**, *44*, 5148-5180.

(8) Gao, Q. S.; Zhang, W. B.; Shi, Z. P.; Yang, L. C.; Tang, Y. Structural Design and Electronic Modulation of Transition-Metal-Carbide Electrocatalysts toward Efficient Hydrogen Evolution. *Adv. Mater.* **2019**, *31*, 1802880.

(9) Shi, Y. M.; Zhang, B. Recent Advances in Transition Metal Phosphide Nanomaterials: Synthesis and Applications in Hydrogen Evolution Reaction. *Chem. Soc. Rev.* **2016**, *45*, 1529-1541.

(10) Xiong, B. Y.; Chen, L. S.; Shi, J. L. Anion-Containing Noble-Metal-Free Bifunctional Electrocatalysts for Overall Water Splitting. *ACS Catal.* **2018**, *8*, 3688-3707.

(11) Jamesh, M. I. Recent Progress on Earth Abundant Hydrogen Evolution Reaction and Oxygen Evolution Reaction Bifunctional Electrocatalyst for Overall Water Splitting in Alkaline Media. *J. Power Sources* **2016**, *333*, 213-236.

(12) Jiang, K.; Wang, H. Electrocatalysis over Graphene Defect-Coordinated Transition-Metal Single-Atom Catalysts. *Chem* **2018**, *4*, 194-195.

(13) Li, K.; Li, Y.; Wang, Y.; Ge, J.; Liu, C.; Xing, W. Enhanced Electrocatalytic Performance for the Hydrogen Evolution Reaction Through Surface Enrichment of Platinum Nanoclusters Alloying with Ruthenium in Situ Embedded in Carbon. *Energy Environ. Sci.* **2018**, *11*, 1232-1239.

(14) Bhowmik, T.; Kundu, M. K.; Barman, S. Growth of One-Dimensional RuO_2 Nanowires on g-Carbon Nitride: An Active and Stable Bifunctional Electrocatalyst for Hydrogen and Oxygen Evolution Reactions at All pH Values. *ACS Appl. Mater. Interfaces* **2016**, *8*, 28678-28688.

(15) Du, X. C.; Huang, J. W.; Zhang, J. J.; Yan, Y. C.; Wu, C. Y.; Hu, Y.; Yan, C. Y.; Lei, T. Y.; Chen, W.; Fan, C.; Xiong, J. Modulating Electronic Structures of Inorganic Nanomaterials for Efficient Electrocatalytic Water Splitting. *Angew. Chem. Int. Ed.* **2019**, *58*, 4484-4502.

(16) Yu, J.; Zhong, Y.; Wu, X.; Sunarso, J.; Ni, M.; Zhou, W.; Shao, Z. Bifunctionality from Synergy: CoP Nanoparticles Embedded in Amorphous CoO_x Nanoplates with Heterostructures for Highly Efficient Water Electrolysis. *Adv. Sci.* **2018**, *5*, 1800514.

(17) Zheng, Y.; Jiao, Y.; Zhu, Y. H.; Li, L. H.; Han, Y.; Chen, Y.; Jaroniec, M.; Qiao, S. Z. High Electrocatalytic Hydrogen Evolution Activity of an Anomalous Ruthenium Catalyst. *J. Am. Chem. Soc.* **2016**, *138*, 16174-16181.

(18) Higgins, S. Regarding Ruthenium. *Nat. Chem.* **2010**, *2*, 1100-1100.

(19) Li, Y. T.; Zhang, L. A.; Qin, Y.; Chu, F. Q.; Kong, Y.; Tao, Y. X.; Li, Y. X.; Bu, Y. F.; Ding, D.; Liu, M. L. Crystallinity Dependence of Ruthenium Nanocatalyst toward Hydrogen Evolution Reaction. *ACS Catal.* **2018**, *8*, 5714-5720.

(20) Kong, X. K.; Xu, K.; Zhang, C. L.; Dai, J.; Oliaee, S. N.; Li, L. Y.; Zeng, X. C.; Wu, C. Z.; Peng, Z. M. Free-Standing Two-Dimensional Ru Nanosheets with High Activity toward Water Splitting. *ACS Catal.* **2016**, *6*, 1487-1492.

(21) Chang, S. H.; Danilovic, N.; Chang, K. C.; Subbaraman, R.; Paulikas, A. P.; Fong, D. D.; Highland, M. J.; Baldo, P. M.; Stamenkovic, V. R.; Freeland, J. W.; Eastman, J. A.; Markovic, N. M. Functional Links between Stability and Reactivity of Strontium Ruthenate Single Crystals during Oxygen Evolution. *Nat. Commun.* **2014**, *5*, 4191.

(22) Rao, R. R.; Kolb, M. J.; Halck, N. B.; Pedersen, A. F.; Mehta, A.; You, H.; Stoerzinger, K. A.; Feng, Z. X.; Hansen, H. A.; Zhou, H.; Giordano, L.; Rossmeisl, J.; Vegge, T.; Chorkendorff, I.; Stephens, I. E. L.; Shao-Horn, Y. Towards Identifying the Active Sites on RuO_2(110) in Catalyzing Oxygen Evolution. *Energy Environ. Sci.* **2017**, *10*, 2626-2637.

(23) Salvatore, D. A.; Pena, B.; Dettelbach, K. E.; Berlinguette, C. P. Photodeposited Ruthenium Dioxide Films for Oxygen Evolution Reaction Electrocatalysis. *J. Mater. Chem. A* **2017**, *5*, 1575-1580.

(24) Shan, J. Q.; Guo, C. X.; Zhu, Y. H.; Chen, S. M.; Song, L.; Jaroniec, M.; Zheng, Y.; Qiao, S. Z. Charge-Redistribution-Enhanced Nanocrystalline Ru@IrO_x Electrocatalysts for Oxygen Evolution in Acidic Media. *Chem* **2019**, *5*, 445-459.

(25) Galizzioli, D.; Tantardini, F.; Trasatti, S. Ruthenium Dioxide: A New Electrode Material. II. Non-Stoichiometry and Energetics of Electrode Reactions in Acid Solutions. *J. Appl. Electrochem.* **1975**, *5*, 203-214.

(26) Lu, Q. P.; Wang, A. L.; Cheng, H. F.; Gong, Y.; Yun, Q. B.; Yang, N. L.; Li, B.; Chen, B.; Zhang, Q. H.; Zong, Y.; Gu, L.; Zhang, H. Synthesis of Hierarchical 4H/fcc Ru Nanotubes for Highly Efficient Hydrogen Evolution in Alkaline Media. *Small* **2018**, *14*, 1801090.

(27) Mahmood, J.; Li, F.; Jung, S. M.; Okyay, M. S.; Ahmad, I.; Kim, S. J.; Park, N.; Jeong, H. Y.; Baek, J. B. An Efficient and pH-Universal Ruthenium-Based Catalyst for the Hydrogen Evolution Reaction. *Nat. Nanotech.* **2017**, *12*, 441-446.

(28) Wang, J.; Ji, Y.; Yin, R.; Li, Y.; Shao, Q.; Huang, X. Transition Metal-Doped Ultrathin RuO_2 Networked Nanowires for Efficient Overall Water Splitting Across A Broad pH Range. *J. Mater. Chem. A* **2019**, *7*, 6411-6416.

(29) Zhu, Y. L.; Tahini, H. A.; Hu, Z. W.; Dai, J.; Chen, Y. B.; Sun, H. N.; Zhou, W.; Liu, M. L.; Smith, S. C.; Wang, H. T.; Shao, Z. P. Unusual Synergistic Effect in Layered Ruddlesden -Popper Oxide Enables Ultrafast Hydrogen Evolution. *Nat. Commun.* **2019**, *10*, 149.

(30) Yu, J.; Guo, Y. N.; She, S. X.; Miao, S. S.; Ni, M.; Zhou, W.; Liu, M. L.; Shao, Z. P. Bigger is Surprisingly Better: Agglomerates of Larger RuP Nanoparticles Outperform Benchmark Pt Nanocatalysts for the Hydrogen Evolution Reaction. *Adv. Mater.* **2018**, *30*, 1800047.

(31) Bandal, H.; Reddy, K. K.; Chaugule, A.; Kim, H. Iron-Based Heterogeneous Catalysts for Oxygen Evolution Reaction; Change in Perspective from Activity Promoter to Active Catalyst. *J. Power Sources* **2018**, *395*, 106-127.

(32) Miao, M.; Pan, J.; He, T.; Yan, Y.; Xia, B. Y.; Wang, X. Molybdenum Carbide-Based Electrocatalysts for Hydrogen Evolution Reaction. *Chem. Eur. J.* **2017**, *23*, 10947-10961.

(33) Vij, V.; Sultan, S.; Harzandi, A. M.; Meena, A.; Tiwari, J. N.; Lee, W. G.; Yoon, T.; Kim, K. S. Nickel-Based Electrocatalysts for Energy-Related Applications: Oxygen Reduction, Oxygen Evolution, and Hydrogen Evolution Reactions. *ACS Catal.* **2017**, *7*, 7196-7225.

(34) Wang, J. H.; Cui, W.; Liu, Q.; Xing, Z. C.; Asiri, A. M.; Sun, X. P. Recent Progress in Cobalt-Based Heterogeneous Catalysts for Electrochemical Water Splitting. *Adv. Mater.* **2016**, *28*, 215-230.

(35) Wang, J.; Xu, F.; Jin, H. Y.; Chen, Y. Q.; Wang, Y. Non-Noble Metal-based Carbon Composites in Hydrogen Evolution Reaction: Fundamentals to Applications. *Adv. Mater.* **2017**, *29*, 1605838.

(36) Kalamaras, C. M.; Efstathiou, A. M. Hydrogen Production Technologies: Current State and Future Developments. *Conference Papers in Energy* **2013**, *2013*, 1-9.

(37) Suen, N. T.; Hung, S. F.; Quan, Q.; Zhang, N.; Xu, Y. J.; Chen, H. M. Electrocatalysis for the Oxygen Evolution Reaction: Recent Development and Future Perspectives. *Chem. Soc. Rev.* **2017**, *46*, 337-365.

(38) Huang, Z. F.; Song, J.; Du, Y.; Xi, S.; Dou, S.; Nsanzimana, J. M. V.; Wang, C.; Xu, Z. J.; Wang, X. Chemical and Structural Origin of Lattice Oxygen Oxidation in Co-Zn Oxyhydroxide Oxygen Evolution Electrocatalysts. *Nature Energy* **2019**, *4*, 329-338.

(39) Huang, Z. F.; Wang, J.; Peng, Y.; Jung, C. Y.; Fisher, A.; Wang, X. Design of Efficient Bifunctional Oxygen Reduction/Evolution Electrocatalyst: Recent Advances and Perspectives. *Adv. Energy Mater.* **2017**, *7*, 1700544.

(40) Guo, Y.; Park, T.; Yi, J. W.; Henzie, J.; Kim, J.; Wang, Z.; Jiang, B.; Bando, Y.; Sugahara, Y.; Tang, J.; Yamauchi, Y. Nanoarchitectonics for Transition-Metal-Sulfide-Based Electrocatalysts for Water Splitting. *Adv. Mater.* **2019**, *31*, 1807134.

(41) Morales-Guio, C. G.; Stern, L. A.; Hu, X. L. Nanostructured Hydrotreating Catalysts for Electrochemical Hydrogen Evolution. *Chem. Soc. Rev.* **2014**, *43*, 6555-6569.

(42) You, B.; Tang, M. T.; Tsai, C.; Abild-Pedersen, F.; Zheng, X.; Li, H. Enhancing Electrocatalytic Water Splitting by Strain Engineering. *Adv. Mater.* **2019**, *31*, 1807001.

(43) Man, I. C.; Su, H. Y.; Calle-Vallejo, F.; Hansen, H. A.; Martinez, J. I.; Inoglu, N. G.; Kitchin, J.; Jaramillo, T. F.; Norskov, J. K.; Rossmeisl, J. Universality in Oxygen Evolution Electrocatalysis on Oxide Surfaces. *ChemCatChem* **2011**, *3*, 1159-1165.

(44) Geiger, S.; Kasian, O.; Shrestha, B. R.; Mingers, A. M.; Mayrhofer, K. J. J.; Cherevko, S. Activity and Stability of Electrochemically and Thermally Treated Iridium for The Oxygen Evolution Reaction. *J. Electrochem. Soc.* **2016**, *163*, F3132-F3138.

(45) Sanabria-Chinchilla, J.; Soriaga, M. P.; Bussar, R.; Baltruschat, H. A DEMS Study of The Electrocatalytic Hydrogenation and Oxidation of p-dihydroxybenzene at Polycrystalline and Monocrystalline Platinum Electrodes. *J. Appl. Electrochem.* **2006**, *36*, 1253-1260.

(46) Planes, G. A.; García, G.; Pastor, E. High Performance Mesoporous Pt Electrode for Methanol Electrooxidation. A DEMS Study. *Electrochem. Commun.* **2007**, *9*, 839-844.

(47) Trasatti, S. Work Function, Electronegativity, and Electrochemical Behaviour of Metals: III. Electrolytic Hydrogen Evolution in Acid Solutions. *J. Electroanal. Chem.* **1972**, *39*, 163-184.

(48) Cook, T. R.; Dogutan, D. K.; Reece, S. Y.; Surendranath, Y.; Teets, T. S.; Nocera, D. G. Solar Energy Supply and Storage for the Legacy and Nonlegacy Worlds. *Chem. Rev.* **2010**, *110*, 6474-6502.

(49) Jin, H.; Wang, J.; Su, D.; Wei, Z.; Pang, Z.; Wang, Y. In Situ Cobalt-cobalt Oxide/N-doped Carbon Hybrids as Superior Bifunctional Electrocatalysts for Hydrogen and Oxygen Evolution. *J. Am. Chem. Soc.* **2015**, *137*, 2688-2694.

(50) Chen, S.; Zhao, Y.; Sun, B.; Ao, Z.; Xie, X.; Wei, Y.; Wang, G. Microwave-assisted Synthesis of Mesoporous Co_3O_4 Nanoflakes for Applications in Lithium Ion Batteries and Oxygen Evolution Reactions. *ACS Appl. Mater. Interfaces* **2015**, *7*, 3306-3313.

(51) Xu, L.; Jiang, Q.; Xiao, Z.; Li, X.; Huo, J.; Wang, S.; Dai, L. Plasma-engraved Co_3O_4 Nanosheets with Oxygen Vacancies and High Surface Area for the Oxygen Evolution Reaction. *Angew. Chem. Int. Ed.* **2016**, *55*, 5277-5281.

(52) Quaino, P.; Juarez, F.; Santos, E.; Schmickler, W. Volcano Plots in Hydrogen Electrocatalysis-uses and Abuses. *Beilstein J. Nanotechnol.* **2014**, *5*, 846-854.

(53) Nørskov, J. K.; Bligaard, T.; Logadottir, A.; Kitchin, J. R.; Chen, J. G.; Pandelov, S.; Stimming, U. Trends in the Exchange Current for Hydrogen Evolution. *J. Electrochem. Soc.* **2005**, *152*, J23-J26.

(54) Paoli, E. A.; Masini, F.; Frydendal, R.; Deiana, D.; Schlaup, C.; Malizia, M.; Hansen, T. W.; Horch, S.; Stephens, I. E. L.; Chorkendorff, I. Oxygen Evolution on Well-Characterized Mass-Selected Ru and RuO_2 Nanoparticles. *Chem. Sci.* **2015**, *6*, 190-196.

(55) Elezovic, N. R.; Babic, B. M.; Radmilovic, V. R.; Krstajic, N. V. Synthesis and Characterization of Pt Catalysts on SnO_2 Based Supports for Oxygen Reduction Reaction. *J. Electrochem. Soc.* **2013**, *160*, F1151-F1158.

(56) Lee, Y.; Suntivich, J.; May, K. J.; Perry, E. E.; Shao-Horn, Y. Synthesis and Activities of Rutile IrO_2 and RuO_2 Nanoparticles for Oxygen Evolution in Acid and Alkaline Solutions. *J. Phys. Chem. Lett.* **2012**, *3*, 399-404.

(57) Cherevko, S.; Geiger, S.; Kasian, O.; Kulyk, N.; Grote, J. P.; Savan, A.; Shrestha, B. R.; Merzlikin, S.; Breitbach, B.; Ludwig, A.; Mayrhofer, K. J. J. Oxygen and Hydrogen Evolution Reactions on Ru, RuO_2, Ir, and IrO_2 Thin Film Electrodes in Acidic and Alkaline Electrolytes: A Comparative Study on Activity and Stability. *Catal. Today* **2016**, *262*, 170-180.

(58) Frydendal, R.; Paoli, E. A.; Knudsen, B. P.; Wickman, B.; Malacrida, P.; Stephens, I. E. L.; Chorkendorff, I. Benchmarking the Stability of Oxygen Evolution Reaction Catalysts: The Importance of Monitoring Mass Losses. *ChemElectroChem* **2014**, *1*, 2075-2081.

(59) Cherevko, S.; Zeradjanin, A. R.; Topalov, A. A.; Keeley, G. P.; Mayrhofer, K. J. J. Effect of Temperature on Gold Dissolution in Acidic Media. *J. Electrochem. Soc.* **2014**, *161*, H501-H507.

(60) Kolotyrkin, Y. M.; Losev, V. V.; Chemodanov, A. N. Relationship between Corrosion Processes and Oxygen Evolution on Anodes Made from Noble Metals and Related Metal Oxide Anodes. *Mater. Chem. Phys.* **1988**, *19*, 1-95.

(61) Roy, C.; Rao, R. R.; Stoerzinger, K. A.; Hwang, J.; Rossmeisl, J.; Chorkendorff, I.; Shao-Horn, Y.; Stephens, I. E. L. Trends in Activity and Dissolution on RuO_2 under Oxygen Evolution Conditions: Particles versus Well-Defined Extended Surfaces. *ACS Energy Lett.* **2018**, *3*, 2045-2051.

(62) Over, H.; Kim, Y. D.; Seitsonen, A. P.; Wendt, S.; Lundgren, E.; Schmid, M.; Varga, P.; Morgante, A.; Ertl, G. Atomic-scale Structure and Catalytic Reactivity of the RuO_2 (110) Surface. *Science* **2000**, *287*, 1474-1476.

(63) Madhavaram, H.; Idriss, H.; Wendt, S.; Kim, Y. D.; Knapp, M.; Over, H.; Aßmann, J.; Loffler E.; Muhler, M. Oxidation Reactions over RuO_2: A Comparative Study of the Reactivity of the (110) Single Crystal and Polycrystalline Surfaces. *J. Catal.* **2001**, *202*, 296-307.

(64) Wang, W.; Su, C.; Wu, Y.; Ran, R.; Shao, Z. Progress in Solid Oxide Fuel Cells with Nickel-Based Anodes Operating on Methane and Related Fuels. *Chem. Rev.* **2013**, *113*, 8104-8151.

(65) Exner, K. S.; Anton, J.; Jacob, T.; Over, H. Full Kinetics from First Principles of the Chlorine Evolution Reaction over a RuO_2(110) Model Electrode. *Angew. Chem. Int. Ed.* **2016**, *55*, 7501-7504.

(66) Kim, Y. D.; Seitsonen, A. P.; Wendt, S.; Wang, J.; Fan, C.; Jacobi, K.; Over H.; Ertl, G. Characterization of Various Oxygen Species on an Oxide Surface: RuO_2(110). *J. Phys. Chem. B* **2001**, *105*, 3752-3758.

(67) Mu, R.; Zhao, Z. J.; Dohnalek, Z.; Gong, J. Structural Motifs of Water on Metal Oxide Surfaces. *Chem. Soc. Rev.* **2017**, *46*, 1785-1806.

(68) Sun, Q.; Reuter, K.; Scheffler, M. Effect of a Humid Environment on the Surface Structure of RuO_2 (110). *Phys. Rev. B: Condens. Matter Mater. Phys.* **2003**, *67*, 205424.

(69) Seitsonen, A. P.; Crihan, D.; Knapp, M.; Resta, A.; Lundgren, E.; Andersen, J. N.; Over, H. Reaction Mechanism of Ammonia Oxidation over RuO_2(110): A Combined Theory/Experiment Approach. *Surf. Sci.* **2009**, *603*, L113-L116.

(70) Yao, Y.; He, D. S.; Lin, Y.; Feng, X.; Wang, X.; Yin, P.; Hong, X.; Zhou, G.; Wu, Y.; Li, Y. Modulating fcc and hcp Ruthenium on the Surface of Palladium-Copper Alloy through Tunable Lattice Mismatch. *Angew. Chem. Int. Ed.* **2016**, *55*, 5501-5505.

(71) Li, W. Z.; Liu, J. X.; Gu, J.; Zhou, W.; Yao, S. Y.; Si, R.; Guo, Y.; Su, H. Y.; Yan, C. H.; Li, W. X.; Zhang, Y. W.; Ma, D. Chemical Insights into the Design and Development of Face-Centered Cubic Ruthenium Catalysts for Fischer-Tropsch Synthesis. *J. Am. Chem. Soc.* **2017**, *139*, 2267-2276.

(72) Kusada, K.; Kobayashi, H.; Yamamoto, T.; Matsumura, S.; Sumi, N.; Sato, K.; Nagaoka, K.; Kubota, Y.; Kitagawa, H. Discovery of Face-Centered-Cubic Ruthenium Nanoparticles: Facile Size-Controlled Synthesis Using the Chemical Reduction Method. *J. Am. Chem. Soc.* **2013**, *135*, 5493-5496.

(73) Drouet, S.; Creus, J.; Collière, V.; Amiens, C.; García-Antón, J.; Sala, X.; Philippot, K. A Porous Ru Nanomaterial as An Efficient Electrocatalyst for the Hydrogen Evolution Reaction under Acidic and Neutral Conditions. *Chem. Commun.* **2017**, *53*, 11713-11716.

(74) Wang, Q.; Ming, M.; Niu, S.; Zhang, Y.; Fan, G.; Hu, J. S. Hydrogen Evolution: Scalable Solid-State Synthesis of Highly Dispersed Uncapped Metal (Rh, Ru, Ir) Nanoparticles for Efficient Hydrogen Evolution (Adv. Energy Mater. 31/2018). *Adv. Energy Mater.* **2018**, *8*, 1870135.

(75) Gao, K.; Wang, Y.; Wang, Z.; Zhu, Z.; Wang, J.; Luo, Z.; Zhang, C.; Huang, X.; Zhang, H.; Huang, W. Ru Nanodendrites Composed of Ultrathin fcc/hcp Nanoblades for the Hydrogen Evolution Reaction in Alkaline Solutions. *Chem. Commun.* **2018**, *54*, 4613-4616.

(76) Tee, S. Y.; Lee, C. J. J.; Dinachali, S. S.; Lai, S. C.; Williams, E. L.; Luo, H.-K.; Chi, D.; Andy Hor, T. S.; Han, M.-Y. Amorphous Ruthenium Nanoparticles for Enhanced Electrochemical Water Splitting. *Nanotechnology* **2015**, *26*, 415401.

(77) Pierozynski, B.; Mikolajczyk, T.; Kowalski, I. M. Hydrogen Evolution at Catalytically-Modified Nickel Foam in Alkaline Solution. *J. Power Sources* **2014**, *271*, 231-238.

(78) Franceschini, E. A.; Lacconi, G. I.; Corti, H. R. Kinetics of Hydrogen Evolution Reaction on Nickel Modified by Spontaneous Ru Deposition: A Rotating Disk Electrode and Impedance Spectroscopy Approach. *Int. J. Hydrogen Energ.* **2016**, *41*, 3326-3338.

(79) Zhu, L.; Cai, Q.; Liao, F.; Sheng, M.; Wu, B.; Shao, M. Ru-modified Silicon Nanowires as Electrocatalysts for Hydrogen Evolution Reaction. *Electrochem. Commun.* **2015**, *52*, 29-33.

(80) Pierozynski, B.; Mikolajczyk, T. Hydrogen Evolution Reaction at Ru-Modified Nickel-Coated Carbon Fibre in 0.1 M NaOH. *Pol. J. Chem. Technol.* **2015**, *17*, 18-22.

(81) Jović, B. M.; Jović, V. D.; Lačnjevac, U. Č.; Stevanović, S. I.; Kovač, J.; Radović, M.; Krstajić, N. V. Ru Layers Electrodeposited onto Highly Stable Ti_2AlC Substrates as Cathodes for Hydrogen Evolution in Sulfuric Acid Solutions. N. V. Krstajić, *J. Electroanal. Chem.* **2016**, *766*, 78-86.

(82) Reier, T.; Oezaslan, M.; Strasser, P. Electrocatalytic Oxygen Evolution Reaction (OER) on Ru, Ir, and Pt Catalysts: A Comparative Study of Nanoparticles and Bulk Materials. *ACS Catal.* **2012**, *2*, 1765-1772.

(83) Kim, J. Y.; Choi, J.; Kim, H. Y.; Hwang, E.; Kim, H.-J.; Ahn, S. H.; Kim, S. K. Activity and Stability of the Oxygen Evolution Reaction on Electrodeposited Ru and Its Thermal Oxides. *Appl. Surf. Sci.* **2015**, *359*, 227-235.

(84) Poerwoprajitno, A. R.; Gloag, L.; Benedetti, T. M.; Cheong, S.; Watt, J.; Huber, D. L.; Gooding, J. J.; Tilley, R. D. Formation of Branched Ruthenium Nanoparticles for Improved Electrocatalysis of Oxygen Evolution Reaction. *Small* **2019**, *15*, 1804577.

(85) Shao, Q.; Lu, K.; Huang, X. Platinum Group Nanowires for Efficient Electrocatalysis. *Small Methods* **2019**, 1800545.

(86) Pedersen, A. F.; Ulrikkeholm, E. T.; Escudero-Escribano, M.; Johansson, T. P.; Malacrida, P.; Pedersen, C. M.; Hansen, M. H.; Jensen, K. D.; Rossmeisl, J.; Friebel, D.; Nilsson, A.; Chorkendorff, I.; Stephens, I. E. L. Probing the Nanoscale Structure of the Catalytically Active Overlayer on Pt Alloys with Rare Earths. *Nano Energy* **2016**, *29*, 249-260.

(87) Cullen, D. A.; More, K. L.; Atanasoska, L. L.; Atanasoski, R. T. Impact of IrRu Oxygen Evolution Reaction Catalysts on Pt Nanostructured Thin Films under Start-up/Shutdown Cycling. *J. Power Sources* **2014**, *269*, 671-681.

(88) Liu, S.; Zhang, Q.; Bao, J.; Li, Y.; Dai, Z.; Gu, L. Significantly Enhanced Hydrogen Evolution Activity of Freestanding Pd-Ru Distorted Icosahedral Clusters with less than 600 Atoms. *Chem. Eur. J.* **2017**, *23*, 18203-18207.

(89) Chen, C. H.; Wu, D.; Li, Z.; Zhang, R.; Kuai, C. G.; Zhao, X. R.; Dong, C. K.; Qiao, S. Z.; Liu, H.; Du, X. W. Ruthenium-Based Single-Atom Alloy with High Electrocatalytic Activity for Hydrogen Evolution. *Adv. Energy Mater.* **2019**, *9*, 1803913.

(90) Su, J.; Yang, Y.; Xia, G.; Chen, J.; Jiang, P.; Chen, Q. Ruthenium-Cobalt Nanoalloys Encapsulated in Nitrogen-Doped Graphene as Active Electrocatalysts for Producing Hydrogen in Alkaline Media. *Nat. Commun.* **2017**, *8*, 14969.

(91) Xu, Y.; Yin, S.; Li, C.; Deng, K.; Xue, H.; Li, X.; Wang, H.; Wang, L. Low-Ruthenium-Content NiRu Nanoalloys Encapsulated in Nitrogen-Doped Carbon as Highly Efficient and pH-Universal Electrocatalysts for the Hydrogen Evolution Reaction. *J. Mater. Chem. A* **2018**, *6*, 1376-1381.

(92) Zhang, Z.; Li, P.; Wang, Q.; Feng, Q.; Tao, Y.; Xu, J.; Jiang, C.; Lu, X.; Fan, J.; Gu, M.; Li, H.; Wang, H. Mo Modulation Effect on the Hydrogen Binding Energy of Hexagonal-Close-Packed Ru for Hydrogen Evolution. *J. Mater. Chem. A* **2019**, *7*, 2780-2786.

(93) Niu, X.; Tang, Q.; He, B.; Yang, P. Robust and Stable Ruthenium Alloy Electrocatalysts for Hydrogen Evolution by Seawater Splitting. *Electrochim. Acta* **2016**, *208*, 180-187.

(94) Mao, J.; He, C. T.; Pei, J.; Chen, W.; He, D.; He, Y.; Zhuang, Z.; Chen, C.; Peng, Q.; Wang, D.; Li, Y. Accelerating Water Dissociation Kinetics by Isolating Cobalt Atoms into Ruthenium Lattice. *Nat. Commun.* **2018**, *9*, 4958.

(95) Li, H.; Tang, Q.; He, B.; Yang, P. Robust Electrocatalysts from An Alloyed Pt-Ru-M (M = Cr, Fe, Co, Ni, Mo)-Decorated Ti Mesh for Hydrogen Evolution by Seawater Splitting. *J. Mater. Chem. A* **2016**, *4*, 6513-6520.

(96) Shi, Y. C.; Yuan, T.; Feng, J. J.; Yuan, J.; Wang, A.-J. Rapid Fabrication of Support-Free Trimetallic $Pt_{53}Ru_{39}Ni_8$ Nanosponges with Enhanced Electrocatalytic Activity for Hydrogen Evolution And Hydrazine Oxidation Reactions. *J. Colloid Interf. Sci.* **2017**, *505*, 14-22.

(97) Forgie, R.; Bugosh, G.; Neyerlin, K. C.; Liu, Z. C.; Strasser, P. Bimetallic Ru Electrocatalysts for the OER and Electrolytic Water Splitting in Acidic Media. *Electrochem. Solid St.* **2010**, *13*, D36-D39.

(98) Miles, M. H.; Klaus, E. A.; Gunn, B. P.; Locker, J. R.; Serafin, W. E.; Srinivasan, S. The Oxygen Evolution Reaction on Platinum, Iridium, Ruthenium and Their Alloys at 80°C in Acid Solutions. *Electrochim. Acta* **1978**, *23*, 521-526.

(99) Neyerlin, K. C.; Bugosh, G.; Forgie, R.; Liu, Z. C.; Strasser, P. Combinatorial Study of High-Surface-Area Binary and Ternary Electrocatalysts for the Oxygen Evolution Reaction. *J. Electrochem. Soc.* **2009**, *156*, B363-B369.

(100) Yao, Y.; Hu, S.; Chen, W.; Huang, Z. Q.; Wei, W.; Yao, T.; Liu, R.; Zang, K.; Wang, X.; Wu, G.; Yuan, W.; Yuan, T.; Zhu, B.; Liu, W.; Li, Z.; He, D.; Xue, Z.; Wang, Y.; Zheng, X.; Dong, J.; Chang, C. R.; Chen, Y.; Hong, X.; Luo, J.; Wei, S.; Li, W. X.; Strasser, P.; Wu, Y.; Li, Y. Engineering the Electronic Structure of Single Atom Ru Sites via Compressive Strain Boosts Acidic Water Oxidation Electrocatalysis. *Nature Catalysis* **2019**, *2*, 304-313.

(101) Shan, J.; Ling, T.; Davey, K.; Zheng, Y.; Qiao, S. Z. Transition-Metal-Doped RuIr Bifunctional Nanocrystals for Overall Water Splitting in Acidic Environments. *Adv. Mater.* **2019**, *31*, 1900510.

(102) Wang, J. X.; Zhang, Y.; Capuano, C. B.; Ayers, K. E. Ultralow Charge-Transfer Resistance with Ultralow Pt Loading for Hydrogen Evolution and Oxidation Using Ru@Pt Core-Shell Nanocatalysts. *Sci. Rep.* **2015**, *5*, 12220.

(103) Luo, Y.; Luo, X.; Wu, G.; Li, Z.; Wang, G.; Jiang, B.; Hu, Y.; Chao, T.; Ju, H.; Zhu, J.; Zhuang, Z.; Wu, Y.; Hong, X.; Li, Y. Mesoporous Pd@Ru Core-Shell Nanorods for Hydrogen Evolution Reaction in Alkaline Solution. *ACS Appl. Mater. Interfaces* **2018**, *10*, 34147-34152.

(104) Wang, X.; Zhu, Y.; Vasileff, A.; Jiao, Y.; Chen, S.; Song, L.; Zheng, B.; Zheng, Y.; Qiao, S. Z. Strain Effect in Bimetallic Electrocatalysts in the Hydrogen Evolution Reaction. *ACS Energy Lett.* **2018**, *3*, 1198-1204.

(105) AlYami, N. M.; LaGrow, A. P.; Joya, K. S.; Hwang, J.; Katsiev, K.; Anjum, D. H.; Losovyj, Y.; Sinatra, L.; Kim, J. Y.; Bakr, O. M. Tailoring Ruthenium Exposure to Enhance the Performance of fcc Platinum@Ruthenium Core-Shell Electrocatalysts in the Oxygen Evolution Reaction. *Phys. Chem. Chem. Phys.* **2016**, *18*, 16169-16178.

(106) Gloag, L.; Benedetti, T. M.; Cheong, S.; Webster, R. F.; Marjo, C. E.; Gooding, J. J.; Tilley, R. D. Pd–Ru Core-Shell Nanoparticles with Tunable Shell Thickness for Active and Stable Oxygen Evolution Performance. *Nanoscale* **2018**, *10*, 15173-15177.

(107) Gloag, L.; Benedetti, T. M.; Cheong, S.; Marjo, C. E.; Gooding, J. J.; Tilley, R. D. Cubic-Core Hexagonal-Branch Mechanism to Synthesize Bimetallic Branched and Faceted Pd-Ru Nanoparticles for Oxygen Evolution Reaction Electrocatalysis. *J. Am. Chem. Soc.* **2018**, *140*, 12760-12764.

(108) Gloag, L.; Benedetti, T. M.; Cheong, S.; Li, Y.; Chan, X. H.; Lacroix, L. M.; Chang, S. L. Y.; Arenal, R.; Florea, I.; Barron, H.; Barnard, A. S.; Henning, A. M.; Zhao, C.; Schuhmann, W.; Gooding, J. J.; Tilley, R. D. Three-Dimensional Branched and Faceted Gold–Ruthenium Nanoparticles: Using Nanostructure to Improve Stability in Oxygen Evolution Electrocatalysis. *Angew. Chem. Int. Edit.* **2018**, *130*, 10398-10402.

(109) Jin, H.; Lee, K. W.; Khi, N. T.; An, H.; Park, J.; Baik, H.; Kim, J.; Yang, H.; Lee, K. Rational Synthesis of Heterostructured M/Pt (M = Ru or Rh) Octahedral Nanoboxes and Octapods and Their Structure-Dependent Electrochemical Activity Toward the Oxygen Evolution Reaction. *Small* **2015**, *11*, 4462-4468.

(110) Jiang, P.; Yang, Y.; Shi, R.; Xia, G.; Chen, J.; Su, J.; Chen, Q. Pt-like Electrocatalytic Behavior of Ru–MoO_2 Nanocomposites for the Hydrogen Evolution Reaction. *J. Mater. Chem. A* **2017**, *5*, 5475-5485.

(111) Yoon, D.; Lee, J.; Seo, B.; Kim, B.; Baik, H.; Joo, S. H.; Lee, K. Cactus-Like Hollow Cu2-xS@Ru Nanoplates as Excellent and Robust Electrocatalysts for the Alkaline Hydrogen Evolution Reaction. *Small* **2017**, *13*, 1700052.

(112) Liu, Y.; Liu, S.; Wang, Y.; Zhang, Q.; Gu, L.; Zhao, S.; Xu, D.; Li, Y.; Bao, J.; Dai, Z. Ru Modulation Effects in the Synthesis of Unique Rod-like Ni@Ni_2P–Ru Heterostructures and Their Remarkable Electrocatalytic Hydrogen Evolution Performance. *J. Am. Chem. Soc.* **2018**, *140*, 2731-2734.

(113) Liu, S.; Liu, Q.; Lv, Y.; Chen, B.; Zhou, Q.; Wang, L.; Zheng, Q.; Che, C.; Chen, C. Ru Decorated with NiCoP: An Efficient and Durable Hydrogen Evolution Reaction Electrocatalyst in Both Acidic and Alkaline Conditions. *Chem. Commun.* **2017**, *53*, 13153-13156.

(114) Demir, E.; Akbayrak, S.; Önal, A. M.; Özkar, S. Nanoceria-Supported Ruthenium(0) Nanoparticles: Highly Active and Stable Catalysts for Hydrogen Evolution from Water. *ACS Appl. Mater. Interfaces* **2018**, *10*, 6299-6308.

(115) Wang, L.; Zhou, Q.; Pu, Z.; Zhang, Q.; Mu, X.; Jing, H.; Liu, S.; Chen, C.; Mu, S. Surface Reconstruction Engineering of Cobalt Phosphides by Ru Inducement to Form Hollow Ru-RuP_x-Co_xP Pre-Electrocatalysts with Accelerated Oxygen Evolution Reaction. *Nano Energy* **2018**, *53*, 270-276.

(116) Chen, Z. J.; Cao, G. X.; Gan, L. Y.; Dai, H.; Xu, N.; Zang, M. J.; Dai, H. B.; Wu, H.; Wang, P. Highly Dispersed Platinum on Honeycomb-like NiO@Ni Film as a Synergistic Electrocatalyst for the Hydrogen Evolution Reaction. *ACS Catal.* **2018**, *8*, 8866-8872.

(117) Ledezma-Yanez, I.; Wallace, W. D. Z.; Sebastián-Pascual, P.; Climent, V.; Feliu, J. M.; Koper, M. T. M. Interfacial Water Reorganization as A pH-Dependent Descriptor of the Hydrogen Evolution Rate on Platinum Electrodes. *Nat. Energy* **2017**, *2*, 17031.

(118) Subbaraman, R.; Tripkovic, D.; Strmcnik, D.; Chang, K. C.; Uchimura, M.; Paulikas, A. P.; Stamenkovic, V.; Markovic, N. M. Enhancing Hydrogen Evolution Activity in Water Splitting by Tailoring Li^+-Ni $(OH)_2$-Pt Interfaces. *Science* **2011**, *334*, 1256-1260.

(119) Liu, Y.; Lu, X.; Che, Z.; Zhang, C.; Han, M.; Bao, J.; Dai, Z. Amorphous $Y(OH)_3$-Promoted Ru/$Y(OH)_3$ Nanohybrids with High Durability for Electrocatalytic Hydrogen Evolution in Alkaline Media. *Chem. Commun.* **2018**, *54*, 12202-12205.

(120) Liu, J.; Zheng, Y.; Zhu, D.; Vasileff, A.; Ling, T.; Qiao, S. Z. Identification of pH-Dependent Synergy on Ru/MoS_2 Interface: A Comparison of Alkaline and Acidic Hydrogen Evolution. *Nanoscale* **2017**, *9*, 16616-16621.

(121) Zhong, C.; Zhou, Q.; Li, S.; Cao, L.; Li, J.; Shen, Z.; Ma, H.; Liu, J.; Lu, M.; Zhang, H. Enhanced Synergistic Catalysis by A Novel Triple-Phase Interface Design of NiO/Ru@Ni for the Hydrogen Evolution Reaction. *J. Mater. Chem. A* **2019**, *7*, 2344-2350.

(122) Liu, Z.; Li, Z.; Li, J.; Xiong, J.; Zhou, S.; Liang, J.; Cai, W.; Wang, C.; Yang, Z.; Cheng, H. Engineering of Ru/Ru_2P Interfaces Superior to Pt Active Sites for Catalysis of the Alkaline Hydrogen Evolution Reaction. *J. Mater. Chem. A* **2019**, *7*, 5621-5625.

(123) Marques Mota, F.; Choi, C. H.; Boppella, R.; Lee, J.-E.; Kim, D. H. Arising Synergetic and Antagonistic Effects in the Design of Ni- and Ru-Based Water Splitting Electrocatalysts. *J. Mater. Chem. A* **2019**, *7*, 639-646.

(124) Ding, J.; Shao, Q.; Feng, Y.; Huang, X. Ruthenium-Nickel Sandwiched Nanoplates for Efficient Water Splitting Electrocatalysis. *Nano Energy* **2018**, *47*, 1-7.

(125) Yang, K.; Xu, P.; Lin, Z.; Yang, Y.; Jiang, P.; Wang, C.; Liu, S.; Gong, S.; Hu, L.; Chen, Q. Ultrasmall Ru/Cu-doped RuO_2 Complex Embedded in Amorphous Carbon Skeleton as Highly Active Bifunctional Electrocatalysts for Overall Water Splitting. *Small* **2018**, *14*, 1803009.

(126) Li, P.; Wang, M.; Duan, X.; Zheng, L.; Cheng, X.; Zhang, Y.; Kuang, Y.; Li, Y.; Ma, Q.; Feng, Z.; Liu, W.; Sun, X. Boosting Oxygen Evolution of Single-Atomic Ruthenium through Electronic Coupling with Cobalt-Iron Layered Double Hydroxides. *Nat. Commun.* **2019**, *10*, 1711.

(127) Chen, Q. Q.; Yang, X.; Hou, C. C.; Li, K.; Chen, Y. Inlay of Ultrafine Ru Nanoparticles into a Self-Supported $Ni(OH)_2$ Nanoarray for Hydrogen Evolution with Low Overpotential and Enhanced Kinetics. *J. Mater. Chem. A* **2019**, *7*, 11062-11608.

(128) Hwang, H.; Kwon, T.; Kim, H. Y.; Park, J.; Oh, A.; Kim, B.; Baik, H.; Joo, S. H.; Lee, K. Ni@ Ru and NiCo@ Ru Core-Shell Hexagonal Nanosandwiches with a Compositionally Tunable Core and a Regioselectively Grown Shell. *Small* **2018**, *14*, 1702353.

(129) Joo, J.; Jin, H.; Oh, A.; Kim, B.; Lee, J.; Baik, H.; Joo, S. H.; Lee, K. An IrRu Alloy Nanocactus on $Cu_{2-x}S$@IrS_y as a Highly Efficient Bifunctional Electrocatalyst toward Overall Water Splitting in Acidic Electrolytes. *J. Mater. Chem. A* **2018**, *6*, 16130-16138.

(130) Zhang, J.; Hao, J.; Ma, Q.; Li, C.; Liu, Y.; Li, B.; Liu, Z. Polyvinylpyrrolidone Stabilized-Ru Nanoclusters Loaded onto Reduced Graphene Oxide as High Active Catalyst for Hydrogen Evolution. *J. Nanopart. Res.* **2017**, *19*, 227.

(131) Chen, Z.; Lu, J.; Ai, Y.; Ji, Y.; Adschiri, T.; Wan, L. Ruthenium/Graphene-like Layered Carbon Composite as an Efficient Hydrogen Evolution Reaction Electrocatalyst. *ACS Appl. Mater. Interfaces* **2016**, *8*, 35132-35137.

(132) Li, Y.; Chu, F.; Liu, Y.; Kong, Y.; Tao, Y.; Li, Y.; Qin, Y. An Ultrafine Ruthenium Nanocrystal with Extremely High Activity for the Hydrogen Evolution Reaction in Both Acidic and Alkaline Media. *Chem. Commun.* **2018**, *54*, 13076-13079.

(133) Santosh, B.; Wu, Z.; Sai Siddhartha, R.; Krishna Prasad, G.; Ramamurthy, S. S.; Mitra, S.; Dandamudi, R. B. Ruthenium Decorated Carbon Nanoink as Highly Active Electrocatalyst in Hydrogen Evolution Reaction. *Int. J. Hydrogen Energ.* **2016**, *41*, 23007-23014.

(134) Zhang, J.; Liu, P.; Wang, G.; Zhang, P. P.; Zhuang, X. D.; Chen, M. W.; Weidinger, I. M.; Feng, X. L. Ruthenium/Nitrogen-Doped Carbon as An Electrocatalyst for Efficient Hydrogen Evolution in Alkaline Solution. *J. Mater. Chem. A* **2017**, *5*, 25314-25318.

(135) Wang, J.; Wei, Z.; Mao, S.; Li, H.; Wang, Y. Highly Uniform Ru Nanoparticles over N-Doped Carbon: pH and Temperature-Universal Hydrogen Release from Water Reduction. *Energy Environ. Sci.* **2018**, *11*, 800-806.

(136) Wang, Z. L.; Sun, K.; Henzie, J.; Hao, X.; Li, C.; Takei, T.; Kang, Y. M.; Yamauchi, Y. Spatially Confined Assembly of Monodisperse Ruthenium Nanoclusters in a Hierarchically Ordered Carbon Electrode for Efficient Hydrogen Evolution. *Angew. Chem. Int. Ed.* **2018**, *57*, 5848-5852.

(137) Qiu, T.; Liang, Z.; Guo, W.; Gao, S.; Qu, C.; Tabassum, H.; Zhang, H.; Zhu, B.; Zou, R.; Shao-Horn, Y. Highly Exposed Ruthenium-based Electrocatalysts from Bimetallic Metal-Organic Frameworks for Overall Water Splitting. *Nano Energy* **2019**, *58*, 1-10.

(138) Luo, D.; Zhou, B.; Li, Z.; Qin, X.; Wen, Y.; Shi, D.; Lu, Q.; Yang, M.; Zhou, H.; Liu, Y. Biomimetic Organization of a Ruthenium-Doped Collagen-Based Carbon Scaffold for Hydrogen Evolution. *J. Mater. Chem. A* **2018**, *6*, 2311-2317.

(139) Barman, B. K.; Das, D.; Nanda, K. K. Facile Synthesis of Ultrafine Ru Nanocrystal Supported N-Doped Graphene as An Exceptional Hydrogen Evolution Electrocatalyst in Both Alkaline and Acidic Media. *Sustain. Energ. Fuels* **2017**, *1*, 1028-1033.

(140) Li, F.; Han, G.-F.; Noh, H.-J.; Ahmad, I.; Jeon, I.-Y.; Baek, J.-B. Mechanochemically Assisted Synthesis of a Ru Catalyst for Hydrogen Evolution with Performance Superior to Pt in Both Acidic and Alkaline Media. *Adv. Mater.* **2018**, *30*, 1803676.

(141) Peng, Z.; Wang, H.; Zhou, L.; Wang, Y.; Gao, J.; Liu, G.; Redfern, S. A. T.; Feng, X.; Lu, S.; Li, B.; Liu, Z. Hollow Carbon Shells Enhanced by Confined Ruthenium as Cost-Efficient and Superior Catalysts for the Alkaline Hydrogen Evolution Reaction. *J. Mater. Chem. A* **2019**, *7*, 6676-6685.

(142) Chen, X.; Zheng, J.; Zhong, X.; Jin, Y.; Zhuang, G.; Li, X.; Deng, S.; Wang, J.-g. Tuning the Confinement Space of N-Carbon Shell-Coated Ruthenium Nanoparticles: Highly Efficient Electrocatalysts for Hydrogen Evolution Reaction. *Catal. Sci. Technol.* **2017**, *7*, 4964-4970.

(143) Wei, S.; Li, A.; Liu, J. C.; Li, Z.; Chen, W.; Gong, Y.; Zhang, Q.; Cheong, W. C.; Wang, Y.; Zheng, L.; Xiao, H.; Chen, C.; Wang, D.; Peng, Q.; Gu, L.; Han, X.; Li, J.; Li, Y. Direct Observation of Noble Metal Nanoparticles Transforming to Thermally Stable Single Atoms. *Nat. Nanotech.* **2018**, *13*, 856-861.

(144) Lu, B.; Guo, L.; Wu, F.; Peng, Y.; Lu, J. E.; Smart, T. J.; Wang, N.; Finfrock, Y. Z.; Morris, D.; Zhang, P.; Li, N.; Gao, P.; Ping, Y.; Chen, S. Ruthenium Atomically Dispersed in Carbon Outperforms Platinum toward Hydrogen Evolution in Alkaline Media. *Nat. Commun.* **2019**, *10*, 631.

(145) Melsheimer, J.; Ziegler, D. The Oxygen Electrode Reaction in Acid Solutions on RuO_2 Electrodes Prepared by the Thermal Decomposition Method. *Thin Solid Films* **1988**, *163*, 301-308.

(146) Licht, S. Multiple Band Gap Semiconductor/Electrolyte Solar Energy Conversion. *J. Phys. Chem. B* **2001**, *105*, 6281-6294.

(147) Ma, H.; Liu, C.; Liao, J.; Su, Y.; Xue, X.; Xing, W. Study of Ruthenium Oxide Catalyst for Electrocatalytic Performance in Oxygen Evolution. *J. Mol. Catal. A-Chem.* **2006**, *247*, 7-13.

(148) Rossmeisl, J.; Qu, Z. W.; Zhu, H.; Kroes, G. J.; Nørskov, J. K. Electrolysis of Water on Oxide Surfaces. *J. Electroanal. Chem.* **2007**, *607*, 83-89.

(149) Danilovic, N.; Subbaraman, R.; Chang, K. C.; Chang, S. H.; Kang, Y. J.; Snyder, J.; Paulikas, A. P.; Strmcnik, D.; Kim, Y. T.; Myers, D.; Stamenkovic, V. R.; Markovic, N. M. Activity–Stability Trends for the Oxygen Evolution Reaction on Monometallic Oxides in Acidic Environments. *J. Phys. Chem. Lett.* **2014**, *5*, 2474-2478.

(150) Nazir, R.; Basak, U.; Pande, S. Synthesis of One-Dimensional RuO_2 Nanorod for Hydrogen and Oxygen Evolution Reaction: An Efficient and Stable Electrocatalyst. *Colloid. Surface. A*, **2019**, *560*, 141-148.

(151) Lyu, F.; Wang, Q.; Choi, S. M.; Yin, Y. Noble-Metal-Free Electrocatalysts for Oxygen Evolution. *Small* **2019**, *15*, 1804201.

(152) Hodnik, N.; Jovanovič, P.; Pavlišič, A.; Jozinović, B.; Zorko, M.; Bele, M.; Šelih, V. S.; Šala, M.; Hočevar, S.; Gaberšček, M. New Insights into Corrosion of Ruthenium and Ruthenium Oxide Nanoparticles in Acidic Media. *J. Phys. Chem. C* **2015**, *119*, 10140-10147.

(153) Stoerzinger, K. A.; Qiao, L.; Biegalski, M. D.; Shao-Horn, Y. Orientation-Dependent Oxygen Evolution Activities of Rutile IrO_2 and RuO_2. *J. Phys. Chem. Lett.* **2014**, *5*, 1636-1641.

(154) Nguyen, T. D.; Scherer, G. G.; Xu, Z. J. A Facile Synthesis of Size-Controllable IrO_2 and RuO_2 Nanoparticles for the Oxygen Evolution Reaction. *Electrocatalysis* **2016**, *7*, 420-427.

(155) DeSario, P. A.; Chervin, C. N.; Nelson, E. S.; Sassin, M. B.; Rolison, D. R. Competitive Oxygen Evolution in Acid Electrolyte Catalyzed at Technologically Relevant Electrodes Painted with Nanoscale RuO_2. *ACS Appl. Mater. Interfaces* **2017**, *9*, 2387-2395.

(156) Kibsgaard, J.; Hellstern, T. R.; Choi, S. J.; Reinecke, B. N.; Jaramillo, T. F. Mesoporous Ruthenium/Ruthenium Oxide Thin Films: Active Electrocatalysts for the Oxygen Evolution Reaction. *ChemElectroChem* **2017**, *4*, 2480-2485.

(157) Salvatore, D. A.; Peña, B.; Dettelbach, K. E.; Berlinguette, C. P. Photodeposited Ruthenium Dioxide Films for Oxygen Evolution Reaction Electrocatalysis. *J. Mater. Chem. A* **2017**, *5*, 1575-1580.

(158) Tsuji, E.; Imanishi, A.; Fukui, K.-i.; Nakato, Y. Electrocatalytic Activity of Amorphous RuO_2 Electrode for Oxygen Evolution in an Aqueous Solution. *Electrochim. Acta* **2011**, *56*, 2009-2016.

(159) Stoerzinger, K. A.; Rao, R. R.; Wang, X. R.; Hong, W. T.; Rouleau, C. M.; Shao-Horn, Y. The Role of Ru Redox in pH-Dependent Oxygen Evolution on Rutile Ruthenium Dioxide Surfaces. *Chem* **2017**, *2*, 668-675.

(160) Heras-Domingo, J.; Sodupe, M.; Solans-Monfort, X. Interaction between Ruthenium Oxide Surfaces and Water Molecules. Effect of Surface Morphology and Water Coverage. *J. Phys. Chem. C* **2019**, *123*, 7786-7798.

(161) Hansen, H. A.; Man, I. C.; Studt, F.; Abild-Pedersen, F.; Bligaard, T.; Rossmeisl, J. Electrochemical Chlorine Evolution at Rutile Oxide (110) Surfaces. *Phys. Chem. Chem. Phys.* **2010**, *12*, 283-290.

(162) Kuo, D.-Y.; Paik, H.; Kloppenburg, J.; Faeth, B.; Shen, K. M.; Schlom, D. G.; Hautier, G.; Suntivich, J. Measurements of Oxygen Electroadsorption Energies and Oxygen Evolution

Reaction on RuO_2(110): A Discussion of the Sabatier Principle and Its Role in Electrocatalysis. *J. Am. Chem. Soc.* **2018**, *140*, 17597-17605.

(163) Iwakura, C.; Hirao, K.; Tamura, H. Preparation of Ruthenium Dioxide Electrodes and Their Anodic Polarization Characteristics in Acidic Solutions. *Electrochim. Acta* **1977**, *22*, 335.

(164) Galizzioli, D.; Tantardini, F.; Trasatti, S. Ruthenium Dioxide: A New Electrode Material. I. Behaviour in Acid Solutions of Inert Electrolytes. *J. Appl. Electrochem.* **1974**, *4*, 57-67.

(165) Vukmirovic, M. B.; Sabatini, R. L.; Adzic, R. R. Growth of RuO_2 by Electrochemical and Gas-Phase Oxidation of an Ru (0001) Surface. Adzic, *Surf. Sci.* **2004**, *572*, 269-276.

(166) Paoli, E. A.; Masini, F.; Frydendal, R.; Deiana, D.; Malacrida, P.; Hansen, T. W.; Chorkendorff, I.; Stephens, I. E. L. Fine-Tuning the Activity of Oxygen Evolution Catalysts: The Effect of Oxidation Pre-Treatment on Size-Selected Ru Nanoparticles. *Catal. Today* **2016**, *262*, 57-64.

(167) Lee, J.; Sher Shah, S. A.; Yoo, P. J.; Lim, B. Hydrous RuO_2 Nanoparticles as Highly Active Electrocatalysts for Hydrogen Evolution Reaction. *Chem. Phys. Lett.* **2017**, *673*, 89-92.

(168) Galizzioli, D.; Tantardini, F.; Trasatti, S. Ruthenium Dioxide: A New Electrode Material. II. Non-Stoichiometry and Energetics of Electrode Reactions in Acid Solutions. *J. Appl. Electrochem.* **1975**, *5*, 203-214.

(169) Chen L.; Guay, D. Kinetics of the Hydrogen Evolution Reaction on RuO_2 and IrO_2 Oxide Electrodes in H_2SO_4 Solution: An AC Impedance Study. *J. Electrochem. Soc.* **1996**, *143*, 3576-3584.

(170) Chabanier, C.; Irissou, E.; Guay, D.; Pelletier, J. F.; Sutton, M.; Lurio, L. B. Hydrogen absorption in Thermally Prepared RuO_2 Electrode. *Electrochem. Solid St.* **2002**, *5*, E40-E42.

(171) Chabanier, C.; Guay, D. Activation and Hydrogen Absorption in Thermally Prepared RuO_2 and IrO_2. *J. Electroanal. Chem.* **2004**, *570*, 13-27.

(172) Burke, L. D.; Naser, N. S. Metastability and Electrocatalytic Activity of Ruthenium Dioxide Cathodes Used in Water Electrolysis cells. *J. Appl. Electrochem.* **2005**, *35*, 931-938.

(173) Rochefort, D.; Dabo, P.; Guay, D.; Sherwood, P. M. A. XPS Investigations of Thermally Prepared RuO_2 Electrodes in Reductive Conditions. *Electrochim. Acta* **2003**, *48*, 4245-4252.

(174) Näslund, L.-Å.; Ingason, Á. S.; Holmin, S.; Rosen, J. Formation of $RuO(OH)_2$ on RuO_2-Based Electrodes for Hydrogen Production. *J. Phys. Chem. C* **2014**, *118*, 15315-15323.

(175) Karlsson, R. K. B.; Cornell, A.; Pettersson, L. G. M. Structural Changes in RuO_2 during Electrochemical Hydrogen Evolution. *J. Phys. Chem. C* **2016**, *120*, 7094-7102.

(176) Kötz, R.; Stucki, S. Stabilization of RuO_2 by IrO_2 for Anodic Oxygen Evolution in Acid Media. *Electrochim. Acta* **1986**, *31*, 1311-1316.

(177) Angelinetta, C.; Falciola, M.; Trasatti, S. Heterogenous Acid-Base Equilibria and Reaction Order of Oxygen Evolution on Oxide Electrodes. *J. Electroanal. Chem.* **1986**, *205*, 347-353.

(178) Wen, T. C.; Hu, C. C. Hydrogen and Oxygen Evolutions on Ru-Ir Binary Oxides. *J. Electrochem. Soc.* **1992**, *139*, 2158-2163.

(179) Mattos-Costa, F. I.; de Lima-Neto, P.; Machado, S. A. S.; Avaca, L. A. Characterisation of Surfaces Modified by Sol-Gel Derived $Ru_xIr_{1-x}O_2$ Coatings for Oxygen Evolution in Acid Medium. *Electrochim. Acta* **1998**, *44*, 1515-1523.

(180) Marshall, A.; Børresen, B.; Hagen, G.; Tsypkin, M.; Tunold, R. Electrochemical Characterization of $Ir_xSn_{1-x}O_2$ Powders as Oxygen Evolution Electrocatalysts. *Electrochim. Acta* **2006**, *51*, 3161-3167.

(181) Cheng, J.; Zhang, H.; Chen, G.; Zhang, Y. Study of $Ir_xRu_{1-x}O_2$ Oxides as Anodic Electrocatalysts for Solid Polymer Electrolyte Water Electrolysis. *Electrochim. Acta* **2009**, *54*, 6250-6256.

(182) Mamaca, N.; Mayousse, E.; Arrii-Clacens, S.; Napporn, T. W.; Servat, K.; Guillet, N.; Kokoh, K. B. Electrochemical Activity of Ruthenium and Iridium-Based Catalysts for Oxygen Evolution Reaction. *Appl. Catal. B-Environ.* **2012**, *111-112*, 376-380.

(183) Pham, H. H.; Nguyen, N. P.; Do, C. L.; Le, B. T. Nanosized $Ir_xRu_{1-x}O_2$ Electrocatalysts for Oxygen Evolution Reaction in Proton Exchange Membrane Water Electrolyzer. *Advances in Natural Sciences: Nanoscience and Nanotechnology*, **2015**, *6*, 025015.

(184) Reksten, A. H.; Thuv, H.; Seland, F.; Sunde, S. The Oxygen Evolution Reaction Mechanism at $Ir_xRu_{1-x}O_2$ Powders Produced by Hydrolysis Synthesis. *J. Electroanal. Chem.* **2018**, *819*, 547-561.

(185) Audichon, T.; Napporn, T. W.; Canaff, C.; Morais, C.; Comminges, C.; Kokoh, K. B. IrO_2 Coated on RuO_2 as Efficient and Stable Electroactive Nanocatalysts for Electrochemical Water Splitting. *J. Phys. Chem. C* **2016**, *120*, 2562-2573.

(186) Marshall, A. T.; Sunde, S.; Tsypkin, M.; Tunold, R. Performance of a PEM Water Electrolysis Cell using $Ir_xRu_yTa_zO_2$ Electrocatalysts for the Oxygen Evolution Electrode. *Int. J. Hydrogen Energ.* **2007**, *32*, 2320-2324.

(187) Lervik, I. A.; Tsypkin, M.; Owe, L.-E.; Sunde, S. Electronic Structure vs. Electrocatalytic Activity of Iridium Oxide. *J. Electroanal. Chem.* **2010**, *645*, 135-142.

(188) Marshall, A. T.; Haverkamp, R. G. Electrocatalytic Activity of IrO_2–RuO_2 Supported on Sb-Doped SnO_2 Nanoparticles., *Electrochim. Acta* **2010**, *55*, 1978-1984.

(189) Owe, L.-E.; Tsypkin, M.; Wallwork, K. S.; Haverkamp, R. G.; Sunde, S. Iridium–Ruthenium Single Phase Mixed Oxides for Oxygen Evolution: Composition Dependence of Electrocatalytic Activity. *Electrochim. Acta* **2012**, *70*, 158-164.

(190) Lyons, M. E. G.; Floquet, S. Mechanism of Oxygen Reactions at Porous Oxide Electrodes. Part 2—Oxygen Evolution at RuO_2, IrO_2 and $Ir_xRu_{1-x}O_2$ Electrodes in Aqueous Acid and Alkaline Solution. *Phys. Chem. Chem. Phys.* **2011**, *13*, 5314-5335.

(191) Li, G.; Yu, H.; Song, W.; Wang, X.; Li, Y.; Shao, Z.; Yi, B. Zeolite-Templated $Ir_xRu_{1-x}O_2$ Electrocatalysts for Oxygen Evolution Reaction in Solid Polymer Electrolyte Water Electrolyzers. *Int. J. Hydrogen Energ.* **2012**, *37*, 16786-16794.

(192) Roller, J. M.; Arellano-Jimenez, M. J.; Jain, R.; Yu, H. R.; Carter, C. B.; Maric, R. Oxygen Evolution during Water Electrolysis from Thin Films Using Bimetallic Oxides of Ir-Pt and Ir-Ru. *J. Electrochem. Soc.* **2013**, *160*, F716-F730.

(193) Li, G.; Li, S.; Ge, J.; Liu, C.; Xing, W. Discontinuously Covered IrO_2–RuO_2@Ru Electrocatalysts for the Oxygen Evolution Reaction: How High Activity and Long-Term Durability Can Be Simultaneously Realized in the Synergistic and Hybrid Nano-Structure. *J. Mater. Chem. A* **2017**, *5*, 17221-17229.

(194) Yeo, R. S.; Orehotsky, J.; Visscher, W.; Srinivasan, S. Ruthenium-Based Mixed Oxides as Electrocatalysts for Oxygen Evolution in Acid Electrolytes. *J. Electrochem. Soc.* **1981**, *128*, 1900-1904.

(195) Cheng, J.; Zhang, H.; Ma, H.; Zhong, H.; Zou, Y. Preparation of $Ir_{0.4}Ru_{0.6}Mo_xO_y$ for Oxygen Evolution by Modified Adams' Fusion Method. *Int. J. Hydrogen Energ.* **2009**, *34*, 6609-6613.

(196) Petrykin, V.; Macounová, K.; Okube, M.; Mukerjee, S.; Krtil, P. Local Structure of Co Doped RuO_2 Nanocrystalline Electrocatalytic Materials for Chlorine and Oxygen Evolution. *Catal. Today* **2013**, *202*, 63-69.

(197) Corona-Guinto, J. L.; Cardeño-García, L.; Martínez-Casillas, D. C.; Sandoval-Pineda, J. M.; Tamayo-Meza, P.; Silva-Casarin, R.; González-Huerta, R. G. Performance of a PEM Electrolyzer Using $RuIrCoO_x$ Electrocatalysts for the Oxygen Evolution Electrode. *Int. J. Hydrogen Energ.* **2013**, *38*, 12667-12673.

(198) Audichon, T.; Morisset, S.; Napporn, T. W.; Kokoh, K. B.; Comminges, C.; Morais, C. Effect of Adding CeO_2 to RuO_2–IrO_2 Mixed Nanocatalysts: Activity towards the Oxygen Evolution Reaction and Stability in Acidic Media. *ChemElectroChem* **2015**, *2*, 1128-1137.

(199) Blouin, M.; Guay, D. Activation of Ruthenium Oxide, Iridium Oxide, and mixed Ru_xIr_{1-x} Oxide Electrodes during Cathodic Polarization and Hydrogen Evolution. *J. Electrochem. Soc.* **1997**, *144*, 573-581.

(200) Cho, Y.-B.; Yu, A.; Lee, C.; Kim, M. H.; Lee, Y. Fundamental Study of Facile and Stable Hydrogen Evolution Reaction at Electrospun Ir and Ru Mixed Oxide Nanofibers. *ACS Appl. Mater. Interfaces* **2018**, *10*, 541-549.

(201) Petrykin, V.; Macounova, K.; Shlyakhtin, O. A.; Krtil, P. Tailoring the Selectivity for Electrocatalytic Oxygen Evolution on Ruthenium Oxides by Zinc Substitution. *Angew. Chem. Int. Ed.* **2010**, *49*, 4813-4815.

(202) Petrykin, V.; Macounova, K.; Franc, J.; Shlyakhtin, O.; Klementova, M.; Mukerjee, S.; Krtil, P. Zn-Doped RuO_2 electrocatalyts for Selective Oxygen Evolution: Relationship between Local Structure and Electrocatalytic Behavior in Chloride Containing Media. *Chem. Mater.* **2011**, *23*, 200-207.

(203) Wu, X.; Tayal, J.; Basu, S.; Scott, K. Nano-Crystalline $Ru_xSn_{1-x}O_2$ Powder Catalysts for Oxygen Evolution Reaction in Proton Exchange Membrane Water Electrolysers. *Int. J. Hydrogen Energ.* **2011**, *36*, 14796-14804.

(204) Jirkovský, J.; Makarova, M.; Krtil, P. Particle Size Dependence of Oxygen Evolution Reaction on Nanocrystalline RuO_2 and $Ru_{0.8}Co_{0.2}O_{2-x}$. *Electrochem. Commun.* **2006**, *8*, 1417-1422.

(205) Macounova, K.; Makarova, M.; Krtil, P. Oxygen Evolution on Nanocrystalline RuO_2 and $Ru_{0.9}Ni_{0.1}O_{2-\delta}$ Electrodes–DEMS Approach to Reaction Mechanism Determination. *Electrochem. Commun.* **2009**, *11*, 1865-1868.

(206) Halck, N. B.; Petrykin, V.; Krtil, P.; Rossmeisl, J. Beyond the Volcano Limitations in Electrocatalysis-Oxygen Evolution Reaction. *Phys. Chem. Chem. Phys.* **2014**, *16*, 13682-13688.

(207) Oh, A.; Kim, H. Y.; Baik, H.; Kim, B.; Chaudhari, N. K.; Joo, S. H.; Lee, K. Topotactic Transformations in an Icosahedral Nanocrystal to Form Efficient Water-Splitting Catalysts. *Adv. Mater.* **2019**, *31*, 1805546.

(208) Yi, J.; Lee, W. H.; Choi, C. H.; Lee, Y.; Park, K. S.; Min, B. K.; Hwang, Y. J.; Oh, H. S. Effect of Pt Introduced on Ru-based Electrocatalyst for Oxygen Evolution Activity and Stability. *Electrochem. Commun.* **2019**, *104*, 106469.

(209) Wu, Y.; Tariq, M.; Zaman, W. Q.; Sun, W.; Zhou, Z.; Yang, J. Ni-Co Codoped RuO_2 with Outstanding Oxygen Evolution Reaction Performance. *ACS Appl. Energy Mater.* **2019**, *2*, 4105-4110.

(210) Su, J.; Ge, R.; Jiang, K.; Dong, Y.; Hao, F.; Tian, Z.; Chen, G.; Chen, L. Assembling Ultrasmall Copper-Doped Ruthenium Oxide Nanocrystals into Hollow Porous Polyhedra: Highly Robust Electrocatalysts for Oxygen Evolution in Acidic Media. *Adv. Mater.* **2018**, *30*, 1801351.

(211) Lin, Y.; Tian, Z.; Zhang, L.; Ma, J.; Jiang, Z.; Deibert, B. J.; Ge, R.; Chen, L. Chromium-Ruthenium Oxide Solid Solution Electrocatalyst for Highly Efficient Oxygen Evolution Reaction in Acidic Media. *Nat. Commun.* **2019**, *10*, 162.

(212) Gaudet, J.; Tavares, A. C.; Trasatti, S.; Guay, D. Physicochemical Characterization of Mixed RuO_2–SnO_2 Solid Solutions. *Chem. Mater.* **2005**, *17*, 1570-1579.

(213) Kadakia, K.; Datta, M. K.; Velikokhatnyi, O. I.; Jampani, P.; Park, S. K.; Chung, S. J.; Kumta, P. N. High Performance Fluorine Doped (Sn, Ru)O_2 Oxygen Evolution Reaction Electro-catalysts for Proton Exchange Membrane Based Water Electrolysis. *J. Power Sources* **2014**, *245*, 362-370.

(214) Terezo, A. J.; Pereira, E. C. Preparation and Characterization of Ti/RuO_2–Nb_2O_5 Electrodes Obtained by Polymeric Precursor Method. *Electrochim. Acta* **1999**, *44*, 4507-4513.

(215) Ribeiro, J.; Moats, M. S.; De Andrade, A. R. Morphological and Electrochemical Investigation of RuO_2–Ta_2O_5 Oxide Films Prepared by the Pechini–Adams Method. *J. Appl. Electrochem.* **2008**, *38*, 767-775.

(216) Da Silva, L. M.; Boodts, J. F. C.; De Faria, L. A. Oxygen Evolution at $RuO_2(x)+Co_3O_4(1-x)$ Electrodes from Acid Solution. *Electrochim. Acta* **2001**, *46*, 1369-1375.

(217) Fernández, J. L.; Gennero De Chialvo, M. R.; Chialvo, A. C. Preparation and Electrochemical Characterization of $Ti/Ru_xMn_{1-x}O_2$ Electrodes. *J. Appl. Electrochem.* **2002**, *32*, 513-520.

(218) Baruffaldi, C.; Cattarin, S.; Musiani, M. Deposition of Non-Stoichiometric Tungsten Oxides+MO_2 Composites (M=Ru or Ir) and Study of Their Catalytic Properties in Hydrogen or Oxygen Evolution Reactions. *Electrochim. Acta* **2003**, *48*, 3921-3927.

(219) Shrivastava, P.; Moats, M. S. Ruthenium Palladium Oxide-Coated Titanium Anodes for Low-Current-Density Oxygen Evolution. *J. Electrochem. Soc.* **2008**, *155*, E101-E107.

(220) Puthiyapura, V. K.; Pasupathi, S.; Basu, S.; Wu, X.; Su, H.; Varagunapandiyan, N.; Pollet, B.; Scott, K. $Ru_xNb_{1-x}O_2$ Catalyst for the Oxygen Evolution Reaction in Proton Exchange Membrane Water Electrolysers. *Int. J. Hydrogen Energ.* **2013**, *38*, 8605-8616.

(221) Browne, M. P.; Nolan, H.; Duesberg, G. S.; Colavita, P. E.; Lyons, M. E. G. Low-Overpotential High-Activity Mixed Manganese and Ruthenium Oxide Electrocatalysts for Oxygen Evolution Reaction in Alkaline Media. *ACS Catal.* **2016**, *6*, 2408-2415.

(222) Shiva Kumar, S.; Ramakrishna, S. U. B.; Bhagawan, D.; Himabindu, V. Preparation of $Ru_xPd_{1-x}O_2$ Electrocatalysts for the Oxygen Evolution Reaction (OER) in PEM Water Electrolysis. *Ionics*, **2018**, *24*, 2411-2419.

(223) Yoon, K. R.; Lee, G. Y.; Jung, J.-W.; Kim, N.-H.; Kim, S. O.; Kim, I.-D. One-Dimensional RuO_2/Mn_2O_3 Hollow Architectures as Efficient Bifunctional Catalysts for Lithium–Oxygen Batteries. *Nano Lett.* **2016**, *16*, 2076-2083.

(224) Browne, M. P.; Nolan, H.; Twamley, B.; Duesberg, G. S.; Colavita, P. E.; Lyons, M. E. G. Thermally Prepared Mn_2O_3/RuO_2/Ru Thin Films as Highly Active Catalysts for the Oxygen Evolution Reaction in Alkaline Media. *ChemElectroChem* **2016**, *3*, 1847-1855.

(225) Yoon, K. R.; Kim, D. S.; Ryu, W.-H.; Song, S. H.; Youn, D.-Y.; Jung, J.-W.; Jeon, S.; Park, Y. J.; Kim, I.-D. Tailored Combination of Low Dimensional Catalysts for Efficient Oxygen Reduction and Evolution in Li–O_2 Batteries. *ChemSusChem* **2016**, *9*, 2080-2088.

(226) He, C.; Wang, G. X.; Parrondo, J.; Sankarasubramanian, S.; Ramani, V. Pt/RuO_2-TiO_2 Electrocatalysts Exhibit Excellent Hydrogen Evolution Activity in Alkaline Media. *J. Electrochem. Soc.* **2017**, *164*, F1234-F1240.

(227) Zhang, L.; Xiong, K.; Chen, S.; Li, L.; Deng, Z.; Wei, Z. In Situ Growth of Ruthenium Oxide-Nickel Oxide Nanorod Arrays on Nickel Foam as a Binder-Free Integrated Cathode for Hydrogen Evolution. *J. Power Sources* **2015**, *274*, 114-120.

(228) Shibli, S. M. A.; Ameen Sha, M. Development and Characterization of Electro Active CeO_2–RuO_2 Mixed Oxide and Its Role in Alkaline Hydrogen Evolution Reaction. *J. Alloy Compd.* **2018**, *749*, 250-261.

(229) Cheng, J.; Zhang, H.; Ma, H.; Zhong, H.; Zou, Y. Study of Carbon-Supported IrO_2 and RuO_2 for Use in the Hydrogen Evolution Reaction in a Solid Polymer Electrolyte Electrolyzer. *Electrochim. Acta* **2010**, *55*, 1855-1861.

(230) Jebakumar Immanuel Edison, T. N.; Atchudan, R.; Lee, Y. R. Facile Synthesis of Carbon Encapsulated RuO_2 Nanorods for Supercapacitor and Electrocatalytic Hydrogen Evolution Reaction. *Int. J. Hydrogen Energ.* **2019**, *44*, 2323-2329.

(231) Park, H.-S.; Yang, J.; Cho, M. K.; Lee, Y.; Cho, S.; Yim, S.-D.; Kim, B.-S.; Jang, J. H.; Song, H.-K. RuO_2 Nanocluster as a 4-in-1 Electrocatalyst for Hydrogen and Oxygen Electrochemistry. *Nano Energy* **2019**, *55*, 49-58.

(232) Xie, K.; Xia, W.; Masa, J.; Yang, F.; Weide, P.; Schuhmann, W.; Muhler, M. Promoting Effect of Nitrogen Doping on Carbon Nanotube-Supported RuO_2 Applied in the Electrocatalytic Oxygen Evolution Reaction. *J. Energy Chem.* **2016**, *25*, 282-288.

(233) Yuan, C.-Z.; Jiang, Y.-F.; Zhao, Z.-W.; Zhao, S.-J.; Zhou, X.; Cheang, T.-Y.; Xu, A.-W. Molecule-Assisted Synthesis of Highly Dispersed Ultrasmall RuO_2 Nanoparticles on Nitrogen-Doped Carbon Matrix as Ultraefficient Bifunctional Electrocatalysts for Overall Water Splitting. *ACS Sustain. Chem. Eng.* **2018**, *6*, 11529-11535.

(234) Zhang, L.; Zhao, Z.-J.; Norouzi Banis, M.; Li, L.; Zhao, Y.; Song, Z.; Wang, Z.; Sham, T.-K.; Li, R.; Zheng, M.; Gong, J.; Sun, X. Selective Atomic Layer Deposition of RuO_x Catalysts

on Shape-Controlled Pd Nanocrystals with Significantly Enhanced Hydrogen Evolution Activity. *J. Mater. Chem. A* **2018**, *6*, 24397-24406.

(235) Park, H.-S.; Seo, E.; Yang, J.; Lee, Y.; Kim, B.-S.; Song, H.-K. Bifunctional Hydrous RuO_2 Nanocluster Electrocatalyst Embedded in Carbon Matrix for Efficient and Durable Operation of Rechargeable Zinc–Air Batteries. *Sci. Rep.* **2017**, *7*, 7150.

(236) Park, J.; Park, M.; Nam, G.; Kim, M. G.; Cho, J. Unveiling the Catalytic Origin of Nanocrystalline Yttrium Ruthenate Pyrochlore as a Bifunctional Electrocatalyst for Zn–Air Batteries. *Nano Lett.* **2017**, *17*, 3974-3981.

(237) Kim, J.; Shih, P.-C.; Tsao, K.-C.; Pan, Y.-T.; Yin, X.; Sun, C.-J.; Yang, H. High-Performance Pyrochlore-Type Yttrium Ruthenate Electrocatalyst for Oxygen Evolution Reaction in Acidic Media. *J. Am. Chem. Soc.* **2017**, *139*, 12076-12083.

(238) Kim, J.; Shih, P.-C.; Qin, Y.; Al-Bardan, Z.; Sun, C.-J.; Yang, H. A Porous Pyrochlore $Y_2[Ru_{1.6}Y_{0.4}]O_{7-\delta}$ Electrocatalyst for Enhanced Performance towards the Oxygen Evolution Reaction in Acidic Media. *Angew. Chem. Int. Edit.* **2018**, *130*, 14073-14077.

(239) Feng, Q.; Wang, Q.; Zhang, Z.; Xiong, Y.; Li, H.; Yao, Y.; Yuan, X.-Z.; Williams, M. C.; Gu, M.; Chen, H.; Li, H.; Wang, H. Highly Active and Stable Ruthenate Pyrochlore for Enhanced Oxygen Evolution Reaction in Acidic Medium Electrolysis. *Appl. Catal. B-Environ.* **2019**, *244*, 494-501.

(240) Horowitz, H. S.; Longo, J. M.; Horowitz, H. H. Oxygen Electrocatalysis on Some Oxide Pyrochlores. *J. Electrochem. Soc.* **1983**, *130*, 1851-1859.

(241) Park, J.; Risch, M.; Nam, G.; Park, M.; Shin, T. J.; Park, S.; Kim, M. G.; Shao-Horn, Y.; Cho, J. Single Crystalline Pyrochlore Nanoparticles with Metallic Conduction as Efficient Bi-functional Oxygen Electrocatalysts for Zn–Air Batteries. *Energy Environ. Sci.* **2017**, *10*, 129-136.

(242) Parrondo, J.; George, M.; Capuano, C.; Ayers, K. E.; Ramani, V. Pyrochlore Electrocatalysts for Efficient Alkaline Water Electrolysis. *J. Mater. Chem. A* **2015**, *3*, 10819-10828.

(243) Sardar, K.; Petrucco, E.; Hiley, C. I.; Sharman, J. D. B.; Wells, P. P.; Russell, A. E.; Kashtiban, R. J.; Sloan, J.; Walton, R. I. Water-Splitting Electrocatalysis in Acid Conditions Using Ruthenate-Iridate Pyrochlores. *Angew. Chem. Int. Ed.* **2014**, *53*, 10960-10964.

(244) Akbashev, A. R.; Zhang, L.; Mefford, J. T.; Park, J.; Butz, B.; Luftman, H.; Chueh, W. C.; Vojvodic, A. Activation of Ultrathin $SrTiO_3$ with Subsurface $SrRuO_3$ for the Oxygen Evolution Reaction. *Energy Environ. Sci.* **2018**, *11*, 1762-1769.

(245) Abreu-Sepulveda, M.; Trinh, P.; Malkhandi, S.; Narayanan, S. R.; Jorné, J.; Quesnel, D. J.; Postonr, J. A.; Manivannan, A. Investigation of Oxygen Evolution Reaction at $LaRuO_3$, $La_{3.5}Ru_4O_{13}$, and La_2RuO_5. *Electrochim. Acta* **2015**, *180*, 401-408.

(246) Rincón, R. A.; Ventosa, E.; Tietz, F.; Masa, J.; Seisel, S.; Kuznetsov, V.; Schuhmann, W. Evaluation of Perovskites as Electrocatalysts for the Oxygen Evolution Reaction. *ChemPhysChem*, **2014**, *15*, 2810-2816.

(247) Laha, S.; Lee, Y.; Podjaski, F.; Weber, D.; Duppel, V.; Schoop, L. M.; Pielnhofer, F.; Scheurer, C.; Müller, K.; Starke, U.; Reuter, K.; Lotsch, B. V. Ruthenium Oxide Nanosheets for Enhanced Oxygen Evolution Catalysis in Acidic Medium. *Adv. Energy Mater.* **2019**, *9*, 1803795.

(248) Jiang, P.; Liu, Q.; Sun, X. NiP_2 Nanosheet Arrays Supported on Carbon Cloth: An Efficient 3D Hydrogen Evolution Cathode in Both Acidic and Alkaline Solutions. *Nanoscale* **2014**, *6*, 13440-13445.

(249) Son, C. Y.; Kwak, I. H.; Lim, Y. R.; Park, J. FeP and FeP_2 Nanowires for Efficient Electrocatalytic Hydrogen Evolution Reaction. *Chem. Commun.* **2016**, *52*, 2819-2822.

(250) Zhu, W.; Tang, C.; Liu, D.; Wang, J.; Asiri, A. M.; Sun, X. A Self-Standing Nanoporous MoP_2 Nanosheet Array: An Advanced pH-Universal Catalytic Electrode for the Hydrogen Evolution Reaction. *J. Mater. Chem. A* **2016**, *4*, 7169-7173.

(251) Pu, Z.; Amiinu, I. S.; Kou, Z.; Li, W.; Mu, S. RuP_2-Based Catalysts with Platinum-like Activity and Higher Durability for the Hydrogen Evolution Reaction at All pH Values. *Angew. Chem. Int. Ed.* **2017**, *56*, 11559-11564.

(252) Qin, Q.; Jang, H.; Chen, L.; Nam, G.; Liu, X.; Cho, J. Low Loading of Rh_xP and RuP on N, P Codoped Carbon as Two Trifunctional Electrocatalysts for the Oxygen and Hydrogen Electrode Reactions. *Adv. Energy Mater.* **2018**, *8*, 1801478.

(253) Liu, T.; Feng, B.; Wu, X.; Niu, Y.; Hu, W.; Li, C. M. Ru_2P Nanoparticle Decorated P/N-Doped Carbon Nanofibers on Carbon Cloth as a Robust Hierarchical Electrocatalyst with Platinum-Comparable Activity toward Hydrogen Evolution. *ACS Appl. Energy Mater.* **2018**, *1*, 3143-3150.

(254) Liu, T.; Wang, S.; Zhang, Q.; Chen, L.; Hu, W.; Li, C. M. Ultrasmall Ru_2P Nanoparticles on Graphene: A Highly Efficient Hydrogen Evolution Reaction Electrocatalyst in Both Acidic and Alkaline Media. *Chem. Commun*. **2018**, *54*, 3343-3346.

(255) Yu, J.; Wu, X.; Zhang, H.; Ni, M.; Zhou, W.; Shao, Z. Core Effect on the Performance of N/P Codoped Carbon Encapsulating Noble-Metal Phosphide Nanostructures for Hydrogen Evolution Reaction. *ACS Appl. Energy Mater*. **2019**, *2*, 2645-2653.

(256) Chang, Q.; Ma, J.; Zhu, Y.; Li, Z.; Xu, D.; Duan, X.; Peng, W.; Li, Y.; Zhang, G.; Zhang, F.; Fan, X. Controllable Synthesis of Ruthenium Phosphides (RuP and RuP_2) for pH-Universal Hydrogen Evolution Reaction. *ACS Sustain. Chem. Eng.* **2018**, *6*, 6388-6394.

(257) Ge, R.; Wang, S.; Su, J.; Dong, Y.; Lin, Y.; Zhang, Q.; Chen, L. Phase-Selective Synthesis of Self-supported RuP Films for Efficient Hydrogen Evolution Electrocatalysis in Alkaline Media. *Nanoscale* **2018**, *10*, 13930-13935.

(258) Chi, J.-Q.; Gao, W.-K.; Lin, J.-H.; Dong, B.; Yan, K.-L.; Qin, J.-F.; Liu, B.; Chai, Y.-M.; Liu, C.-G. Hydrogen Evolution Activity of Ruthenium Phosphides Encapsulated in Nitrogen- and Phosphorous-Codoped Hollow Carbon Nanospheres. *ChemSusChem* **2018**, *11*, 743-752.

(259) Wang, K.; Chen, Q.; Hu, Y.; Wei, W.; Wang, S.; Shen, Q.; Qu, P. Crystalline $Ru_{0.33}Se$ Nanoparticles-Decorated TiO_2 Nanotube Arrays for Enhanced Hydrogen Evolution Reaction. *Small* **2018**, *14*, 1802132.

(260) Yu, J.; Guo, Y.; Miao, S.; Ni, M.; Zhou, W.; Shao, Z. Spherical Ruthenium Disulfide-Sulfur-Doped Graphene Composite as an Efficient Hydrogen Evolution Electrocatalyst. *ACS Appl. Mater. Interfaces* **2018**, *10*, 34098-34107.

(261) Li, Q.; Zou, X.; Ai, X.; Chen, H.; Sun, L.; Zou, X. Revealing Activity Trends of Metal Diborides Toward pH-Universal Hydrogen Evolution Electrocatalysts with Pt-Like Activity. *Adv. Energy Mater.* **2019**, *9*, 1803369.

(262) Chen, G.; Wang, T.; Zhang, J.; Liu, P.; Sun, H.; Zhuang, X.; Chen, M.; Feng, X. Accelerated Hydrogen Evolution Kinetics on NiFe-Layered Double Hydroxide Electrocatalysts by Tailoring Water Dissociation Active Sites. *Adv. Mater.* **2018**, *30*, 1706279.

(263) Chala, S. A.; Tsai, M.-C.; Su, W.-N.; Ibrahim, K. B.; Duma, A. D.; Yeh, M.-H.; Wen, C.-Y.; Yu, C.-H.; Chan, T.-S.; Dai, H.; Hwang, B.-J. Site Activity and Population Engineering of NiRu-

Layered Double Hydroxide Nanosheets Decorated with Silver Nanoparticles for Oxygen Evolution and Reduction Reactions. *ACS Catal.* **2019**, *9*, 117-129.

(264) Liyanage, D. R.; Li, D.; Cheek, Q. B.; Baydoun, H.; Brock, S. L. Synthesis and Oxygen Evolution Reaction (OER) Catalytic Performance of $Ni_{2-x}Ru_xP$ Nanocrystals: Enhancing Activity by Dilution of the Noble Metal. *J. Mater. Chem. A* **2017**, *5*, 17609-17618.

(265) Zhang, Z.; Li, P.; Feng, Q.; Wei, B.; Deng, C.; Fan, J.; Li, H.; Wang, H. Scalable Synthesis of a Ruthenium-Based Electrocatalyst as a Promising Alternative to Pt for Hydrogen Evolution Reaction. *ACS Appl. Mater. Interfaces* **2018**, *10*, 32171-32179.

(266) Nong, S.; Dong, W.; Yin, J.; Dong, B.; Lu, Y.; Yuan, X.; Wang, X.; Bu, K.; Chen, M.; Jiang, S.; Liu, L.-M.; Sui, M.; Huang, F. Well-Dispersed Ruthenium in Mesoporous Crystal TiO_2 as an Advanced Electrocatalyst for Hydrogen Evolution Reaction. *J. Am. Chem. Soc.* **2018**, *140*, 5719-5727.

(267) Vasu, K.; Meiron, O. E.; Enyashin, A. N.; Bar-Ziv, R.; Bar-Sadan, M. Effect of Ru Doping on the Properties of $MoSe_2$ Nanoflowers. *J. Phys. Chem. C* **2019**, *123*, 1987-1994.

(268) Faustini, M.; Giraud, M.; Jones, D.; Rozière, J.; Dupont, M.; Porter, T. R.; Nowak, S.; Bahri, M.; Ersen, O.; Sanchez, C.; Boissière, C.; Tard, C.; Peron, J. Porous Electrocatalysts: Hierarchically Structured Ultraporous Iridium-Based Materials: A Novel Catalyst Architecture for Proton Exchange Membrane Water Electrolyzers. *Adv. Energy Mater.* **2019**, *9*, 1970012.

(269) Yu, J.; Wu, X.; Zhong, Y.; Yang, G.; Ni, M.; Zhou, W.; Shao, Z. Multifold Nanostructuring and Atomic-Scale Modulation of Cobalt Phosphide to Significantly Boost Hydrogen Production. *Chem. Eur. J.* **2018**, *24*, 13800-13806.

(270) Masaki, Y.; Shigeyuki, M.; Ken, S. Oxygen Evolution from Water Catalyzed by Mononuclear Ruthenium Complexes with a Triazamacrocyclic Ligand in a Facial Fashion. *Chem. Lett.* **2009**, *38*, 702-703.

(271) Mbemba Kiele, N.; Herrero, C.; Ranjbari, A.; Aukauloo, A.; Grigoriev, S. A.; Villagra, A.; Millet, P. Ruthenium-based Molecular Compounds for Oxygen Evolution in Acidic Media. *Int. J. Hydrogen Energ.* **2013**, *38*, 8590-8596.

(272) Udachyan, I.; Vishwanath, R. S.; Pradeepa Kumara, C. S.; Kandaiah, S. Ruthenium Ion Containing N and S Rich Triazine Based Metallopolymer as a Low Overpotential Acid Stable Electrocatalyst for Hydrogen Evolution. *J. Catal.* **2018**, *357*, 138-146.

(273) Creus, J.; Drouet, S.; Suriñach, S.; Lecante, P.; Collière, V.; Poteau, R.; Philippot, K.; García-Antón, J.; Sala, X. Ligand-Capped Ru Nanoparticles as Efficient Electrocatalyst for the Hydrogen Evolution Reaction. *ACS Catal.* **2018**, *8*, 11094-11102.

(274) Wang, L.; Fan, K.; Chen, H.; Daniel, Q.; Philippe, B.; Rensmo, H.; Sun, L. Towards Efficient and Robust Anodes for Water Splitting: Immobilization of Ru Catalysts on Carbon Electrode and Hematite by in Situ Polymerization. *Catal. Today* **2017**, *290*, 73-77.

(275) Han, X.; Wu, X.; Deng, Y.; Liu, J.; Lu, J.; Zhong, C.; Hu, W. Ultrafine Pt Nanoparticle-Decorated Pyrite-Type CoS_2 Nanosheet Arrays Coated on Carbon Cloth as a Bifunctional Electrode for Overall Water Splitting. *Adv. Energy Mater.* **2018**, *8*, 1800935.

(276) Anantharaj, S.; Karthick, K.; Venkatesh, M.; Simha, T. V.; Salunke, A. S.; Ma, L.; Liang, H.; Kundu, S. Enhancing Electrocatalytic total Water Splitting at Few Layer Pt-NiFe Layered Double Hydroxide Interfaces. *Nano Energy* **2017**, *39*, 30-43.

(277) Zhu, M.; Shao, Q.; Qian, Y.; Huang, X. Superior Overall Water Splitting Electrocatalysis in Acidic Conditions Enabled by Bimetallic Ir-Ag Nanotubes. *Nano energy* **2019**, *56*, 330-337.

(278) Lv, F.; Feng, J.; Wang, K.; Dou, Z.; Zhang, W.; Zhou, J.; Yang, C.; Luo, M.; Yang, Y.; Li, Y.; Gao, P.; Gao, S. Iridium-Tungsten Alloy Nanodendrites as pH-Universal Water-Splitting Electrocatalysts. *ACS Central Sci.* **2018**, *4*, 1244-1252.

(279) Zhu, Y.; Zhou, W.; Zhong, Y.; Bu, Y.; Chen, X.; Zhong, Q.; Liu, M.; Shao, Z. A Perovskite Nanorod as Bifunctional Electrocatalyst for Overall Water Splitting. *Adv. Energy Mater.* **2017**, *7*, 1602122.

(280) Zhang, B.; Xiao, C.; Xie, S.; Liang, J.; Chen, X.; Tang, Y. Iron-Nickel Nitride Nanostructures in Situ Grown on Surface-Redox-Etching Nickel Foam: Efficient and Ultrasustainable Electrocatalysts for Overall Water Splitting. *Chem. Mater.* **2016**, *28*, 6934-6941.

(281) Wei, S.; Cui, X.; Xu, Y.; Shang, B.; Zhang, Q.; Gu, L.; Fan, X.; Zheng, L.; Hou, C.; Huang, H.; Wen, S.; Zheng, W. Iridium-Triggered Phase Transition of MoS_2 Nanosheets Boosts Overall Water Splitting in Alkaline Media. *ACS Energy Lett.* **2018**, *4*, 368-374.

(282) Li, W.; Gao, X.; Xiong, D.; Wei, F.; Song, W. G.; Xu, J.; Liu, L. Hydrothermal Synthesis of Monolithic Co_3Se_4 Nanowire Electrodes for Oxygen Evolution and Overall Water Splitting with High Efficiency and Extraordinary Catalytic Stability. *Adv. Energy Mater.* **2017**, *7*, 1602579.

(283) Li, H.; Wen, P.; Li, Q.; Dun, C.; Xing, J.; Lu, C.; Adhikari, S.; Jiang, L.; Carroll, D. L.;

Geyer, S. M. Earth-Abundant Iron Diboride (FeB_2) Nanoparticles as Highly Active Bifunctional Electrocatalysts for Overall Water Splitting. *Adv. Energy Mater.* **2017**, *7*, 1700513.

(284) Jiang, Y.; Lu, Y.; Lin, J.; Wang, X.; Shen, Z. A hierarchical MoP Nanoflake Array Supported on Ni Foam: A Bifunctional Electrocatalyst for Overall Water Splitting. *Small Methods* **2018**, *2*, 1700369.

(285) Dai, Z.; Geng, H.; Wang, J.; Luo, Y.; Li, B.; Zong, Y.; Yang, J.; Guo, Y.; Zheng, Y.; Wang, X.; Yan, Q. Hexagonal-phase Cobalt Monophosphosulfide for Highly Efficient Overall Water Splitting. *ACS Nano* **2017**, *11*, 11031-11040.

(286) Yu, Z. Y.; Duan, Y.; Gao, M. R.; Lang, C. C.; Zheng, Y. R.; Yu, S. H. A One-Dimensional Porous Carbon-Supported Ni/Mo_2C Dual Catalyst for Efficient Water Splitting. *Chem. Sci.* **2017**, *8*, 968-973.

TOC: